European Cells and Materials Vol. 3. Suppl. 1, 2002 (pages 1-2) ISSN 1473-2262

MICROSTRUCTURE DESIGN OF ADVANCED BIOCERAMICS

P. Greil and F. Mueller, University of Erlangen-Nuernberg, Erlangen, FRG

INTRODUCTION: Bioceramics are increasingly being used clinically due to their compatibility with the physiological environment. While load bearing implants are made of high strength and wear resistant oxides such as Al_2O_3 and ZrO_2 a number of bioactive glasses and glass ceramics in the system Na_2O-CaO-SiO_2-P_2O_5-CaF_2 and Ca-Phosphate ceramics showing osteoconductive behavior serve for bone-repair and reconstruction of deseased or damaged skeletal parts [1]. Thus, applications of bioceramics include implants and restaurations in dentistry, joint replacements in orthopedics, bone reconstruction in maxillofacial surgery, and drug release and tissue engineering systems in pharmaceutical technology.

In the field of materials science and engineering zero shrinkage manufacturing, fiber composites processing and biomimetic interface bonding are among the current topics of advanced bioceramics development. In the following, recent work on microstructure design involving volume compensating reaction bonding systems, bioceramic fiber composite architecture, and *in situ* formation of calcium phosphate reaction layer at the implant/ tissue interface will be discussed.

RESULTS AND DISCUSSION:

A) Zero Shrinkage Manufacturing: Volume compensation of a bonding reaction which takes place between a matrix phase and a filler phase has recently become a promising approach for achieving a dimensional invariant shaping and densification of bioceramic components. Ideally, the volume change associated with the formation of the ceramic body from a starting powder mixture, Ψ, is given as

$$\Psi = \sum V_{educts} + P_{educt} - \sum V_{products} - P_{product} \ .$$

Making use of a selective expansion reaction in the educt powder mixture, zero shrinkage with $\Psi = 0$ can be obtained upon densification (e.g. porosity in the product $P_{product} \rightarrow 0$) when the volume of the reaction product, $\sum V_{products}$, equals that of the green body, $\sum V_{educts} + P_{educts}$. Possible reactions involving metal powders (Al, $ZrSi_2$, Ti) and gaseous (O_2) or liquid and solid polymeric ($CH_3SiO_{1.5}$) reactants are for example [2-4]

$2Al+3/2\ O_2 \rightarrow Al_2O_3$

$ZrSi_2+3O_2 \rightarrow ZrSiO_4+SiO_2$

$Ti+2(CH_3SiO_{1.5}) \rightarrow TiC+SiO_2+SiC+(H_2O+2H_2)\uparrow$

Typical reaction bonding temperatures can be rather low (< 1100°C) and the reaction bonded ceramics are distinguished by excellent mechanical properties (strength of RBAO Al_2O_3 > 700 MPa) which may further be improved by ZrO_2-toughening. Zero shrinkage manufacturing of bioceramic components is of particular relevance for complex shaped dental restaurations.

B) Bioceramic Fiber Composite Architecture: Bioactive as well as bioresorbable fibers are of particular interest for reinforcement of osteosynthetic biopolymer matrix composites and for cell carrying scaffold substrates. Hollow fibers of hydroxylapatite (HAP) ($Ca_5(PO_4)_3/OH$) and tricalciumphosphate (ß-TCP) ($Ca_3(PO_4)_2$) can be prepared by coating a template fiber with a powder slurry of controlled rheology, removal of the template and subsequent sintering. Continous as well as short fibers with an outer and inner diameter ranging from 50 to 200 µm and 10 to 100 µm, respectively, were prepared by coating polyamide or cellulose template fibers, Fig. 1, and subsequently used for reinforcement of polylactide composites.

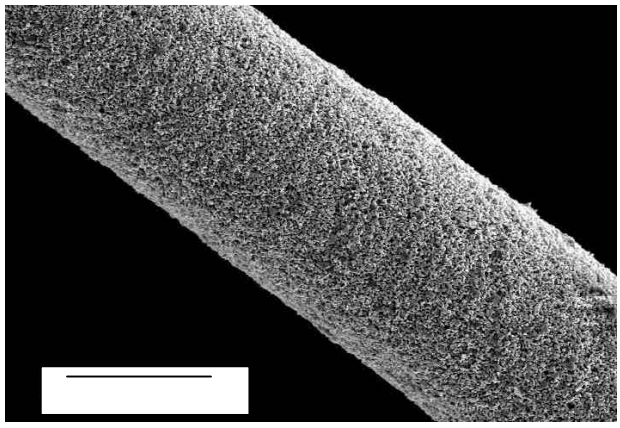

Fig. 1: ß-TCP hollow fiber derived by a continuous slurry coating process.

Electrochemical and electrophoretic deposition of the calcium phosphate phases from aqueous solutions or powder suspensions on fibrillar biocarbon templates derived from plant tissue is a novel approach which makes use of the hierarchical cellular anatomy of naturally grown tissue. Templates of appropriate cellular morphology mimicking the anatomical features of bone can be selected from a huge variety of biostructures as for example the one shown in Fig. 2.

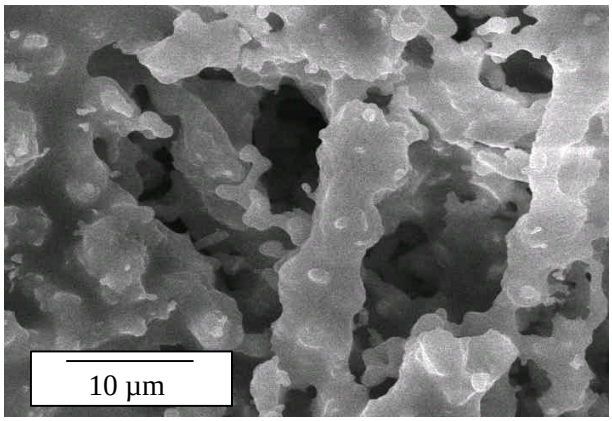

Fig. 2: Cellular HAP-bioceramic derived from a lingocellulosic template.

C) Biomimetic in situ formation of HAP interface layers: Todays implants have a variety of shortcomings related to their fixation behavior, and unlike living tissues, cannot self-repair or adapt to local physiological conditions. Conventionally physical (plasma spraying) and chemical (sol-gel) deposition processes are applied to form ceramic coatings on the implant surface. *In situ* formation of biologically active bone-like calcium phosphate interface bonding layers on metals, polymers and ceramics can be triggered in the physiological environment via a cation exchange process which induces local pH variation [5,6].

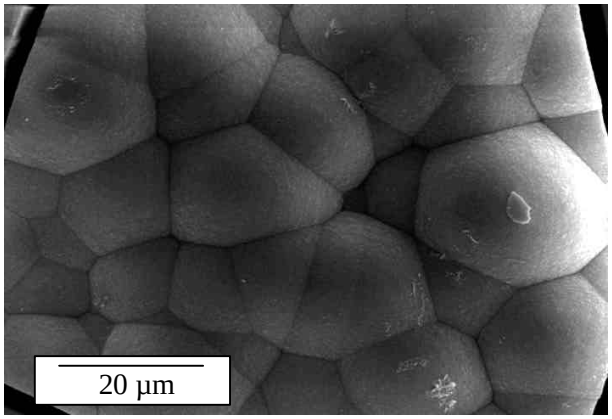

Fig. 3: SEM micrograph of Ti surface soaked for 14 days in SBF showing in situ grown HAP reaction layer.

Fig. 3 shows typical HAP surface structure of alkaline treated Ti after soaking in simulated body fluid (SBF) for 14 days. Formation of interface apatite at low alkaline concentrations is of particular relevance in order to reduce inflammatory response at the early stages of implant fixation [7].

The long-term alternatives to the more traditional use of bioceramics and bioceramic fabrications processes include the use of nanoceramics coupled with biofunctional molecules [8]. Enzymes, anti-bodies or specific receptors linked to nanoceramic particles are supposed to make new applications possible such as diffusible bio-markers and bio-sensors for medical diagnostics or nanoparticle carrier systems to be applied in therapeutics. Hierarchically structured biomaterial surfaces with a porous microstructure extending over several length scales provide the opportunity of improving the biomaterial/ tissue interface with respect to molecular, supramolecular and cellular interaction.

CONCLUSIONS: Tailoring the microstructure on various hierarchical levels is of particular significance for the development of advanced bioceramics with improved biomechanical and biochemical behavior. Novel approaches such as zero shrinkage and biomimetic processing offer the possibility for manufacturing of bioceramics which exhibit a better adaption to the physiological environment, performance and reliability.

REFERENCES: [1]L.L. Hench, Bioceramics, *J.Am.Ceram.Soc. 81* (1998) 1705-28. [2]S. Wu, D. Holz, N. Claussen, Mechanisms and kinetics of reaction-bonded aluminium oxide ceramics, *J.Am. Ceram.Soc. 76* (1993) 970-80. [3]V.D. Hennige, J. Haußelt, H.J. Ritzhaupt-Kleissl, T. Windmann, Shrinkage-free $ZrSiO_4$-ceramics: Characterisation and Applications, *J.Europ.Ceram.Soc. 19* (1999) 2901-08. [4]P. Greil, Pyrolysis of Active and Passive Filler-Loaded Preceramic Polymers, in *Handbook Advanced Ceramic Materials Science*, edt. S. Somiya, Academic Press. (2002), [5]T. Kokubo, Forma-tion of biologically active bone-like apatite on metals and polymers by a biomimetic process, *Thermoch.Acta 280/281* (1996) 479-90. [6]H. Barrere, P. Layrolle, C.A. Van Blitterswijk, K. De Groot, Biomimetic coatings on titanium: a crystal growth study of octacalcium phosphate, *J.Mat.Sci. Med. 12* (2001) 529-34. [7]L. Janasova, F.A. Müller, A. Helebrant, J. Strnad, P. Greil, Hydroxyapatite formation on alkali-treated titanium with different content of Na^+ in the surface layer, to be publ. in *Biomaterials* (2002). [8]C.M. Niemeyer, Nanopartikel, Proteine und Nucleinsäuren: Die Biotechnologie begegnet den Materialswissenschaften, *Angew. Chem. 113* (2001) 4254-87.

European Cells and Materials Vol. 3. Suppl. 1, 2002 (pages 3-4) ISSN 1473-2262

CONTROLLED LOCALIZED DELIVERY OF INSULIN LIKE GROWTH FACTOR I (IGF I) INDUCES NEW BONE FORMATION: THE SIGNIFICANCE OF RELEASE KINETICS

V. Luginbühl[1], B. v. Rechenberg[2], J. Zapf[3], E. Zoidis[3], J. A. Auer[2], H. P. Merkle[1], L. Meinel[1]

[1]Drug formulation and delivery, ETH Zürich, CH, [2]Department of Veterinary Surgery, University of Zürich, CH, [3]Division of Endocrinology, University of Zürich, CH

INTRODUCTION: It is estimated that five to ten percent of the 6.2 million fractures occurring annually in the United States result in delayed or impaired healing. Osteoinductive agents are a possible avenue to augment surgical procedures or treat the plethora of standard fractures. A great challenge presented in the science of biological bone growth factors at this time seems to be developing the best delivery mechanism and kinetic. Direct injection or oral applications do not present appropriate remedy, but the controlled localized delivery of osteoinductive therapeutics from polymeric biodegradable implants is a valid alternative. We have demonstrated a marked capacity of IGF I to bridge non-union defects, when delivered in a controlled localized fashion[1,2]. We report the impact of release kinetics and polymer choice on new bone formation within sheep fracture models and concomitant changes in the expression of various marker genes relevant for bone formation, resorption, and turnover.

METHODS: IGF I was encapsulated in various types of poly (lactide-co-glycolide) (PLGA 502H, 502, 503H, 752) and poly-lactide (PLA 202) microspheres (MS) using solvent evaporation (loading 0,1%). IGF I in vitro release kinetics from the microspheres were monitored for 72 days by radioimmunoassay (RIA) analysis. The in vivo study was performed in 6 sheeps in an 8 mm drill hole defect model (8 defects per animal). Each defect received either (i) 100 mg unloaded microspheres or (ii) 100 mg MS loaded with 100 µg IGF I (IGF I-MS) or (iii) were left unfilled (negative control). Three animals were sacrificed after 3 weeks and another three 6 weeks post operation. The bones were cut, and slices prepared for histology (acrylic resin embedding, grinding and thin sections were stained with toluidine blue/von Kossa) and for RNA extraction[3]. Upon reverse transcription, the gene expression of pro- and inflammatory proteins (interleukins 1α and 6, cyclooxygenase 2), inducible NO synthetase, and morphogeneic factors (platelet derived growth factor A, transforming growth factor β 1, fibroblast growth factor, IGF I) was analysed by real-time polymerase chain reaction.

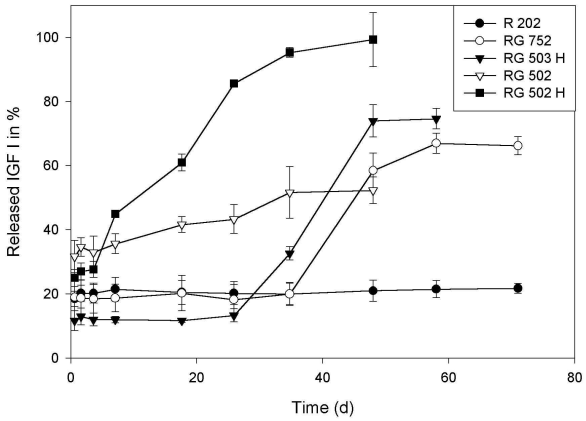

Fig. 1: In vitro release of IGF I from different microsphere formulations.

RESULTS: IGF I in vitro release was monitored over 72 days (Fig. 1).

Three weeks postoperatively, all IGF I treated defects showed consistent new bone formation adjacent to the defect borders. In case of defects treated with IGF I encapsulated in faster degrading PLGA 502H an increased density of granulation tissue and capillaries was observed in the interior defect. Hypertrophic osteoblasts lined the bone surfaces, actively depositing osteoid. In all IGF I treated defects the inflammatory infiltrate characteristic for early reparative changes of fracture healing was highly reduced and foreign body cells were rarely found.

Defects treated with unloaded microspheres showed a fatty in-growth, some granulation tissue formation and an increased inflammatory reaction. This inflammation was more pronounced in defects treated with faster degrading microspheres. On a genome level this finding is corroborated by a reduced expression of inflammatory genes in IGF I treated defects. Little numbers of osteoblasts lining bone surfaces laid down significantly less osteoid compared to IGF I treated defects.

After six weeks, all IGF I-MS treated defects showed a well-organized network of woven bone

within the defects and the pre-existing trabeculae were lined with hypertrophic osteoblasts that laid down thick layers of osteoid (except IGF I loaded PLGA 502 MS). Osteoblast number and matrix deposition rates were especially advanced in defects receiving slow degrading IGF I microspheres prepared with either PLGA 752 or PLA 202 (Fig. 2), respectively.

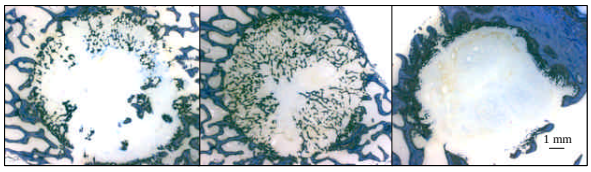

Fig. 2: Grinding sections of IGF I-MS loaded defects 6 weeks post operation (staining toluidine blue).

In defects treated with unloaded microspheres, osteoblasts were inactive depositing few osteoid. In some of these defects the bone ends were covered by fibrous and fibrocartilaginous tissue and showed signs of increased osteoclastic activity.

DISCUSSION & CONCLUSIONS: Controlled localized delivery of IGF I induces efficiently new bone formation. The degree of new bone formation largely depends on release kinetics. This new bone formation is due to an increased osteoblastic and a decreased osteoclastic activity upon IGF I delivery compared to control defects and those treated with unloaded MS. Presence of inflammatory cells is low in IGF I treated defects and this finding is corroborated by a reduced expression of inflammatory marker genes in IGF I-MS treated defects.

REFERENCES: [1] Meinel L, Auer JA , Schneider R, Illi OE, Merkle HP, Rechenberg B (2001) Complete bridging of critical-size bone defects in sheep following controlled localized delivery of insulin-like growth factor I. *submitted*. [2] Meinel L, Zapf J, Zoidis E, Auer JA, Illi OE, Gander B, Merkle HP, Rechenberg B (2001) Enhanced bridging of experimental bone defects in sheep by controlled localized delivery of insulin like growth factor I. *submitted*. [3] Chirgwin JM Przybyla AE MacDonald RJ Rutter WJ (1979) Isolation of biologically active ribonucleic acid from sources enriched in ribonuclease. *Biochemistry*, **18**, 5294-5299.

ACKNOWLEDGEMENTS: We are deeply indepted to Kati Zilinsky, Sabrina Wunderlin and Jessica Müller.

European Cells and Materials Vol. 3. Suppl. 1, 2002 (pages 5-6) ISSN 1473-2262

EARLY DURAL REACTION TO POLYLACTIDE IN CRANIAL DEFECTS OF RABBITS

A. A. Mueller[1], C. S. Leiggener[2], R. Curtis[3], B. Rahn[4]

[1,4]*AO Research Institute, Davos, CH,* [2]*University Hospital Basel, CH,* [3]*AO Development Institute, Davos , CH*

INTRODUCTION: Cranial through-and-through defects, exceeding a certain size do not heal spontaneously[1] and therefore frequently require surgical treatment. One approach uses the principle of guided tissue regeneration[2] by placing a mechanical barrier to preclude soft tissue ingrowth and thus to enhance the regeneration of new bone. The application of biodegradable instead of non-biodegradable material leads to various advantages e.g.: no second surgical procedure for membrane removal, no sequels due to permanent membrane retention, no growth restrictions, spontaneous disintegration in case of passive translocation during growth. These advantages are very useful in cranial surgery, particularly in the growing skull.

Before application in the neurocranium and therefore in vicinity to neural tissue can be considered any hazards must be excluded. In the early stage of polymer degradation biological reaction depends on the material itself and on possible chemical residues from the processing, while in the later stage the biological reaction depends mainly on the degradation products and their molecular weight.

In this study we investigated the dural reaction during the early stage after implantation of polylactide implants into cranial defects in rabbits.

METHODS: We used two implant systems, which consisted of a burr hole cover, four fixation dowels, a perforated strip and an endocranial membrane. One series was manufactured from poly(L/DL-lactide) 70:30 the other was manufactured from poly(L/DL-lactide) 80:20. The membranes were all 0.3 mm thick.

The burr hole covers, endocranial membranes and perforated strips were manufactured by the melt extrusion process, followed by laser cutting. Fixation dowels were injection moulded. The molecular weight of the raw materials was approximately 600’000 Daltons. All implants were sterilised by 30 kGy gamma irradiation.

Implants were applied to the bone in a sandwich manner. The endocranial membrane was placed at the inner surface of the neurocranium in direct contact to the dural tissue without mechanical fixation. The perforated polylactide strip of 3 x 15 mm was then formed in a “z” shape and placed perpendicular to the inner membrane to maintain the bone thickness of approximately 3 mm. The burr hole cover was then fixed onto the outer surface of the skull with four fixation dowels.

Twenty clinically healthy adult female New Zealand rabbits were used in this study. Sixteen underwent surgery and four served as controls. Two 8.3 mm diameter full thickness cranial defects were made, one in each parietal bone, and not touching any cranial sutures. Implants from poly(L/DL-lactide) 70:30 were applied to the first defect and implants from poly(L/DL-lactide) 80:20 were applied to the second defect. The side distribution was randomly assigned in each rabbit.

The animals were sacrificed eight weeks postoperatively. The undecalcified specimens were plastic embedded and sectioned in a coronal direction for contact radiographs, Giemsa/Eosin staining and microradiographs. The light-microscopic evaluation focused on the endocranial polylactide membrane, the interface and the underlying dural tissue. The findings were compared to non-operated specimens and to specimens having only burr hole covers on the outer surface of the skull[3].

RESULTS: All 16 rabbits recovered with no neurological complications. Macroscopically there were no signs of inflammation and no implant was rejected. Microscopically all endocranial membranes prevented the intracranial tissues from herniation into the bony defect. 3 out of 32 membranes had an oblique position protruding into the osseous defect. The formerly transparent polylactide turned to a milky white color. The periphery of the membrane was still continuous with few signs of polymer degradation while the core of the membrane showed variable structural changes.

Along the membrane-dura interface only few giant cells were detected, equal in both types of poly(L/DL-lactide). They were more numerous on the membrane-dura interface than on the bone defect side. The dura had a smooth surface towards

the brain as well as towards the poly(L/DL-lactide) membrane.

In about 80% of all specimens a formation of osseous islets within the dura was detected, equal in both types of poly(L/DL-lactide). The formation of the osseous islets was limited to the dura section along the poly(L/DL-lactide) and raised at any place in the dura. The thickness was variable up to 1 mm while the cranial bone thickness was about 3 mm.

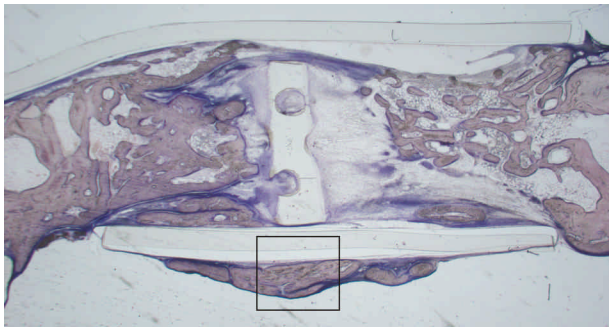

Fig. 1: Osseous islets formation within the dura 8 weeks after insertion of a polylactide disk into a full thickness cranial defect in a rabbit.

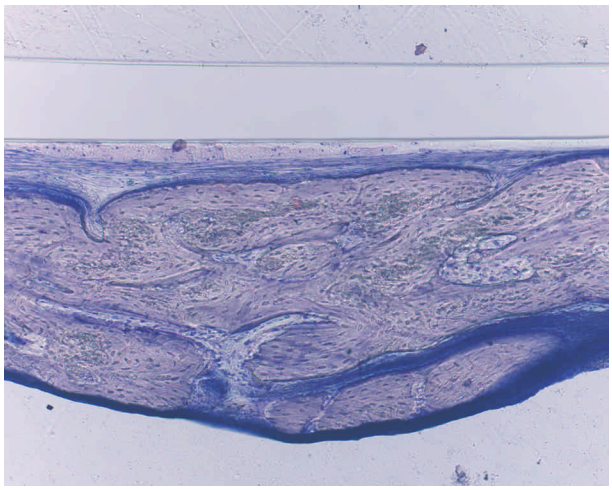

Fig. 2: Details of the osseous islet. The bone is completely lined with connective tissue.

The osseous islets were always limited by a thin dural layer and never stayed in direct contact neither to the poly(L/DL-lactide) membrane nor to the underlying neural tissue. No signs of acute inflammation and no granulation tissue were seen.

The non-operated control specimens showed a normal dura consisting only of dense connective tissue. The specimens having only burr hole covers on the outer surface of the skull showed regular bone formation from the dura towards the defect areas. These bone formations mixed and merged with islets of proper bone regeneration originating from the burr hole edges.

DISCUSSION & CONCLUSIONS: During the observed time the biodegradable poly(L/DL-lactide) membranes were well tolerated by the neurocranium. The dura showed neither acute inflammation nor marked connective tissue reaction. No differences between the two types of poly(L/DL-lactide) were detected. The ectopic osseous formation within the dura shows the osteogenic potential of the dura. This dural bone formation takes place regardless of dura being in direct contact to the regenerating tissue or being separated from the defect by a polylactide membrane. The dural bone formation showed no adverse effect during the observed time, as the amount of bone formation was limited. The biocompatibility of both types of polylactide was good during the observed early stage of biodegradation disclosing no adverse processing residues.

A long-term study would be necessary to investigate first the biocompatibility during the later stage of biodegradation. Second this would demonstrate whether the dural bone islets merge with the cranial bone or not after complete degradation of the endocranial membrane. A persistence of larger zones of dural calcification would be undesired especially in the growing skull of young patients.

REFERENCES: [1] J. P. Schmitz (1986) *The Critical Size Defect as an Experimental Model for Craniomandibulofacial Nonunions*. Clin Orthop (205):299-308. [2] S. Nyman (1982) *The Regenerative Potential of the Periodontal Ligament. An Experimental Study in the Monkey*. J Clin Periodontol 9(3):257-65. [3] C. S. Leiggener (2002) *Effect of Perforations in Burr Hole Covers on Cranial Bone Regeneration in Rabbits.* J Biomed Mater Res (in press).

ACKNOWLEDGEMENTS: Financial support for this work was obtained from the Margarete und Walther Lichtenstein Stiftung, Basel, Switzerland.

European Cells and Materials Vol. 3. Suppl. 1, 2002 (pages 7-8) ISSN 1473-2262

SURFACE MODIFICATION OF POLY(VINYL CHLORIDE) INTUBATION TUBES TO CONTROL BACTERIAL ADHESION : TEFLON-LIKE AND PLURONICS®

D.J. Balazs[1], C. Hollenstein[2] & H.J. Mathieu[1]

[1] *Materials Institute, Swiss Federal Institute of Technology, Lausanne, CH,*
[2] *Plasma Physics Research Center, Swiss Federal Institute of Technology, Lausanne, CH*

INTRODUCTION: *Pseudomonas aeruginosa* is one of the most prevalent bacterial strains in a clinical environment, responsible for 30% of nosocomial pneumonia cases occurring in intubated and mechanically ventilated patients [1]. Colonization of the intubation device leads to mortality for over 40% of these cases, despite aggressive antibiotic therapy. Therefore, a strategy to reduce bacterial adhesion to intubation tubes is desirable. We are developing an approach based on the surface modification of the polymer used for this application, medical grade poly(vinyl chloride) (PVC). This paper investigates a method to prevent protein adsorption and eventual bacterial adhesion, as protein adhesion is believed to be a key event responsible for specific adhesion of bacteria to a surface.

The strategy is to mask the PVC substrate with a chemically inert Teflon-like fluoropolymer layer, which serves as an ideal platform for further surface modification due to its low surface energy properties[2]. By exploiting hydrophobic-hydrophobic interactions, we then bind protein and bacterial resistant[3,4] molecules, such as amphiphilic Pluronics®, to the fluoropolymer film.

METHODS:

This paper investigates fluoropolymer films created on PVC substrates through plasma-enhanced chemical vapor deposition. The films are deposited in a RF-plasma reactor, using C_2F_6 as a precursor and H_2 as a carrier gas. The PVC substrates were 1cm^2 sections cut from Mallinckrodt Medical Hi-Lo endotracheal tubes, which were flattened to allow the eventual microscopic counting of bacteria.

Further surface modification of the Teflon-like surfaces is completed through an incubation in Pluronic® (BASF) F108, a tri-block copolymer containing hydrophilic PEO and hydrophobic PPO chains.

Protein adhesion to the various surfaces is studied by incubating the samples in bovine serum albumin and fibrinogen, for a period of 3 h, at 37°C. The concentrations of albumin and firinogen used were 1 mg/ml, and 0.2 mg/ml, respectively.

XPS analysis of the various surfaces is performed using an imaging Kratos Axis Ultra (UK) X-ray photoelectron spectrometer equipped with a hemispherical analyser. The X-ray source employed is a monochromatized Al *Kα*.

Surface wettability is determined by contact angle measurements of deionized water sessile drops, using a microscope equipped with a goniometer (Krüss GmbH, Hamburg, Germany).

RESULTS: Teflon-like deposition on PVC yields a 21° increase in contact angle to a value of 104° for an 80% flow of C_2F_6 (*Fig. 1*). When C_2F_6 percentage is varied from 20% up to 80%, the contact angle increase is shown to be directly related to the quantity of CF_x groups incorporated in the film (data not shown), where 80% C_2F_6 shows the highest amount of fluorinated groups.

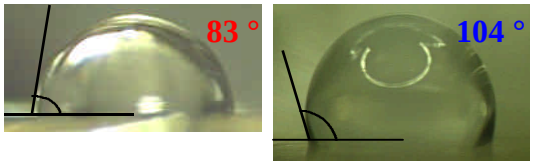

Fig. 1:Effect of Teflon-like deposition on surface wettability: native (left) and Teflon-like (right).

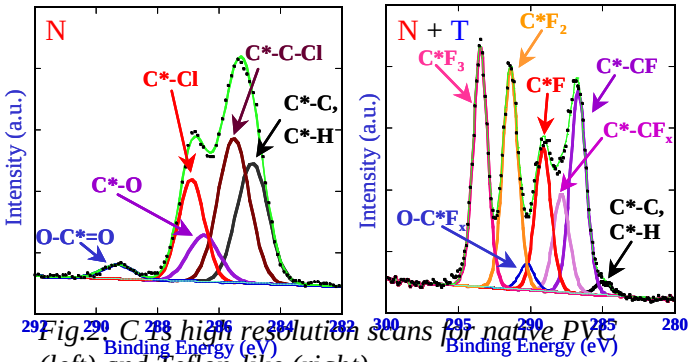

Fig.2: C 1s high resolution scans for native PVC (left) and Teflon-like (right).

The C 1s high resolution scans of the Teflon-like films show that the native PVC is completely masked as there are no signatures, such as C-Cl, remaining (*Fig. 2*). Moreover, there is significant fluorocarbon group incorporation, including C-CF_x, C-F, C-F_2, C-F_3, which are all indicative of a Teflon-like layer. Pluronic® F108 does not adsorb to untreated native PVC. There is no change in contact angle for the native PVC following incubation with the F108 (Fig.3). Pluronic® F108 adsorption is achieved following Teflon-like

deposition on native PVC. Contact angle measurements confirm this as the contact angle of Teflon-like decreases by 14° following the F108 incubation (Fig.3). The O 1s high resolution scan of F108 incubates samples shows the incorporation of O-C groups, which are not present prior to incubation (data not shown).

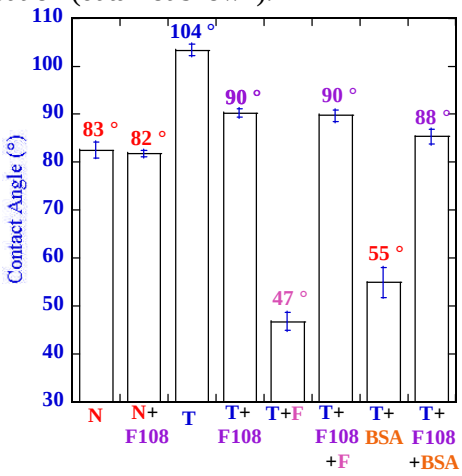

Fig.3: Contact angle evolution for native, Teflon-like and F108 modified samples. The graph also illustrates the evaluation of protein adhesion.

Pluronic® F108 incubation prevents fibrinogen adsorption to Teflon-like coated Native PVC. The T + F108 + Fibrinogen contact angle is identical to T + F108 (Fig.3), and nitrogenated functional groups representative of fibrinogen adsorption are absent on the O 1s high resolution scan following F108 modification. Pluronic® F108 also prevents albumin adsorption, as the contact angle follows the same trend as fibrinogen (Fig.3).

DISCUSSION & CONCLUSIONS: Teflon-like deposition on native PVC yields, a reproducible, hydrophobic surface modification, which serves as an excellent platform for further surface modification with Pluronic® F108. As shown by XPS analysis, the fluoropolymer completely masks the native surface, as no signatures of PVC are detectable following deposition. Contact angle measurements of the Teflon-like surfaces show that the PE-CVD techniques used yield a highly hydrophobic film (104°), where the contact angle achieved directly depends on the feed of C_2F_6 used during the deposition. Higher feeds of C_2F_6 allow for a greater incorporation of hydrophobic fluorocarbon groups in the film.

Pluronic® F108 does not adsorb to untreated native PVC, because the hydrophobic interactions are not strong enough to attract and bind the molecule. Pluronic® adsorption to PVC is only achieved following deposition of a Teflon-like film. XPS analysis shows evidence of F108 adsorption to Teflon-like surfaces through the detection of O-C functional groups, which are not present following incubation of the molecule with native PVC. The reason for the adsorption to the Teflon-like film is the increased hydrophobicity, a 21° increase compared to native PVC surfaces. Contact angle measurements confirm the XPS data. Following Pluronic® F108 incubation with the Teflon-like samples there is a 14° decrease in contact angle, which indicates a surface modification. Following incubation with native PVC substrates, the contact angle remains unchanged.

Pluronic® F108 incubation is capable of preventing albumin and fibrinogen adsorption to Teflon-like coated PVC. Following incubation of fibrinogen and albumin to Teflon-like surfaces the contact angle drops from 104° to 47° and 55°, respectively. This decrease in contact angle indicates adsorption of proteins to the Teflon-like surface. This hypothesis is confirmed by XPS analysis, which detects nitrogenated functional groups characteristic of protein adsorption, such as O=C-N. However, following F108 modification of the Teflon-like surfaces, XPS analysis does not detect the functional groups indicative of protein adsorption. The O 1s high resolution spectra for the F108 modified samples which had been incubated in the protein solutions is identical to that of the F108 modified samples. Moreover, the contact angle of F108 modified surfaces following protein incubation, remains unchanged demonstrating the anti-fouling properties of the Pluronic® F108 molecules.

In conclusion, data from XPS analysis and contact angle measurements confirms that Pluronic® F108 modification of Teflon-like films is capable of producing surfaces resistant to protein adhesion. As protein adhesion is believed to be the triggering event in the inflammatory response and eventual failure of biomaterials, this method could prove to be useful in creating anti-fouling surfaces.

REFERENCES: [1] J. L. Vincent, D. J. Bihari, P. M. Suter et al (1995) *JAMA* **274**: 639-644. [2] I. Noh, K. Chittur, S. Goodman, J. Hubbell (1997) *J Polym Sci Poly Chem* **35**: 1499-1514. [3] M. J. Bridgett, M.C. Davies, S. P. Denyer (1992) *Biomaterials* **13**: 411-416. [4] M. Paulsson, M. Kober, C. Freij-Larsson et al (1993) *Biomaterials* **14**: 845-853.

ACKNOWLEDGEMENTS: We acknowledge financial support of Common Program on Bio-medical Engineering and Research, Univ.of Geneva and EPFL, (1999-2002).

European Cells and Materials Vol. 3. Suppl. 1, 2002 (pages 9-10) ISSN 1473-2262

ELECTRON MICROSCOPY ON TITANIUM IMPLANTS FOR BONE REPLACEMENT AFTER "SLA" SURFACE TREATMENT

E. Conforto[1], D. Caillard[2], B-O. Aronsson[3]& P. Descouts[3]

[1]*Swiss Federal Institute of Technology, Lausanne, CH,* [2]*CEMES/CNRS, Toulouse, FR,*
[3]*GAP Biomedical, University of Geneva, CH*

INTRODUCTION: Because the chemical interaction between the implant and the biological tissue is too weak to account for the fixation, the implant stability depends on good mechanical interlocking. The interest for the influence of surface roughness on biological interactions has recently increased as well as that for bone-anchored implants. Titanium is a very good material for this kind of implant due to its biocompatibility.

The SLA ("Sand-blasting and acid etching") surface treatment on Ti implants has as goal to control the surface roughness, to improve osseointegration and to increase the stability of bone-anchored dental implants. This treatment consists of bombarding the surface with a jet of Al_2O_3 particles followed by an acid etching. From this treatment results a two-level roughness: sub-micron porosity, caused by the acid etching, superimposed to the 30-200 µm roughness, due to the bombardment.

Previous works[1] highlighted the presence of hydrogen in the sub-surface layer after acid etching. Authors have formulated the hypothesis of the formation of another phase, a titanium hydride. The aim of this work is to identify this layer highlighting the crystallographic relationships with the substrate. The layer adherence will be evaluated as well as its mechanical properties.

METHODS: Commercially pure titanium disks were submitted to the SLA surface treatment after polishing. Samples were provided by Institut Straumann AG, Waldenburg, CH. Surface observations after SLA treatment were performed by scanning electron microscopy (Philips XL-30, 10 kV). Crystallographic relationships between the surface layer and the substrate as well as dislocations in the layer were observed in cross-sectional specimens by transmission electron microscopy (Philips EM-430, 300 KV). Specimens were prepared by mechanical polishing followed by ion bombardment. Observation techniques were: Bright and Dark Field images and Electron Diffraction.

RESULTS: SEM observations clearly show the desired porosity (Fig. 1) after SLA treatment on Ti surface. TEM cross-sectional observations confirmed the expected surface profile and also revealed the existence of an interface between the α-Ti substrate, with a hexagonal structure, and tips formed during the acid etching (Fig. 2, top). No other layers, either interfacial or superficial, were detected. In all cases examined these tips are constituted of one or several grains of an FCC phase identified as $TiH_{1.971}$.

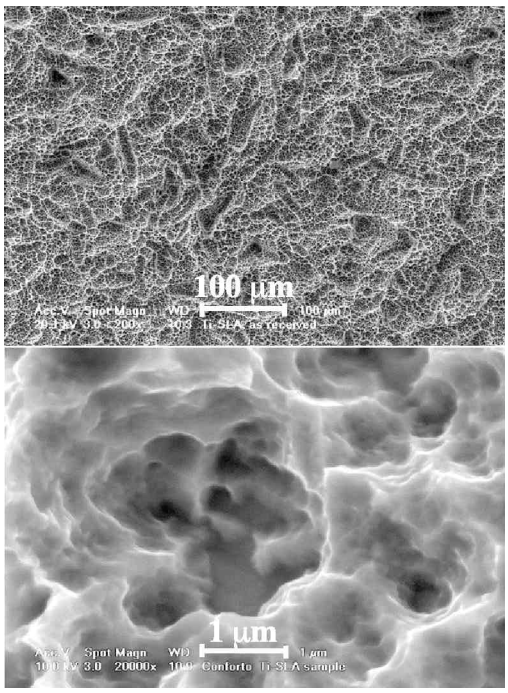

Fig. 1: Ti surface after SLA treatment: general view showing the 30 µm roughness (left); detail, showing micro-porosities (right).

These grains can be of round or column-shape and show, in all samples examined, a crystallographic orientation relationship at the interface with α-Ti grains that have, in average, several tens microns in size. Differences between the two types of hydride grains are not only in shape, but also in the parallelism of their orientation and that of the Ti. Fig. 2 shows the interface between columnar $TiH_{1.971}$ grains and the adjacent Ti, in Bright (Fig. 2, middle) and Dark Field (Fig. 2, bottom) views. The latter was obtained with the diffraction of (311) family of atomic planes of the FCC structure. These grains

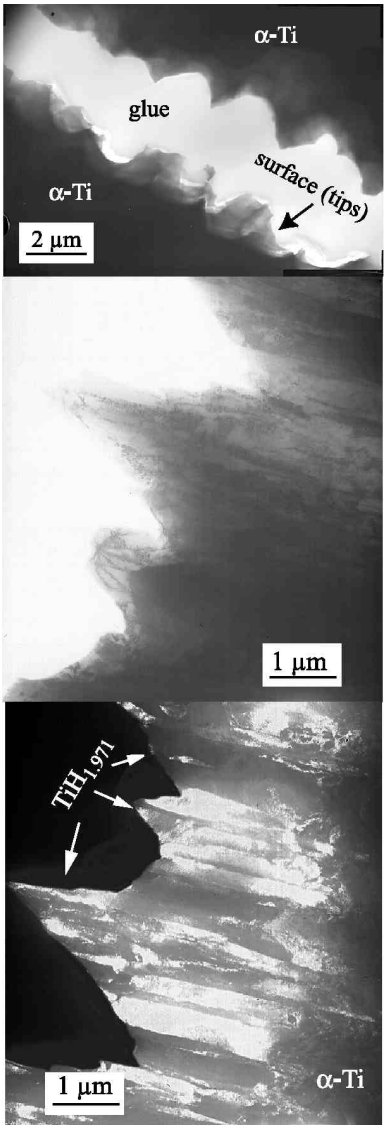

Fig. 2: Cross-sectional TEM observations of the $TiH_{1.971}$/α-Ti interface: low magnification bright field image of the profile (top); Detail, showing $TiH_{1.971}$ FCC columnar grains (middle); Dark Field image of the same region, obtained with the diffraction of (3-11) planes (bottom).

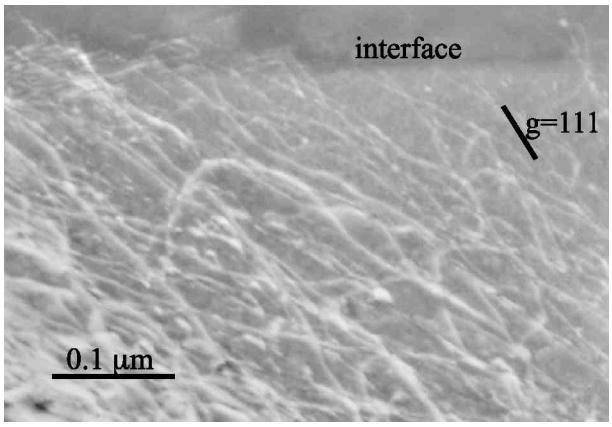

Fig. 3 - Dislocations in a $TiH_{1.971}$ grain close to the interface with the Ti substrate.

extend from the interface up to the surface and belong to one (311) family among three equivalent ones that exhibit an epitaxial relationship with the Ti substrate. These three families can exist simultaneously due to the six-fold symmetry of the adjacent Ti grain in the substrate, in [0001] orientation.

Fig. 3 shows high density of dislocations in the hydride layer forming a three-dimensional network. Using the classical extinction rules, their Burgers vectors are found to be of the 1/2<110> type, as in FCC metals and alloys.

DISCUSSION & CONCLUSIONS: The formation of the hydride layer directly on the Ti substrate, without any interfacial layer, as observed even in very high magnification images, suggests that the acid etching reduced the superficial native titanium oxide layer. Moreover, the crystallographic relationship between the two structures is an evidence that the hydride layer grows epitaxially to the immediate neighbor grain in the substrate. The crystallographic coherence between the two phases at the interface guarantees the best possible adherence of the hydride layer to the Ti substrate.

The dislocation arrangement observed in Fig.3 is typical of a fairly ductile but highly plastically deformed material, which denotes a substantial strain accommodation during the elaboration process. Our observations are in good agreement with previous studies[2] demonstrating the plastic deformation of TiH_x (x = 1.58 – 1.99). According to the Hall-Petch law, good mechanical properties can be expected a priori, since the hydride layer is formed by slightly misoriented subgrains smaller in size than the roughness.

REFERENCES: [1] Aronsson B-O, Hjörvarsson B, Frauchiger L, Taborelli M, Valloton P-H, and Descouts P (2001) Hydrogen desorption from sand-blasted and acid-etched titanium surfaces after glow-discharge treatment. *J. Biomed. Mater. Res.* **54**(1), 20-29. [2] Irving PE, and Beevers CJ (1972) Some observations on the deformation characteristics of titanium hydrides. *J. Mater. Sci.* **7**, 23-30.

ACKNOWLEDGEMENTS: This research was supported by Swiss National Science Foundation that is gratefully acknowledged.

European Cells and Materials Vol. 3. Suppl. 1, 2002 (pages 11-12) ISSN 1473-2262

INVESTIGATION OF FERROFLUIDS FOR BIOMEDICAL APPLICATIONS

M. Chastellain[1], A. Petri[1], M. Hofmann and H. Hofmann[1]

[1]*Powder Technology Laboratory, DMX, EPFL, Lausanne, Switzerland;* [2]*Laboratoire de Photonique et Interfaces (SB/ICMB/LPI) EPFL.*

INTRODUCTION: The recent development of a large variety of ferrofluids has led to a range of new biomedical and diagnostic applications. A major drawback for a lot of applications remains the lack of well-defined and well characterized particles.
Growing attention is paid to iron oxide nanoparticles embedded in a polymer matrix. The matrix fulfills several demands: on the one hand it acts as a stabilizer, or even controls the particle formation, on the other hand it determines the physicochemical properties of the material, or allows surface functionalization.
In this study magnetic nanoparticles were prepared either in the presence of polyvinylic alcohol or were redispersed after precipitation and isolation of iron oxide powder. Aqueous suspensions of magnetic particles were obtained under identical reaction conditions by coprecipitation of Iron(III)- and Iron(II)-salts using aqueous ammonia. The suspensions were finally dialyzed against distilled water to approximately pH 6.5.

METHODS: For a better understanding of the colloidal and magnetic properties, an extensive characterization of the ferrofluids must be carried out. Four major points are discussed in this work: composition, size distribution, magnetic properties, and first tests with human endothelial and synovial cells.

Composition: The iron oxide particles were analyzed with and without coating using XRD as well as FTIR. High resolution TEM measurements were also carried out to obtain qualitative information about the presence of an amorphous phase.

Size distribution: Different techniques were applied in order to obtain information about the iron oxide particle size distribution. Among these are: X-ray diffraction peak broadening, TEM picture analysis, magnetic characterization techniques, photon correlation spectroscopy, or analytical ultracentrifugation. Although the obtained results are not always comparable, valuable information is provided by their interconnection.

Cell survival tests: In collaboration with the Tierspital Zuerich (Musculoskeletal Research Unit) first tests with human endothelial cells and synovial cells have been carried out. The cell survival after different time periods has been

compared for different concentrations as well as different methods of synthesis.

RESULTS: The main characterization results are summarized in the following.

Composition: XRD patterns show a large amorphous zone as well as typical peaks, which can be attributed to nanocrystalline magnetite (Fe_3O_4) or maghemite (γ-Fe_2O_3). After close examination the presence of two distinct phases was excluded and the composition is thought to consist of a defect magnetite structure with a lattice parameter in between the one of bulk magnetite and bulk maghemite. FTIR investigations yield the same results.

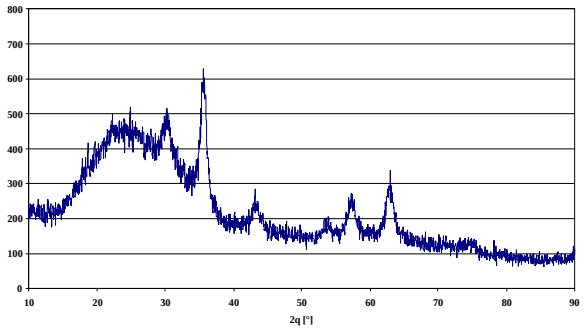

Fig. 1: XRD pattern of uncoated iron oxide nanoparicles showing a wide amorphous zone and typical inverse spinel peaks.

Size distribution: Typical monomodal distributions were found with an average size slightly smaller than 10nm.

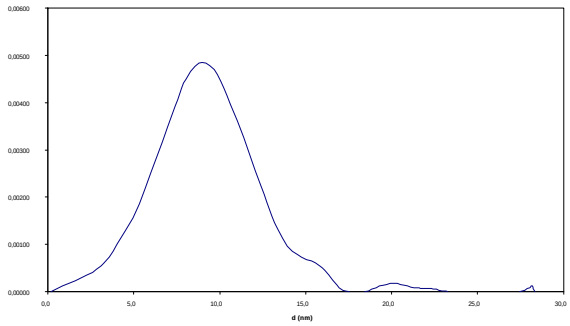

Fig. 2: AUC size distribution of bare iron oxide

The differences in size distribution determined by various methods show the necessity of combined size characterization for particles of that size. The comparison of the results also gives qualitative information about other properties such as the density or the refractive index. In particular the spherical assumption for the particles shape proved to be satisfactory.

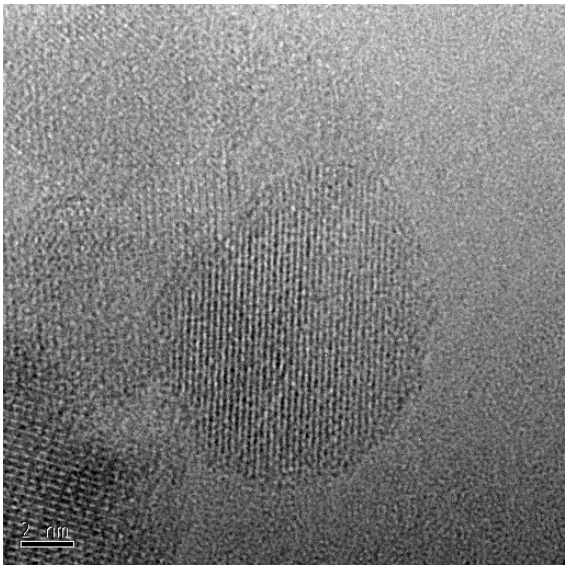

Fig. 3: High resolution TEM picture showing crystalline iron oxide particles.

Cell survival tests: It could be shown that the concentration the polymer as well as the ammonia concentration plays a very important role in the cell survival tests. As a first result it can be concluded that a minimum concentration of ammonia and polymer is essential for cell survival.

CONCLUSION: Ferrofluids were synthesized using PVA to ensure a colloidal stability at neutral pH. The composition, structure and size distribution characterization of iron oxide particles was carried out, showing the influence of the synthesis parameters. After the first tests, the obtained ferrofluids seem to be non-toxic to human endothelial as well as synovial cells.

ACKNOWLEDGMENTS: This project is supported by EU - under the project NANOMAG - Magnetic Nanoparticles for Medical and Biological Diagnostics and Devices.

WORKING CHARACTERISTICS OF RADIO-OPACIFIED BRUSHITE CEMENTS

C. Pittet, J. Lemaître

Laboratoire de Technologie des Poudres, EPFL, MX-Ecublens, 1015-Lausanne

INTRODUCTION: X-Ray opacification of calcium phosphate hydraulic cements (CPHC) is a pre-requisite prior to use them safely in image-guided vertebroplasty. Theoretical calculations (1) have shown that injectable CPHC presently available on the market exhibit linear attenuation coefficients below 1.6 cm^{-1}, whereas the recommended value should be close to 2.5 cm^{-1} in order to achieve enough contrast between the injected cement and the surrounding tissues (2).

According to theoretical calculations, injectable CHPC of the Brushite family – i.e. based on mixtures of $Ca(H_2PO_4)_2•H_2O$ (MCPM) and β-$Ca_3(PO_4)_2$ (β-TCP) transformed into $CaHPO_4•2H_2O$ (Brushite, DCPD) upon consolidation – can be obtained with the requested radio-opacity by incorporating about 100 mg iodine per mL of freshly mixed cement.

This work investigates the effects of different iodine sources on the working characteristics of an injectable Brushite cement formulation containing plaster of Paris (CSH, $CaSO_4•2.H_2O$) as a setting regulator.

METHODS: The Brushite cements were made of 1.201 g β-TCP, 0.781 g MCPM, 0.339 g CSH and mixed with 1.080 mL of distilled water ; 0.09 g of di-sodium di-hydrogen pyrophosphate (NHPP) (Fluka) was added to the mixture in order to adjust the setting time at approximately 20 min.

Four different iodine compounds were tested : NaI, $NaIO_3$ (Merck, pro analysis) Iopentol® (Imagopaque from Nycomed Imaging AS) and Iopamidol® (Iopamiro from Bracco SpA). The two latter compounds are tri-iodinated benzoic molecules commonly used for angiographic diagnosis. In all cases, theamount of iodine-containing substance represented 100 mg of iodine per mL of fresh cement, so as to achieve a theoretical linear attenuation coefficient of 2.47 cm^{-1}. The radio-opacifiers were incorporated by dissolution in the mixing water ; given the low aqueous solubility of $NaIO_3$, only partial dissolution of the additive was achieved. The other ingredients were added in the following order : NHPP, MCPM, CSH, β-TCP ; thorough mixing was effected after each addition. A iodine-free cement was used as control.

The setting times of the cements were measured with the Vicat needle technique (neddle ø = 2 mm, weight 98.4 g). Their mechanial properties were tested on wet cylindrical specimens aged for 24 h at 37 °C and 100 % relative humidity in the uniaxial (ø x h. = 8.7 x 18 mm) and diametral (ø x h = 8.7 x 6 mm) compression modes at a loading rate of 0.3 mm/min ; each composition was tested 4 times.

RESULTS AND DISCUSSION:

Setting times. No significant differences were found between the iodine-containing cements and the control (ST = 24 ± 1 min).

Mechanical properties. The results are summarised in Fig. 1. In diametral compressive strength, cements containing NaI, Iopentol® and Iopamidol® perform better compared to the control and the $NaIO_3$–containing cements In uniaxial compressive strength, Iopentol®–containing cements are significantly better than those containing Iopamidol®, the latter performing the same as the control ; $NaIO_3$ and NaI–loaded cements are worse than the control.

CONCLUSIONS: Brushite cements can be opacified with various iodine–containing additives : NaI, $NaIO_3$ Iopentol® and Iopamidol®. None of these additives affects significantly the setting times of the cements. In general, they do not affect to a large extent the mechanical performances of the consolidated cements, even though NaI appears to improve significantly the diametral compressive strength (3.1 *vs* 2.1 ± 0.8 MPa), immediately followed by Iopentol® ; the latter also improves significantly the uniaxial compressive strength (14.5 *vs* 10.5 ± 2.5 MPa). Thus, from the viewpoint of the working properties, Iopentol® appears to be the first–choice radio-opacifying additive.

REFERENCES:

1 C. Pittet "Development and Characterisation of Injectable Calcium Phosphate Cements for Use in Vertebroplasty." Thesis n° 2509, EPFL, 2001.

2 Deramond H., Wright N.T., Belkoff S.M. Bone 1999, 2 17S-21S.

ACKNOWLEDGEMENTS: This work has been granted by the Foundation of the "Hôpital Orthopédique de la Suisse Romande". Dr A. Uske

(Service de Radiologie, CHUV) is ackowledged for his help in collecting the radio-opacity data.

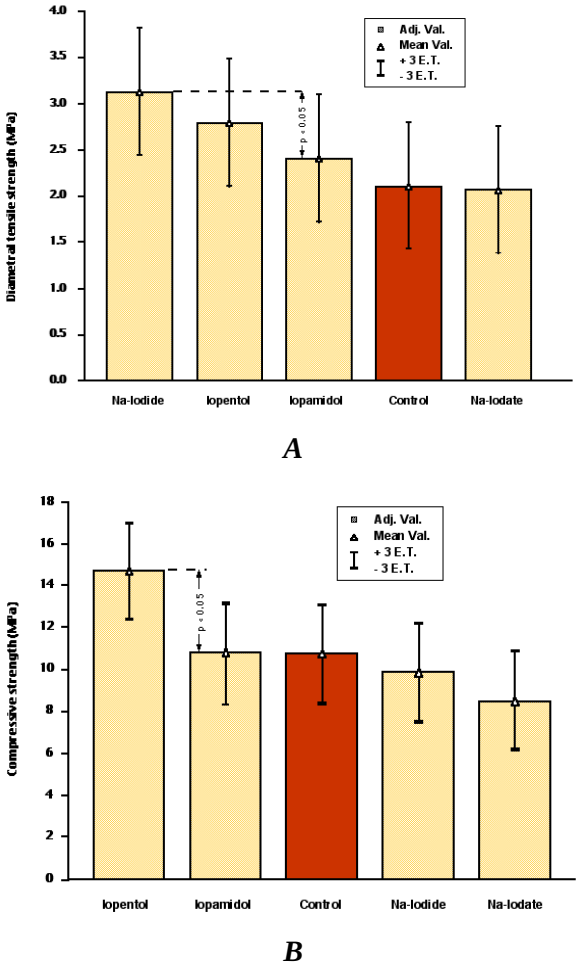

Fig. 1: Mechanical properties of radio-opacified Brushite cements. A) Diametral compressive strength ; B) Uniaxial compressive strength.

THE IMMEDIATE TISSUE REACTION TO A BIORESORBABLE BRUSHITE CEMENT IN EXPERIMENTAL METAPHYSEAL DEFECTS IN SHEEP

F. Theiss[1], D. Apelt[1], M. Bohner[2], Ch. Frei[3], K. Zlinsky[1], J. A. Auer[1], B. von Rechenberg[1]

[1]MSRU, Dept. of Veterinary Surgery, University of Zurich, Winterthurerstr. 260, CH-8057 Zürich, [2]RMS Foundation, Bischmattstrasse 12, CH-2544 Bettlach, [3]STRATEC Medical, Eimattstrasse 3, CH-4436 Oberdorf

INTRODUCTION: Resorbable cements as synthetic bone replacement have been introduced into orthopedic surgery for various applications, such as bone defect filling, augmentation and reinforcement in combination with autogenous grafts. Among those, brushite cements ($CaHPO_4 \cdot 2H_2O$) showed good resorbability and solubility. If applied as a biphasic cement in combination with large granules of β-tricalcium phosphate (β-TCP; β-$Ca_3(PO_4)_2$) <0.5mm in diameter), they proved to be resorbed and replaced with new bone within 4-6 months in a drill hole model in long bone metaphyseal and epiphyseal application in sheep. Although, their biocompatibility was considered optimal at 2, 4 and 6 months, the immediate reaction of the tissue to the biphasic cement was unknown. In this study, the immediate reaction of a brushite biphasic liquid cement (ChronOs Inject) was studied.

METHODS: Eight (8) adult, Swiss Alpine sheep served as experimental animals and were divided in fours groups with 2 animals each. An osteotomy in the proximal tibia was performed, where a rectangular bone wedge of 0.7cm height was removed at the cranial aspect of the tibia plateau. The osteotomy extended ca.60% (2.4 cm) caudally into the tibia shaft and was made according to a standardized template. The defects were stabilized using a 3.5 mm T-plate and 7 x 3.5 mm screws and they were filled with the cements. The hind limbs were operated alternately and additional immobilization of the limbs was provided with splint bandages. A suspension system was used for 4 weeks to protect the animals from refracturing their limbs. The study period until sacrifice of animals was 2,4,6 and 8 weeks. After sacrifice, the bone samples were immediately harvested, macroscopically assessed and processed for histology. Non-decalcified bone specimens were embedded in acrylic resin (HistoDur®). Ground sections (30-40µm) and thin (5µm) were prepared, and stained with either toluidine blue or von Kossa/McNeal.

RESULTS: All cement samples were well integrated at the time of sacrifice, and were easily visible from outside of the bone. Histologic evaluation was performed focusing on cellular reactions and ways of cement degradation. Both cortices of the tibia defects were not remodeled yet at all time points. However, periosteal reactions and new bone formations had started at 6 weeks. A small resorption zone between the old bone matrix and the bulk of the cement was noticed (≈1-2 mm) mainly in the 2 weeks group. It gradually decreased over time. Resorption of the cement matrix (brushite) was quicker compared to the TCP granules. The gap within the resorption zone of the cement was filled with mesenchymal or osteoprogenitor cells and close to the old bone matrix active osteoblasts producing new osteoid were found at the bone surface already at 4 weeks. Small areas of new bone deposition were already noticed on the TCP granules in the 6 weeks group. Only in the 2 weeks group multinuclear foreign body cells were found. Macrophages digesting the cement particles were abundant after 4 weeks as well as actively osteoid synthesizing osteoblasts.

DISCUSSION & CONCLUSIONS: The biphasic resorbable brushite cement (ChronOs Inject) showed good biocompatibility also in short-term experiments. The immediate tissue reaction at short intervals revealed excellent tissue compatibility, such that no significant inflammatory reaction was present at 2,4, 6, and 8 weeks. Foreign body cells were seen only transiently at 2 weeks and were already completely replaced by cement digesting macrophages at 4 weeks. In any case, macrophages are normally involved in cellular debridement and are not considered to be inflammatory cells, at least in bone. The front of cement resorption and bone formation was parallel over time, although the resorption zone of the cement matrix was slightly larger initially at 2 weeks. In conclusion, the brushite cement as investigated in this study appears to be an excellent synthetic bone replacement also in short-term experiments.

ACKNOWLEDGEMENTS: Mathys Medical (Bettlach, Switzerland) and STRATEC Medical (Oberdorf, Switzerland) are thanked for their financial support.

European Cells and Materials Vol. 3. Suppl. 1, 2002 (pages 16-17) ISSN 1473-2262

IMPROVEMENT OF RELIABILITY OF CERAMIC HIP JOINTS

W.Weber[1], M.Zahner[2], W.Rieger[1]

[1] *Metoxit AG, , Thayngen, CH* [2] *EMPA, Dübendorf, CH*

INTRODUCTION:. Ceramic heads have been used for total hip joint replacements successfully for many years due to excellent biocompatibility, low friction and wear and high strength. The failure rate of the ceramic head is very low. However there is still a remaining minimal probability of fracture. This probability is a result of the fracture mechanical behavior of ceramic materials, which is characterized by the Weibull distribution. While metals have a narrow strength distribution, ceramics have a certain probability of low strength elements (figure1).

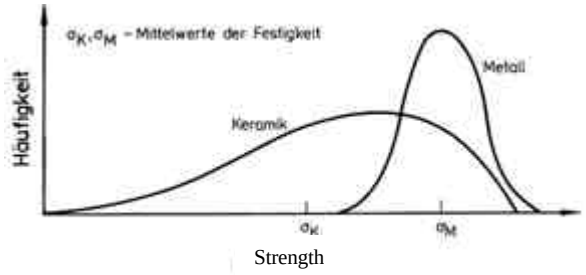

Fig. 1 Strength distribution of metals and ceramic

Therefor proof testing of ceramic hip joints heads has become an accepted method to improve reliability of ceramic hip joints: A static load is applied which is higher than the expected maximum physiological load. Ball heads with a lower strength will be eliminated.

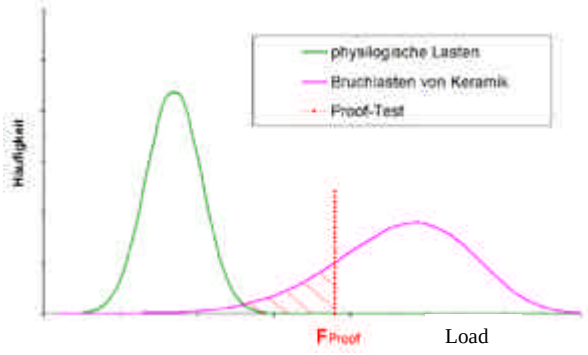

Fig. 2: Effect of proof testing on the strength distribution

While the destructive testing of ceramic heads is described in the standards[1] the way how to perform proof testing is not defined. It is obvious, that proof testing is only of value, if the stress is equivalent to that applied to the component in vivo. Otherwise, failures would not be detected or the test may lead to destruction of good products.

METHODS: The stress distribution in the ceramic head was calculated by finite element methods. The non linear calculation was validated and calibrated by experimental measurements. This was done by measuring the strains and calculating the stresses in dependence of the load by strain gauges. The measurements were carried out for the proof test as well as for the static fracture test according to ISO 7206-5[1] and an "in vivo near" model.

Strain measurement

For the strain measurement each ball head was provided with three strain gauges on the surface. The arrangement of the gauges on the head is shown in fig. 3.

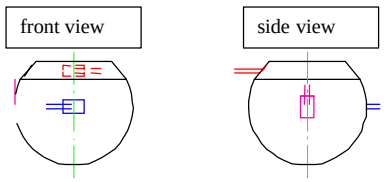

Fig. 3: Arrangement of the strain gauges on the ceramic heads (left side: radial in 38° and 0° position, right side in axial 0° position)

FEM Calculation

In a first step the contact definitions had to be validated by measuring the displacement of the conical shaft and the conical bore of the ceramic head (figure 4) under a definite load.

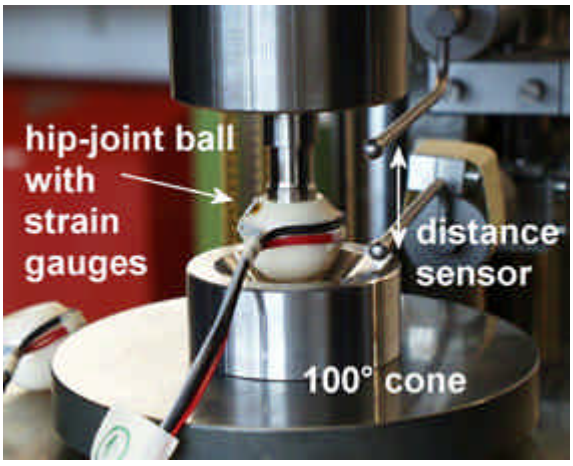

Fig. 4: Test set up for displacement measurement

For two types (cone length L and S) of alumina standard BIO-HIP® ball heads the FEM models for the three load cases were calculated and compared with each other: The static fracture test according to ISO 7206-5, a proof test with hydrostatic pressure inside the cone, and an in vivo near 3D-model.

RESULTS:

Static fracture test

After the calibration of the FEM model, a good agreement between the measured and calculated strains was found. A comparison chart is shown in fig. 5. The best fit was reached with a Youngs-Modulus of 380 MPa for alumina.

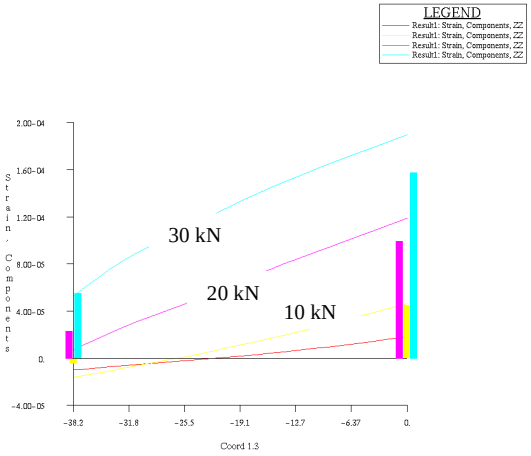

Fig. 5: Calculated (lines) and measured (bars) strains along the outer diameter from the 38° position to the equator for ball head S.

Proof test

The proof test was now designed in order to give a similar strain as in the load case against a 100 ° cone. Figure 6 shows the calculated result of an optimized proof test configuration.

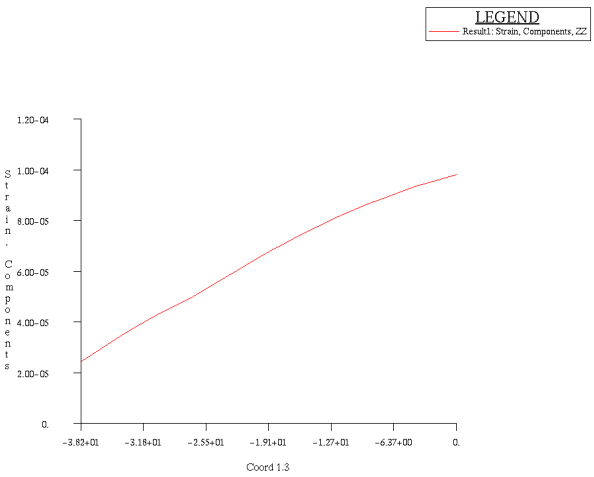

Fig. 6: Calculated strains along the outer diameter from the 38° position to the equator for ball head S.

DISCUSSION: As a result of the calibration of the FEM calculation and a comparison between the three load cases a reliable proof test could be developed. The FEM plots in figure 7 demonstrate good agreement in the stress distribution between the optimized proof test and the static fracture test.

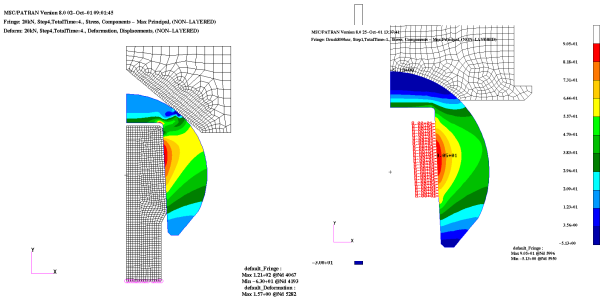

Fig. 7: Stress distribution in the ceramic head type S. Left: static fracture test, right: Optimized proof test.

In addition, for the head type L an “in vivo near” 3D-model with non axial load was also calculated.

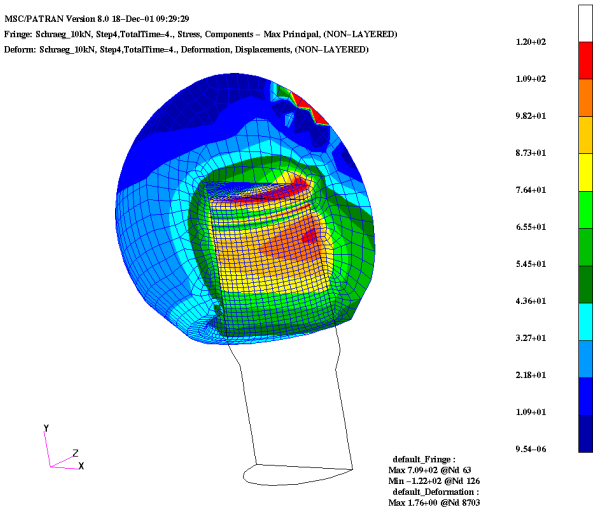

Fig. 8: 3D –model of stress distribution in the ceramic head type L with non axial load.

The influence of the asymmetric load can clearly be seen. However, no principal differences of the stress distribution compared to the axial load cases are found.

CONCLUSIONS: Proof testing of ceramic ball heads was adjusted by strain measurements under load and consecutive FEM calculation to obtain an optimized proof test geometry for increased product reliability.

REFERENCES: [1]ISO 7206-5 “Implants for surgery”

ACKNOWLEDGEMENTS: This study was financially supported by the swiss KTI (Commission for technology and innovation).

European Cells and Materials Vol. 3. Suppl. 1, 2002 (pages 18-19) ISSN 1473-2262

IN VITRO DEGRADATION OF PSEUDOWOLLASTONITE AND IN VITRO CYTOTOXICITY EVALUATION

D. Dufrane [1], M. Anseau [2], I. Mc Kay [3], P. de Asa [4], YJ. Schneider [5], C. Delloye [1].
[1]: Orthopaedic research laboratory: Université catholique de Louvain, Belgium; [2]: Université de Mons-Hainaut; [3]:St Bartholomew's and the Royal London School of Medicine and Dentistry, University of London, UK; [4]: Departamento de Ciencia y Tecnologia de Materiales; Universidad Miguel Hernandez, Spain; [5]: Cell Biochemical Laboratory: Université catholique de Louvain; Louvain-La-Neuve, Belgium.
Mail: denis.dufrane@clin.ucl.ac.be

INTRODUCTION: Bioactive materials including a chain silicate minerals as pseudowollastonite ($CaSiO_3$) (psW) have demonstrated the formation of hydroxyapatite-like layer on their surface both *in vivo* and *in vitro*[1,2,3]. This ceramic material appears to offer therapeutic potential in situation requiring bone augmentation or replacement[4,5]. In previous study, we have demonstrated that psW can released substances able to induce an impact on cellular viability with a kinetic reaction. Indeed, a decrease of cellular viability was observed in the early phase of psW degradation and a better cells viability in function of psW degradation time[6] (Fig.1). Our hypothesis is that the interaction between Silicate and Calcium, released by psW, can play an important role on cell metabolism. The aim of this work consists in the study of calcium and silicate effects on cellular viability.

METHODS: **Cytotoxic assays on silicate and calcium:** Human osteosarcoma cell lines (SaOS-2; ATCC: HTB-85) were incubated with medium [DMEM/HAM-F12 (50% v/v), 10% (v/v) fetal bovine serum, 100 u/ml penicillin, 100µg/ml streptomycin) supplemented with different concentrations of calcium (+ 50%, +100%, +150%) and silicate (sodium silicate solution; 1.6 and 6.25 mM). At 24 and 48 hours after incubation, cells were incubated for 30 min in DMEM/HAM-F12 (no serum) containing 8 µmole/L 2',7'-bis-carboxyethyl)-5- carboxyfluorescein acetoxymethylester (BCECF-AM, Molecular Probes), an esterified dye that, when internalized by living cells, is hydrolyzed by cellular esterases to a membrane-impermeable fluorescent species. The cells were then lyzed by incubation with 1% Triton X-100, and the released dye collected in the supernatant for quantification by spectrofluorimetry (485 nm excitation and 535 nm emission). **Silicon and calcium released of psW pellets:** PsW pellets were incubated in conditioning medium at different concentrations (10, 15, 50 and 100 mg/ml) during 1,2,3,7 and 9 days. Silicon and calcium released were performed by inductively coupled plasma atomic emission spectroscopy (ICP-AES).

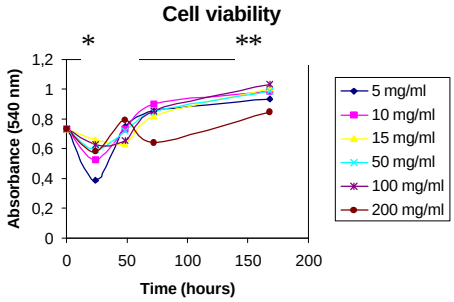

Fig. 1. Cell viability: Relative MTT formazan formation by SaOS-2 cells incubated, during 24 hours, with psW extracts (24, 48, 72, 168 hours of extraction) (n=8) (*: $p<0.005$; **: $p<0.05$).

RESULTS: No significant modification of cellular viability was observed for SaOS-2 cells incubated with medium supplemented with different concentrations of calcium (at 24 and 48 hours) (Fig.2). However, a significant decrease of cell viability was observed for cells exposed to silicate solutions (Fig.2,3). ICP-AES has confirmed that psW samples, incubated in medium, released at day 1 and day 2, a major quantity of silicon compared with sample incubated during 3,7 and 9 days.

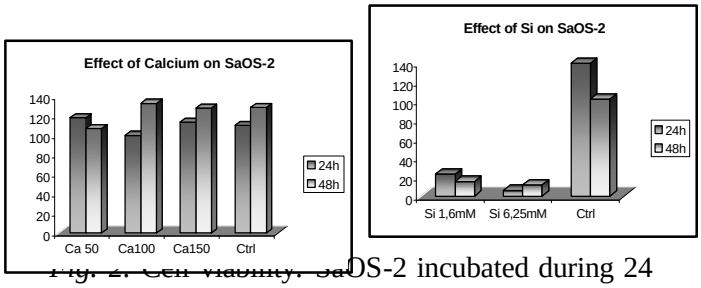

Fig. 2. Cell viability: SaOS-2 incubated during 24 and 48 hours with medium supplemented with calcium (left) and silicon (right).

DISCUSSION & CONCLUSIONS: No cytotoxic effect was demonstrated for psW. However, we

have observed few changes in cell viability or stress for cell exposed to psW extract in the early phase of extraction (24 hours). This phenomenon could be correlated with an increase of silicon released by psW which can initiate a cellular toxicity. Further studies will be necessary to obtain a better understanding of psW degradation which will be primordial to obtain a better interaction between cell and bioactive ceramic.

REFERENCES: [1] Siriphannon P et al (2000) *J Biomed Mater Res* **52**: 30-9.[2] De Aza PN et al (1999) *J Dent* **27**: 107-13.[3] Nishio K et al (2001) *J Biomed Mater Res* **55**: 164-76.[4] Mousa WF et al (2000) *Biomaterials* **21**: 2137-46.[5] Fujita H et al (2000) *J Bone Joint Surg Br* **82**: 614-18.[6] Dufrane D et al (2001) *European Cells and Materials* **1 (supplement 2)**: 64.

European Cells and Materials Vol. 3. Suppl. 1, 2002 (pages 20-21) ISSN 1473-2262

RF-PLASM DEPOSITION AND SURFACE CHARACTERIZATION OF A BIODEGRADABELE THIN FILM COATING

D. Favez [1], D. G. Castner [2], B.D. Ratner [2], H.J. Mathieu [1]

[1] *EPFL, Materials Institute, Lausanne, CH,* [2] *University of Washington, NESAC/BIO, Seattle, USA*

INTRODUCTION: Synthetic biodegradable polymers have become very important materials for applications in biomaterials, tissue engineering and controlled drug delivery. Among these materials, poly(L-lactic acid) (PLLA) has been widely utilized either as temporary scaffolds for cell transplantation in tissue regeneration or as carriers for delivery of bioactive molecules. PLLA breaks down in the body to lactic acid, a component of the normal metabolism [1]. RF-plasma deposition has also been found to be a useful technology for biomaterials applications because of its ability to coat complex shapes with a tightly adherent thin film [2].

The surface analytical techniques X-ray photoelectron spectroscopy (XPS) and Time-of-Flight Secondary Ion Mass Spectrometry (ToF-SIMS) have been used to study the surface chemical nature of many polymeric materials, including plasma deposited polymers [3-4] and degradation of polymers [2]. These techniques probe the chemistry of the polymer surface to a depth of between 20 and 100 Å for XPS and approximately 10 Å for ToF-SIMS. Atomic Force Microscopy (AFM) is also commonly used to probe the topography of plasma deposited polymers [5] or the evolution of polymer degradation, an example being the hydrolysis of polyester [6-7].

The aim of this study is to use plasma deposition techniques to form a thin PLLA coating using the cyclic lactide as a monomer and to study its degradation in a phosphate buffer solution (PBS, pH 7.4) at 37°C (reproducing the saline conditions of human blood) using state-of-the-art surface analysis techniques.

MATERIALS/ METHODS: The substrates used for this experiment were either glass disks (for coating optimization) or silicon wafers (for the degradation studies). The borosilicate glass disks were obtained from Carolina Biological Supply Company (NC, USA) Cat. # D8-63-3029. Their diameter was 12 mm and thickness was 0.13-0.17 mm. The Si wafers were obtained from Silicon Valley Microelectronics, Inc., (CA, USA). The precursor used to form the plasma was L-lactide or (3 S)-cis –3,6-Dimethyl-1,4-dioxane-2,5-dione, purchased from Aldrich Chemical Company, Inc. (Milwaukee, WI, USA), reference 36,704-4.

The plasma chamber consists of a Pyrex tubular glass cylinder, 25.5 in. in length and 4 in. in diameter, wrapped with heating tapes to control the temperature. Two copper capacitor plates are coupled to the 13.56 MHz RF generator via a matching network to increase the power dissipation in the discharge and protect the reactor. A capacitance manometer gauge measures the pressure, using a feedback controller which moves the throttle valve to maintain the pressure as directed.

XPS (ESCA) analyses was performed at the University of Washington (NESAC/BIO) on a Surface Science S-probe or X-probe Instruments. This instrument permits analysis of the outermost 20-100 Angstroms of a sample using a square spot size that can be adjusted from 100 µm x 100 µm to 800 µm x 800 µm. For the present set of measurements the largest spot size (800 microns) was used.

ToF SIMS analysis was conducted using a Physical Electronics Model 7200 time-of-flight secondary ion mass spectrometer at NESAC/BIO. The instrument is equipped with a Cs+ ion source operated at 8keV, a reflectron mass analyzer, and chevron-type multichannel plate detectors. A bunched primary Cs+ beam (50 micron diameter, approximately 1 ns pulse width) is used and the bin width of the time-to-digital converter (TDC) is set at 1.25ns, resulting in mass resolutions (m/Δm) of >7000 at m/z=27 for electrically conducting samples. The beam is rastered over a square area that is 100 microns on a side. Charge neutralization is achieved with a pulsed electron flood gun.

RESULTS / DISCUSSION:

Plasma deposition of cyclic L-lactide has been successfully optimized to yield a poly(lactic acid)-like thin film. The XPS, ToF-SIMS and AFM characterization of such films deposited using a pulsed RF plasma showed that the chemical structure, deposition rate and degradation in phosphate buffer solution (pH 7.4, 37°C) of such

films are strongly dependent on the duty cycle of the pulses. A typical XPS spectrum is shown in Fig. 1.

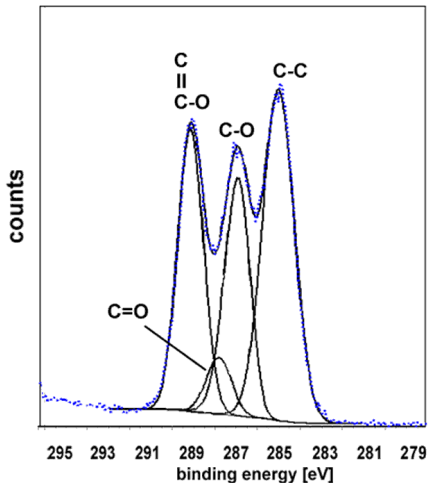

Fig. 1: Four peaks fit of C1s high resolution peak duty cycle = 2%

During the optimization process, it has been shown that the input power is the major parameter which affects the chemical structure of the deposited film. Lowering the input power increases the monomer structure retention. Since the degree of monomer retention was continuing to increase as the lower limit of continuous wave (CW) plasma stability was reached, it was necessary to use a pulsed RF plasma to reach even lower effective powers by decreasing the duty cycles. Other parameters such as sample position or deposition time were shown not to be as significant as the input power for monomer structure retention.

The characterization of the pulsed plasma deposited film showed an increase of oxygen functionalities, present as ester or alcohol groups, with decreasing duty cycle as shown in Fig. 2. The proportion of ketone groups seemed to be independent of the duty cycle. In addition, the deposition rate with a duty cycle of 33% is nearly three times the one corresponding to a duty cycle of 2%. Compared to PLLA, plasma deposited films contain more hydrocarbon species. However, the plasma-deposited PLLA films have several of the same ToF-SIMS fragments observed from a conventionally polymerized PLLA film.

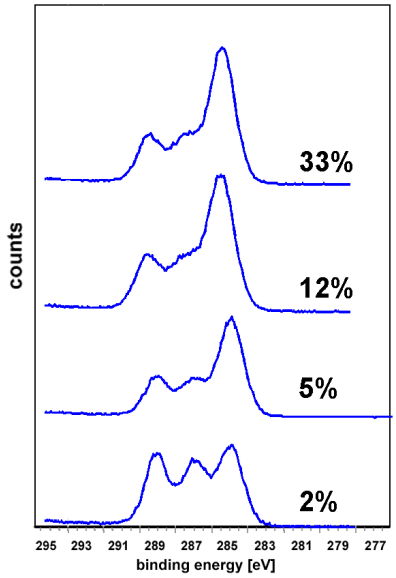

Fig. 2 C1s high-resolution peaks of pulsed plasma polymerized films for various duty cycles..

REFERENCES: [1] Amass, W., A. Amass, et al., *A review of biodegradable polymers: Uses, current developments in the synthesis and characterization of biodegradable polyesters, blends of biodegradable polymers and recent advances in biodegradation studies*, Polymer International, **1998** *47*(2): 89-144; [2] Ratner, B. D. and E. E. Johnston, *Surface characterization of plasma deposited organic thin films*, Journal of Electron Spectroscopy and Related Phenomena, **1996** *81*(3): 303-317; [3] Mackie, N. M., D. G. Castner, et al., *Characterization of pulsed-plasma-polymerized aromatic films*, Langmuir, **1998** *14*(5): 1227-1235; [4] Chen, J. X. and J. A. Gardella, *Time-of-flight secondary ion mass spectrometry studies of in vitro hydrolytic degradation of biodegradable polymers*, Macromolecules, **1999** *32*(22): 7380-7388; [5] Wang, J. H., J. J. Chen, et al., *Plasma Synthesis of a Novel CF3 Dominated Fluorocarbon Film*, Chemistry of Materials, **1996** *8*: 2212-2214; [6] Leadley, S. R., K. M. Shakesheff, et al., *The use of SIMS, XPS and in situ AFM to probe the acid catalyzed hydrolysis of poly(orthoesters)*, Biomaterials, **1998** *19*(15): 1353-1360;[7] Davies, M. C., K. M. Shakesheff, et al., *Surface analysis of biodegradable polymer blends of poly(sebacic anhydride) and poly(DL-lactic acid)*, Macromolecules, **1996** *29*(6): 2205-2212.

ACKNOWLEDGEMENTS: The XPS and ToF-SIMS experiments at NESAC/BIO were funded by NIH grant RR-01296.

European Cells and Materials Vol. 3. Suppl. 1, 2002 (pages 22-23) ISSN 1473-2262

IMMOBILISATION OF STREPTAVIDIN ON POLYSTYRENE

C. Houphouet-Boigny [1], Xin Gao [1] , M. Schawaller [2], H.J. Mathieu [1]

(1) EPFL, Materials Institute, 1015 Lausanne, CH

(2) DiaMed / ADS Applied Diagnostic Systems AG, 1785 Cressier sur Morat, CH

INTRODUCTION: The measurement of certain analytes in blood is an important aspect of clinical diagnosis. There is a need for tests (immuno assays) with high sensitivity to identify and detect enzymes, therapeutic drugs or other specific proteins. In order to achieve this we use a biosensor based on fluorescence measurement [1] To improve analytical performance, allyldextran monolayers were coated on gamma-irradiated polystyrene wells (γ-PS). This study reports the coating of polystyrene wells with allyldextran and chemical properties of the surface analyzed by X-ray Photoelectron Spectroscopy (XPS), contact angle and Total Internal Reflectance Fluorescence Spectroscopy (TIRF) measurements based on a diploma work of one of the authors [2].

METHODS: Surface modification procedures are based on allyldextran layer absorbed on the bottom surface of the polystyrene wells. Allyldextran grade (MW 150'000, Pharmacia 253758-01) provided by Pharmacia is used for all experiments. It is a form of dextran substituted with allyl groups.

Allyldextran solutions with different concentrations 0 –10'000 µg/ml of allyldextran are prepared in water (18.2 MΩcm at 25°C) which has been degassed with nitrogen for about 1h. The wells are filled with the allyldextran solution and stored in a closed box for 16 ± 3 hours. After washing again with water the γ-PS chips are used for further treated with 30mM sodium (meta)periodate $NaIO_4$ (Fluka 71859). After washing with PBS and coupling in a bicarbonate solution (100mM $NaHCO_3$, pH 9.3) with 40µg/ml of Streptavidin (Pierce cat. No. 21122) or Neutravidin (Pierce cat. No. 31000)

The avidin-biotin system has many applications in both research and technology. Due to the very high affinity ($Ka=10^{-15}M^{-1}$) of the complex.

XPS scans were performed to determinethe surface composition in order to analyze changes due to the transformations induced by surface treatment and to detect otherwise contamination. XPS of the samples was performed on a Kratos AXIS Ultra System, utilizing an aluminum Ká monochromatized X-ray source (E=1486.6 eV) and a hemispherical energy analyzer. For this study, XPS spectra were recorded at take-off angles of 0°, 45°, 70° and 80° with respect to the surface. Spectral binding energies were referenced to the C-H peak assigned to 285.0 eV. Evaluation of the XPS data was done by CasaXPS (v. 2.11) and Tougaard-Quasas software packages.

The surface modification and its effects on wettability were analyzed using contact angle measurements. They were performed with a contact angle measuring system G10 by Krüss GmbH (Hamburg, Germany) at the DGR of EPFL (Prof. H. Harms). The contact angle measurements were performed on air-dried sample by placing a water drop on the polystyrene surface. The measured contact angle was the advancing angle between the surface and the water drop.

Total Internal Reflectance Fluorescence measurements were performed at DiaMed by an immunosensor device [3].

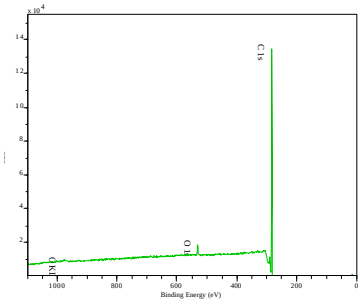

Fig. 1 XPS survey of g-PS radiated Polysytrene

RESULTS:

A typical XPS survey for a polystyrene surface is shown in Figure 1. Carbon C1s peak and the oxygen O 1s are observed. This survey is the standard survey for the gamma irradiated

polystyrene wells prior to any surface treatment. The oxygen amount of the pure gamma irradiated samples (ã-PS) is less than approx. 2 atom%).

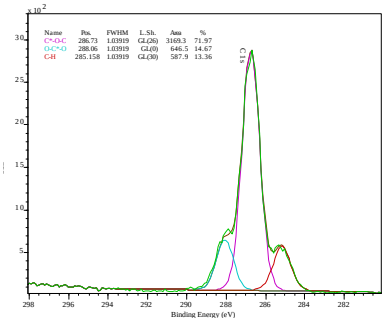

Fig. 2 C1s high resolution XPS of pure allyldextran powder

Fig.2 shows AC1s high resolution scan of pure allyldextran powder is shown in Figure 2, which is compared to allyldextran coating as shown in figure 3.

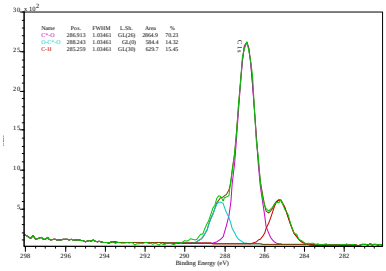

Fig. 3 C1s high resolution XPS of g-radiated Polystyrene coated with an allyldextran layer; è = 0°

SUMMARY: The allyldextran coating provides a stable, hydrophilic surface on γ-radiated Polystyrene wells with repetitive XPS results. Surface treatments were optimised using XPS and contact angle measurements. Functional biotin binding assay using fluorescence measurements of surfaces treated with allyldextran acitvated with iodate and coupled to Neutravidin seem to indicate that the Neutravidin is immobilised. Surfaces treated with allyldextran followed by iodate activation and and Neutravidin are highly hydrophilic and express very good non-specific adsorption characteristics.

REFERENCES: ; [1] Pierce catalogue 2001-2002 ; [2] C. Houhouet-Boigny, EPFL diploma thesis submitted Feb. 2002 to the Mat. Institute;[3] Patent Application WO 01/14859 A1

ACKNOWLEDGEMENTS : The project was partially funded by CTI/KTI, Bern, contract no. 5170.1 MTS. We like to thank N. Xanthopoulos, C. Aeby and M.C. Morandi for their experimental advice and assistance.

European Cells and Materials Vol. 3. Suppl. 1, 2002 (pages 24-25) ISSN 1473-2262

REINFORCEMENT OF COMPOSITE RESINS WITH UNIDIRECTIONAL GLASS FIBERS

J. Kosoric, M. Cattani, S. Bouillaguet, Ch. Godin, & J.-M. Meyer

School of Dentistry, University of Geneva, CH,

INTRODUCTION: Glass fibers have been introduced as reinforcement for composite resins in dentistry more than 20 years ago. They are available in different forms : unidirectional, braid, woven, mesh. They can also be found as pre-impregnated or as material to be impregnated with resin before use when needed. Among different clinical applications we can cite : dentures, overdentures, reinforced temporary/long-term (interim) bridges etc. Even after more than ten years of first clinical experiments the conclusion is that they can be used as long temporary solution (few months up to two years), in case of fixed partial denture (Vallittu[1], Vallittu and Sevelius[2]).

In current research on dental implants there are some intentions for immediate loading : « The results suggest that immediate loading of Branemark System implants at the time of placement in edentulous patients can be a valuable adjunct to therapy and as predictable as delayed loading, in both mandibular and maxillary arches. » Horiuchi K[3], Gatti et al[4] and Copper et al[5] have come to the same results in their own works. We therefore decided to point our research in that direction.

By selecting materials which have a lower rigidity than a cast metal alloy we might be providing better conditions for healing process in the bone surrounding the implant.

First we have decided to evaluate improvement in mechanical behavior, both with laboratory composite resins and with a provisional resin. Thanks to those preliminary results it seemed reasonable to continue our research in making samples shaped like real bridges and to evaluate them under loading.

The aim of this work was to evaluate reinforcement with glass fibers of two dental materials : laboratory composite resins and provisional resins, in order to obtain preliminary results for further studies of provisional bridges as a suprastructure for immediate loading of implants.

METHODS: We have used two different laboratory composite resins (Sinfony, *ESPE* and Cristobal+, *IDR*) and one provisional resin (Protemp Garant 3, *ESPE*) reinforced with unidirectional glass fibers (Stick, *Stick Tech Ltd.*). For all the materials we have used Sinfony Transparent, a flowable composite resin, for a 10 minutes impregnation of glass fibers, in a closed plastic bag. The samples with composite resins were prepared in a 25x2x2 mm mould and cured for 15 sec with a halogen curing lamp Elipar TriLight (*ESPE*), followed by additional curing in the Mpa 2000 light-curing unit for 90 sec, and at the end treated with temperature of 80 degrees C for 8 minutes in the Mpa 2000 Post Cure unit. The samples with provisional resins have been light-cured differently : 15 sec with the Elipar TriLight curing lamp, followed by a post-cure treatment in *ESPE* Beta-Unit, auxiliary program 1. Flexural strength and elastic modulus have been examined with 3 and 4 points bending tests, using an Instron Universal testing machine 1114, at a crosshead speed of 0.5 mm/min. Statistical analysis was performed by multifactorial ANOVA.

RESULTS:

Table 1. Modulus of elasticity of fiber-reinforced composite resins in GPa

4 points test	Without fibers	
	24 h	7 d
Cristobal	13.8 (1.8)	22.7 (6)
Synfony	7.2 (0.5)	7.1 (1.2)
	With fibers	
	24 h	7 d
Cristobal	17.2 (5.3)	15.4 (8.5)
Synfony	16.8 (1.3)	10.5 (1.1)

Table 2. Flexural strength of fiber-reinforced composite resins in MPa

4 points test	Without fibers	
	24 h	7 d
Cristobal	140 (28)	159 (22)
Synfony	163.4 (13)	162 (14)
	With fibers	
	24 h	7 d
Cristobal	460 (130)	340.3 (51)
Synfony	525.6 (36)	462.3 (91)

Multifactorial analysis has shown that glass fibers reinforce the laboratory composite resins but they do not have any influence on their elastic modulus. On the other hand samples become less resistant with time, but their modulus does not change.

Table 3. Flexural strength of fiber-reinforced provisional resins in MPa

4 points test	Without fibers	
Flex strength	24 h	7 d
Protemp Garant 3	134(60)	180(19)
	With fibers	
	24 h	7 d
Protemp Garant 3	110(24)	207(61)

Table 4. Modulus of elasticity of fiber-reinforced provisional resins in GPa

4 points test	Without fibers	
Flex modulus	24 h	7 d
Protemp Garant 3	2.2(0.6)	2.6(0.7)
	With fibers	
	24 h	7 d
Protemp Garant 3	2.9(0.8)	6(2)

Multifactorial analysis has shown that only aging in water has significant influence on flexural strength of provisional resins, but the reinforcement has not. For flexural modulus both, aging in water and reinforcement, give significant difference for tested material.

DISCUSSION & CONCLUSIONS: Post-curing provides better mechanical properties in a short period of time. Glass fibers reinforce significantly the flexural strength of the laboratory composite resins, but strength is more material dependent than condition specific (aging in water, reinforcement) – this is more obvious for Sinfony, a less charged material. On the contrary, flexural strength of provisional resins is condition dependent (aging in water). Also their flexural modulus has become more elevated in simultaneous action of aging and reinforcement.

The work is continuing by the evaluation of provisional reinforced resin characteristics and the development of bridges which simulate more closely the clinical situation.

REFERENCES: [1] Vallittu(1999) *Case report: a glass fibre reinforced composite resin bonded fixed partial denture* (Eur J Prosthodont Restor Dent 2001 Mar;9(1):35-8).[2] Vallittu, Sevelius(2000) *Resin-bonded, glass fiber-reinforced composite fixed partial dentures: Clinical study* (J of Prost Dent 2000 Oct, 413-18,[3] Horiuchi K(2000) *Immediate loading of Branemark system implants following placement in edentulous patients: a clinical report* (Int J Oral Maxillofac Implants 2000 Nov-Dec;15(6):824-30), 4,5 Sadowsky SJ. (2001) *Mandibular implant-retained overdentures: a literature review* J Prosthet Dent 2001 Nov;86(5):468-73

ACKNOWLEDGEMENTS : We would like to thank ESPE, Germany and IDR, France for their generous support in providing theirs material and curing units.

European Cells and Materials Vol. 3. Suppl. 1, 2002 (pages 26-27) ISSN 1473-2262

CORROSION CHARACTERISATION OF PASSIVE FILMS ON CoCrMo WITH ELECTROCHEMICAL TECHNIQUES IN SALINE AND SIMULATED BIOLOGICAL SOLUTIONS

S. Kurz[1], A.W.E Hodgson[1], S. Virtanen[1], V. Fervel[2] & S. Mischler[2]

[1] Institute for Materials Chemistry and Corrosion & Department of Materials, Swiss Federal Institute of Technology Zurich,8093 Zurich, CH, [2] Laboratory of Metallurgical Chemistry, Department of Materials, Swiss Federal Institute of Technology Lausanne, University of Geneva, 1015 Lausanne, CH

INTRODUCTION: CoCrMo alloy is regarded as a highly biocompatible material and has been employed in the fabrication of hip prostheses since the 1940's. Its biocompatibility is linked to the spontaneous formation of a stable oxide film. Nonetheless, the release of metal into the body takes place, which can be the result of uniform passive dissolution, of local breakdown of passivity as a consequence of localized forms of corrosion, or of mechanical events such as fretting corrosion. However, the exact chemical, electrochemical and triboelectrochemical mechanisms that lead to the release of metal from CoCrMo prostheses are not known. In this work an electrochemical characterisation of CoCrMo alloy under simulated biological conditions was sought. In particular, the effects of specific ions present in the electrolyte solution and of time on the properties of the passive film were investigated.

METHODS: CoCrMo disc-shaped samples (Protasul-20, Sulzer Winterthur) of 1 cm^2 area and 5 mm thickness were employed throughout the study. Experiments were performed in simulated body fluid (SBF) and in 0.14 M NaCl solution buffered to pH 7.4 via the use of tris(hydroxyaminomethane) buffer, or to pH 2 and pH 10 by the addition of concentrated HCl and 1 M NaOH. (Table1) The solutions were thermostatted via the use of a water bath to 37 ºC, unless otherwise stated. Potentiodynamic measurements and electrochemical impedance spectroscopy (EIS) were carried out to characterise the alloy and to monitor changes in the passive film as a result of exposure to different environments with time.

***Table 1**: Electrolyte solutions employed in the study. All solutions were adjusted to the desired pH by the addition of HCl (37%) or NaOH (1 M).*

Background Electrolyte	Added ions
0.14 M NaCl	—
0.14 M NaCl	1 mM KH_2PO_4, 2.5 mM $CaCl_2$, 3 mM KCl, 1.5 mM $MgCl_2$, 4.2 mM $NaHCO_3$, 0.5 mM Na_2SO_4 - **Simulated body fluid -**

RESULTS: In Figure 1, potentiodynamic curves acquired after exposure times of 6 min, 90 min, 18 h, 24 h and 7 d to simulated body fluid adjusted to pH 7.4 at 37 ºC are shown. It is evident from the curves that the time of exposure to the solution plays an important role, both on the cathodic and the anodic currents recorded. During the first 18 h the cathodic currents are very similar and the open circuit potentials fall close to one another. In the anodic potential range, the currents are passive, but once again, after 18 h the passive current appears to be much smaller indicating that the passive film has become more protective (e.g. by thickening, by becoming more compact or by changing in composition). At potentials positive to + 0.5 V vs. SCE the peak superimposed upon H_2O oxidation, is due to the transpassive dissolution of Cr. It is important to note that the increase with immediate decrease in current observed at potentials positive to the open circuit potential is not necessarily to be attributed to an active-passive transition but possibly to the discharge of hydrogen ions adsorbed onto the surface under cathodic potentials.

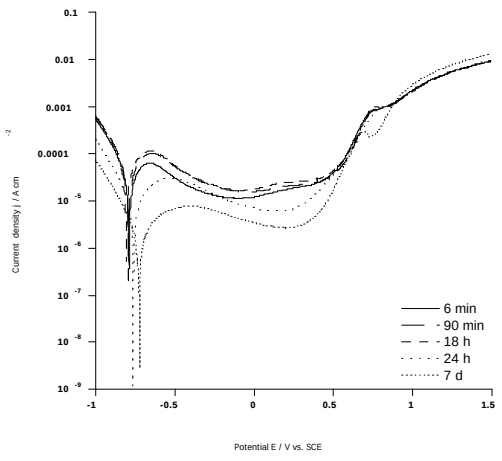

Fig. 1: Current-potential curve recorded at CoCrMo sample at different times of exposure to simulated body fluid adjusted to pH 7.4 at 37 ºC. Sweep rate 5 mVs^{-1}.

Electrochemical impedance spectra acquired under the same solution conditions at different times of exposure ranging from 10 minutes to 7 days, clearly showed an increase in the protectiveness of the passive film with time, which could be observed in the increase in impedance values at low frequency with time and in broadening of the capacitive behaviour of the phase angle to lower frequencies with time.

The effects of ions on the passive film properties were also studied. More specifically, the effects of ions present in simulated body fluid, such as Ca^{2+}, PO_4^{3-}, K^+, Mg^{2+}, were investigated by comparing electrochemical impedance spectra and potentiodynamic measurements with those obtained in 0.14 M NaCl solution also adjusted to pH 7.4 via the use of the same buffer and at 37 ºC. The results clearly showed that, unlike Ti and its alloys[1] which selectively adsorbed Ca^{2+} and PO_4^{3-} ions, CoCrMo does not interact with the ions in the electrolyte and the evolution of the spectra with time obtained in the two solutions are very similar.

Experiments were also performed to investigate the effects of exposure of the CoCrMo sample to air prior to immersion into the electrolyte solution. It was found that the passive films formed in air were different to those formed in solution, but that once the sample had been placed in solution a reconstruction of the passive film takes place.

DISCUSSION & CONCLUSIONS: The electrochemical study showed that the passive film formation on CoCrMo is very sensitive to the conditions under which it takes place, therefore affecting the properties of the films, such as protectiveness and degree of metal ion release. Although the passive film is mainly composed of Cr_2O_3, oxides of Co and Mo can also be present depending on the environment conditions. However the ions present in simulated body fluid do not appear to adsorb or interact with the oxide film. Further studies to investigate the composition of the passive film are currently underway[2].

REFERENCES: [1] A.W.E Hodgson, Y. Mueller, D. Forster, S. Virtanen, (2001) Electrochemical characterisation of passive films on Ti alloys under simulated biological conditions. *Electrochim. Acta* in print. [2] A.W.E. Hodgson, S. Kurz, V. Fervel, S. Virtanen, S. Mischler, (2002) Electrochemical and surface characterization of passive films on CoCrMo in saline and simulated biological solutions, in preparation.

ACKNOWLEDGEMENTS: The authors thank the Foundation "Entwiclungsfonds Seltene Metalle", Switzerland for financial support of the project.

European Cells and Materials Vol. 3. Suppl. 1, 2002 (pages 28-29) ISSN 1473-2262

TRIBOLOGICAL BEHAVIOR OF TITANIUM SLIDING AGAINST BONE

S. Mischler & G. Pax

Laboratoire de Métallurgie Chimique, Ecole Polytechnique Fédérale de Lausanne, CH

INTRODUCTION: In orthopedic implants micro motions are likely to occur at the bone – implant interface. The bone and implant surfaces are thus subject to friction which can cause wear and fretting-corrosion with consequent inflammatory tissue reaction. For this reason, tribological phenomena at bone-implant interface are thought to play a relevant role in aseptic loosening of hip joint implants. Wear and friction are system properties and not materials properties, i.e. the tribological behavior of a material depends, among others, on the nature of the sliding partner. While the tribological behavior of biomedical alloys such as titanium alloys was already investigated when sliding against metals, polymers and ceramics, no results are known for friction against bone.

The goal of this study is to explore possible degradation phenomena (wear, corrosion, changes in surface composition) arising from friction between bone and a Ti6Al4V alloy, a widely used biomedical metal.

METHODS: Tribocorrosion tests were performed using a reciprocating motion plate-on-plate tribometer already described elsewhere. Tests were carried out in a PVC cell that contains 60 ml of solution. The corrosion potential of Ti6Al4V was continuously measured using a silver/silver chloride (+196 mV vs. SHE) reference electrode. Figure 1 shows the details of the contact.

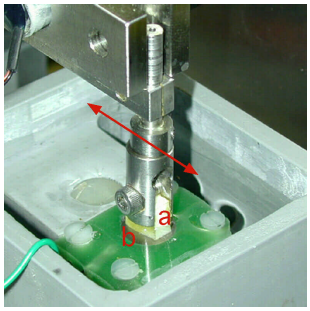

Fig. 1: Detail of the bone (a) – Ti6Al4V (b) contact immersed in 0.14M NaCl at 37°C.

Ti6Al4V discs (10 mm in diameter) were machined from annealed bars supplied by Sieber&Hegner (323HV). The disc were embedded in Technovit, polished using emery paper 240 and subsequently sand blasted. Cow bone specimens were cut in approximately rectangular shape (6 x 4 x 8 mm) from a piece of shin purchased in a butchery. Bone hardness ranged from 35 up to 45 HB62.5 Prior to tests, the samples were cleaned in an ultrasonic ethanol bath. The contact was immersed in a 0.14 M NaCl solution prepared using pa reagent and osmoses de-ionized water. The test procedures involved following steps: first stabilization of the corrosion potential, rubbing at 5 Hz oscillation frequency to establish steady state friction and wear rate (1 hour duration), short rubbing periods (few minutes) at variable motion amplitude by constant oscillation frequency of 1 Hz to monitor changes in corrosion properties. All tests were carried out at 37°C ± 2°C with a normal force of 3 N corresponding to an average load of 0.1 MPa. After tests, the metallic samples were analyzed using optical microscopy, Auger Scanning Electron microscopy (AES), Scanning Electron Microscopy and laser profilometry (UBM apparatus).

RESULTS: The running in period was characterized by severe wear of the bone as evidenced by the large amount of bone debris particles ejected from the contact and the continuous decrease in vertical position of the contact (linear wear). Average of 5 measurements yielded an average bone wear rate of 1.6 ± 0.3 nm/stroke. To check for wear the Ti6Al4V samples were cleaned (after surface analysis) in acetic acid for 12 hours to removed residual bone material. No significant material damage could be observed after rubbing using laser profilometry, SEM and optical microscopy.

The coefficient of friction during rubbing attained, after a few minutes run in, a steady state average value characterized however by large noise (±50% of the average value) due to the large amount of particles trapped within the contact area. Typical average coefficient of friction ranged from 0.34 up to 0.39 for five independent experiments.

Table 1. Shift of the corrosion potential of Ti6Al4V due to rubbing at selected amplitudes.

Motion amplitude	Cathodic shift
1.8 mm	12.7 ± 3.1 mV
0.9 mm	4.5 ± 0.5 mV
0.3 mm	0.3 mV

Rubbing of bone against Ti6Al4V induced a small cathodic shift of the corrosion potential. The shift amplitude was found to depend on the motion amplitude as indicated in Table 1.

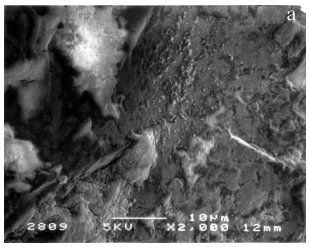

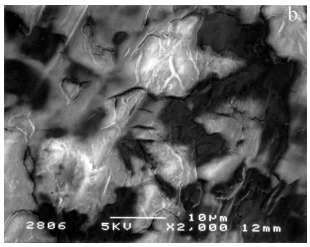

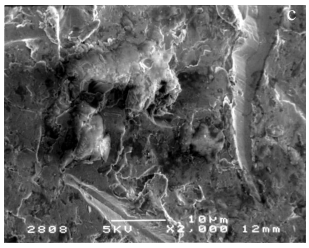

Figure 2: SEM images taken on Ti6Al4V after rubbing against bone in the center (a, top left), at the edge (b, top right) and outside (c) the sliding track.

The rubbed area of all Ti6Al4V samples was found covered by transferred bone material as evidenced by SEM analysis (Figure 2). The transfer morphology was found to depend on whenever the contact was continuous (surface always in contact with the bone) or intermittent (rubbed area exposed to the solution between two strokes). In the intermittent contact area the transfer layer is homogeneous (Figure 2b) while several µm thick patches of bone material characterized the central area (Figure 2a). Interestingly, the transferred bone could not be detached by repeated ultrasonic cleaning but only by dissolution in acetic acid. This indicates a good mechanical adhesion.

AES sputter depth analysis was carried out on three different locations corresponding respectively to thick patches of transfer, areas of the track between patches and areas outside the track. The atomic concentration ratio of the thick patches corresponds to 46% Ca, 32% O, 14% C with P concentrations well below 5%. Areas 2 and 3 are characterized by a passive film of titanium oxide with some contamination by Ca and P, the contamination being more pronounced in the track. The thickness of the passive film is approximately 10 nm. For comparison AES analysis was also carried out on a Ti6Al4V disc loaded against bone (3 N load) during immersion for 2 hours at open circuit potential without sliding. Only carbon (air contamination) oxygen and titanium could be observed. This indicates that friction is necessary to obtain bone transfer onto the metal under the present conditions.

DISCUSSION & CONCLUSIONS: The present work is of preliminary nature and implied several major simplifications of the analyzed tribosystem compared to the complex situation prevailing in vivo. In particular the selected cow bone does not correspond necessarily with clinical situations. The same holds for the applied load and amplitudes. Further the test duration of 1 hour used here is relatively short because it corresponds to an in-vivo activity of only few days assuming a frequency of 10^6 steps per year. Thus, the possibility to extrapolate the present observations to clinical cases is somehow limited.

However, the obtained results clearly illustrate that complex phenomena may occur during rubbing of titanium against bone, phenomena leading to significant bone wear, adhesive transfer of bone onto the metal and modification of the titanium surface composition by contamination of the passive film by Ca and P.

REFERENCES: [1] A, Meunier, L. Sedel (2000), Influence de l'endommagement tribologique des implants orthopédiques sur le milieu biologique: réactions tissulaires et descellement prothétique, *Tribologie et corrosion*. SIRPE pp 193-200. [2] S. Mischler, S. Debaud, D. Landolt (1998) Wear accelerated corrosion of passive metals in tribocorrosion systems. J. Electrochem. Soc **145(3)** pp 750-758.

ACKNOWLEDGEMENTS: Thanks to the Entwicklungsfonds Seltene Metalle, Zürich for financial support.

European Cells and Materials Vol. 3. Suppl. 1, 2002 (pages 30-31) ISSN 1473-2262

EFFICIENCY OF CURING DEVICES FOR DENTAL COMPOSITES

P. Payot*, M. Cattani-Lorente, Ch. Godin, S. Bouillaguet, J. Forchelet* and J.M. Meyer

*Dental School, University of Geneva, * EI-VD, University of applied science, Yverdon-les-bains*

INTRODUCTION: The setting reaction of dental composites is a light-activated radical addition. A high monomer-polymer conversion (DC) is sought, as it is associated with high mechanical properties. The DC depends on the efficiency of the initiator system and on the efficacy of the curing devices. For most dental composites, camphorquinone (CQ) is used as photo initiator. Currently, three different technologies are used in the commercial curing units. The light sources are either halogen lamps, ARC plasma lamps or light emitting diodes (LED).

The aim of the present study is to compare the efficiency of five different curing devices. For that purpose, the curing devices were characterized by their spectra and their irradiance. To test their efficiency, the depth of cure of a dental composite was measured after illumination with different exposure times.

The hypothesis tested is that the efficiency of the curing devices depend on the quantity of energy effectively absorbed by the photo initiator, instead of the total energy supplied by the curing device.

METHODS: The hybrid dental composite Herculite VXR, A2 was used. Two LEDs (Freelight /ESPE; E-light/GC), a halogen (Trilight/ESPE) and two ARC sources (Aurys/DegréK; Flipo/Lokki) were evaluated in the standard mode.

The irradiance was measured using an Avantes fiber optic spectrometer AVS-USB2000 working in the 190 to 850 wavelength range. The irradiance was measured at different distances from the source, as the spectrometer was saturated beyond 4 mW/cm^2.

The depth of cure was determined by measuring the height of cured samples with a micrometer. A PVC opaque mould with a cylindrical cavity of 4mm in diameter and 4 mm in depth was used. The top of the specimens was illuminated using different exposure times (Table 2). The samples were taken out the mold and the uncured material was eventually gently removed. Three samples were made for each illumination condition.Statistical differences in the data were evaluated with a one way analysis of variance, followed by a LSD multiple range test ($p<0.05$).

RESULTS: The obtained spectra are shown in Figure 1.

Fig. 1: Luminous spectra of the five curing units. Their irradiance (mW/cm^2) is given for each

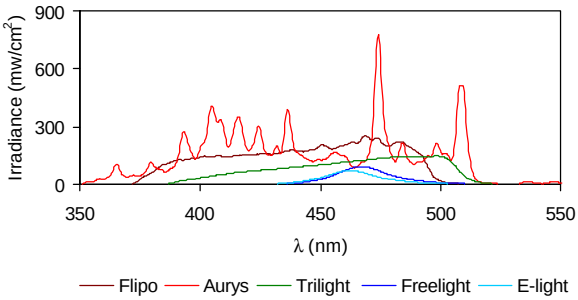

emitted wavelength. The total irradiance is a value integrated over the whole spectrum.

The irradience is given in the Figure 2 for different distances between the source tip and the detector.

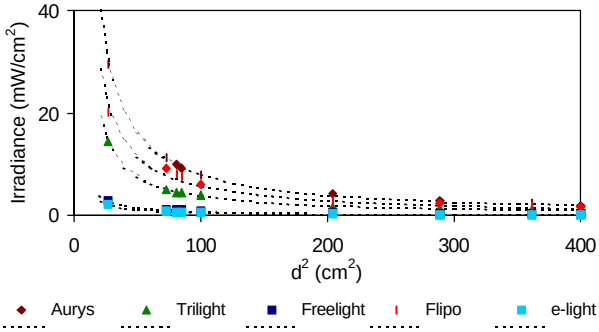

Fig. 2: Irradiance measured at different distances of the source for the five curing devices.

The irradiance in contact with the source was extrapolated from these values, (Table 1). The depths of cure are reported in Table 2.

Table 1. Irradiance Irr (mW/cm2) integrated over two wavelength ranges. Irr are the values given by the manufacturers of the curing devices.*

Curing unit	$Irr_{350-600}$	Irr *	$Irr_{450-490}$
Aurys	1856	1650	523
Flipo	1330	1600	544
Trilight	818	800	297
Freelight	177	400	151
E-light	234	750	203

The energies calculated for the whole spectra range ($E_{350-600}$) and the 450-490 wavelength range (E_{450-}

$_{490}$) are reported in the same table. Values marked with the same letter are not significantly different.

Table 2. Depth of cure for the different conditions and their corresponding energy E (J) emitted over two wavelength ranges .

Curing unit	t (s)	$E_{350-600}$	$E_{450-490}$	Depth (mm)
Flipo	1	0.54	0.23	2.19 ± 0.01 b,c
	2	1.07	0.47	2.34 ± 0.02 c
	3	1.61	0.7	2.79 ± 0.11 d,e
	5	2.68	1.17	3.04 ± 0.16 f
	10	5.37	2.34	4.17 ± 0.01 i
Aurys	1	0.74	0.22	1.42 ± 0.03 a
	2	1.48	0.45	2.09 ± 0.04 b
	3	2.21	0.67	2.84 ± 0.03 e
	5	3.69	1.12	3.05 ± 0.08 f
	10	7.38	2.25	4.06 ± 0.06 i
Freelight	10	0.75	0.65	3.36 ± 0.08 g
	20	1.49	1.3	4.05 ± 0.02 i
	40	2.99	2.6	4.17 ± 0.01 i
E-light	10	0.58	0.49	2.65 ± 0.16 d
	20	1.17	0.98	2.81 ± 0.03 e
	40	2.34	1.95	4.19 ± 0.02 i
Elipar	10	3.1	1.39	3.58 ± 0.14 h
	20	6.2	2.79	4.15 ± 0.02 i
	40	12.4	5.58	4.17 ± 0.01 i

DISCUSSION & CONCLUSIONS: In this work, a single composite was used to exclude the effects of chemical composition on the depth of cure. The maximum depth was obtained by illuminating 10s with the ARC devices, 20s with Elipar and Freelight and 40s with E-light.

The irradiance values given by the manufacturers Irr* are given for the whole emitted. These values correspond to the radiation flux per unit of surface in direct contact with the source. In the present study, the irradiance couldn't be measured in these conditions, because the detector used was saturated at close distances to the sources. However, these values were extrapolated and can be compared to the Irr* (Tab 1). An advantage of measuring the light intensity at different distances is that the source can be considered as being punctual.

To test our hypothesis, the energy emitted by the different sources was calculated by the equation 1,

$$E = IrrSt \quad (1)$$

where S is the surface of the source tip. A relationship between the depth of cure and the emitted energy was established (Figure 3). The data were best fitted by the equation 2,

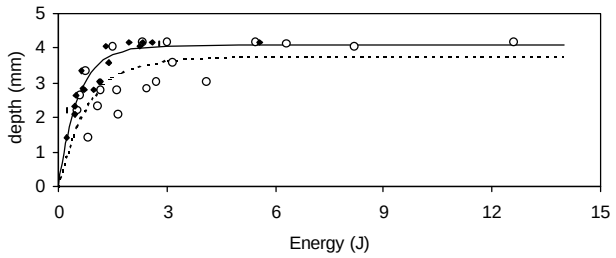

$$Depth = a(1-e^{-bE}) \quad (2)$$

where a and b are constants.

Fig. 3: Relationship between the depth of cure and the energy emitted by the sources at the different exposure conditions.

A poor correlation was obtained between the depth of cure and the total amount of energy $E_{350-600}$ (a:3.77; b:1.21; r:0.81; se:0.66). However, it is well known that only the light emitted in the wavelength interval which corresponds to the absorption of the photo initiator is useful to initiate the composite polymerization. The CQ absorption peak in methacryliate resins ranges from 380 to 510 nm with a maximum at 468 nm [1]. Moreover, Nomoto [2] showed that radiation in the 450-490 nm range activated more efficiently the CQ. Consequently, the energy emitted in this range ($E_{450-490}$) was also calculated. $E_{450-490}$ corresponded to 43% of $E_{350-600}$ for the halogen and the Flipo ARC sources, to 30% for the Aurys ARC and to more than 80% for the LEDs. As expected, a better correlation was obtained between the depth of cure and the $E_{450-490}$ variable (a:4.08; b:1.82; r:0.95; se:0.35), corroborating our working hypothesis.

In conclusion, the five curing devices showed marked differences in the shape and intensity of their emitted light spectra. Despite that the irradiance of the LEDs sources is the lowest, more than 80% of their emitted energy is in the 450-490 wavelength range. 20s were necessary to obtain the maximum depth with the Freelight LED and the halogen source. The exposure time could be reduced by a half by using the two ARC sources. However, for these devices, only 30 % and 43% of the emitted energy is in the wavelength range efficiently absorbed by the CQ.

REFERENCES: [1] F Stahl et al. (2001) *Biomaterials* **21**:1370-1385. [2] R. Nomoto et al. (1997) *Dent Mater J* **16**:60-73.

ACKNOWLEDGEMENTS: We gratefully acknowledge the manufacturers for supplying the unit curing devices.

EXTRACTION OF PLASMA SPRAYED TITANIUM THROUGH A BONE CEMENT USING ELECTROCHEMICAL TECHNIQUES.

L. Reclaru*, A. Blatter*, R. Lerf**, P. Y. Echler*, J. M. Meyer***

** PX Tech SA R&D La Chaux-de-Fonds, ** PI Precision Implant AG , Aarau, ***School of Dentistry, University of Geneva*

Introduction: Titanium and titanium alloys are widely used as orthopedic implants because of their favorable mechanical properties and good biocompatibility. However, some specific cases are known, where highly loaded cemented implants made from Ti alloys produced unsatisfactory results in clinical practise (e.g. 1). Prior *in-vitro* experiments showed that micromotion alone could not explain debonding and osteolysis reported for such cemented implants (2). Electrochemical test on samples of cement + titanium revealed the ability of the polymer to transport electrical charges in the polymer – metal interface (3).

The cement is an ionic conductor and therefore participates in the corrosion process. The corrosion phenomenon is in this case accompanied by titanium cation diffusion into the electrolyte and chloride anions towards the titanium through the cement. In the present study, we have evaluated the corrosion behavior of titanium vacuum plasma spray coating (Ti VPS) with and without bone cement. Electrochemical extraction tests were carried out, with ICP-MS analysis of the electrolyte, in order to verify the ionic permeability of the polymer.

Materials and methods : A layer of CEMEX® bone cement, approximately 0.9 mm thick, was manually pressed onto Ti VPS sample discs of diameter 11 mm.

The quantities of titanium in the electolyte, extracted from the samples by cyclic and potentiostatic voltametry, were determined by the technique of ICP-MS.

After the tests, we eliminated part of the cement on the disc to check for the presence of chloride ions using EDX analysis.

Results and discussion : Figure 1 shows the sweeping curves corresponding to the first and last (#48) cycle recorded during cyclic. The measured current is of the order of a few hundred nano-amperes.

For the second technique used are displayed in Figure 2 the potentiostatic curves of the ten cycles at 650 mV SCE.

The concentrations of titanium cations found in the electrolyte by ICP-MS were smaller than 0.5 ìg/L in both tests.

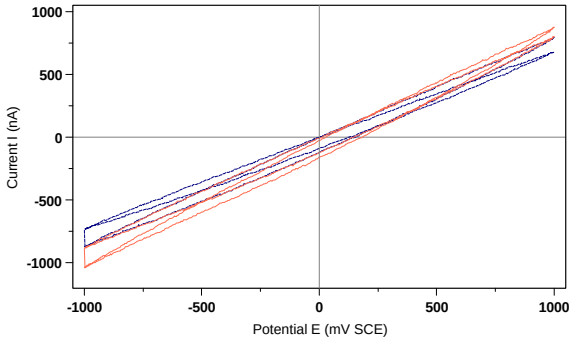

Fig.1 Potentiodynamic curves obtained by the cyclic voltametry technique. First cycle and the last , # 48 .

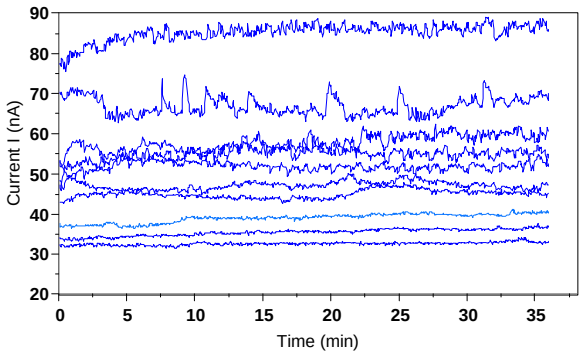

Fig. 2 Potentiostatic curves recorded during 36 minutes, number of cycles, 10 / level

The total quantity of charge recorded during the extraction test was 6106, 6 °C. Based on Faraday's law, which assumes that all the measured electrical charge is used to extricate the Ti^{2+} cations from the disc sample through the membrane of bone cement into the electrolyte, we expect a theoretical quantity of 1.515 ìg of titanium in the solution, corresponding to a titanium concentration of 75ìg/liter. This theoretical concentration by far exceeds the measured quantities of less than 0.5 ìg/liter. This indicates that most of the electrical charges are consumed in the cement by other ions (sodium and chloride), and probably also by the growth of the titanium oxide layer. After the extraction test, we find indeed chloride ions on the surface of the sample disc using EDX analysis.

The presence of titanium in the solution and of chloride on the sample surface confirms the suggested transfer mechanism (Fig.3).

Conclusion: From our results we conclude that the bone cement is permeable for titanium cations, leading to a corrosion process of the titanium underneath the cement. The corrosion process comprises the formation of titanium cations as well as the growth of the titanium oxide layer.

References:

1Willert HG. et al., 1996, Clin Orthop, 333: 51-75.
2 Schmotzer H. et al., 2000, ORS Orlando, 0572.
3 Deportes C., Duclo M., Fabry P., Fouletier J., Hammou A., Kleitz M., Siebert E., Souquet J-L., Electrochimie des Solides, Ed. Presses Universitaires de Grenoble, 1994, 1782-186, 300-320.

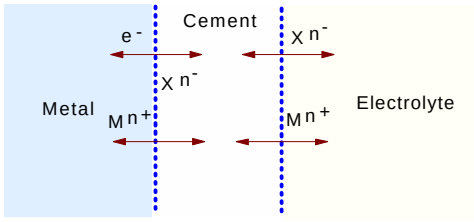

Fig. 3 Schematic representation of the exchange process between the metal - cement – electrolyte**.**

European Cells and Materials Vol. 3. Suppl. 1, 2002 (pages 34-35) ISSN 1473-2262

THERMOMETRIC STUDY OF BRUSHITE CEMENTS

S. Rousseau, M. Bühler, J. Lemaître

Laboratoire de Technologie des Poudres, EPFL, MX-Ecublens, 1015-Lausanne

INTRODUCTION: This study is part of a broader work on Brushite cements [1]. The effects of various experimental factors on the working characteristics of Brushite cements are being investigated, with the aim of understanding the physico-chemical aspects of the setting and consolidation processes, and the mechanisms of the chemical reactions leading to consolidation.

In the present study, thermometric measurements are being used in order to monitor the early stages of the setting and hardenig processes of Brushite cements. The thermometric approach gives acces to useful working characteristics such as working and setting times, in very good agreement with standard experimental techniques such as the Vicat needle method.

METHODS:

Principle of the method : Advantage is taken of the fact that the setting reactions leading to brushite formation are slightly exothermic.

A freshly prepared cement paste (about 2 mL) is inserted into a polyurethane foam block placed within a Dewar flask, and covered with an insulating lid ; thus, the sample is thermally insulated in a way similar as it would be upon implantation into cancellous bone. A thermocouple is stuck in the middle of the cement sample. Temperature is sampled every few seconds and recorded by a computer (Fig. 1). The thermometric curve results from two competing processes : heat is generated by the chemical reactions responsible for the consolidation of the cement and slowly dissipated by thermal conduction through the walls of the container and through the thermocouple. Compensation for thermal dissipation can be calculated from a control thermometric curve (Fig. 2), obtained by placing in the measuring cell a sample of hardened cement preheated to about 45°C, and recording its cooling curve.

The kinetics of enthalpy production due to the consolidation reactions is obtained by summing the apparent enthalpic curve and the thermal dissipation curve deduced from the experimental and control thermometric curves (Fig. 3).

The progress of the cementation reaction is calculated by taking the ratio of the measured enthalpy over the theoretical reaction enthalpy (which can be calculated on the basis of known thermochemical data). The kinetic curve (Fig. 4) shows a sigmoidal shape, from which several characteristics of the consolidation process can be deduced : induction (or working) time, setting time, maximum β-TCP conversion.

Full details on the experimental setup and on the treatment of the experimental data are presented in reference [2].

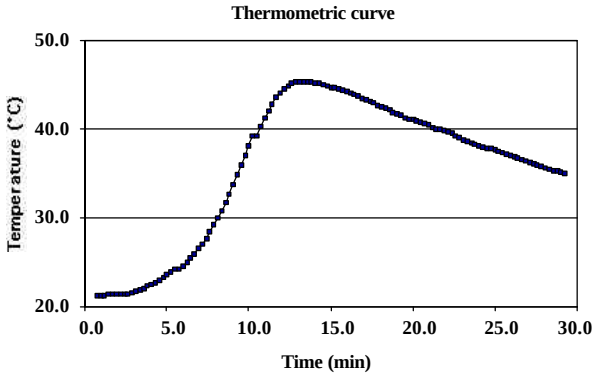

Figure 1. Experimental thermometric curve.

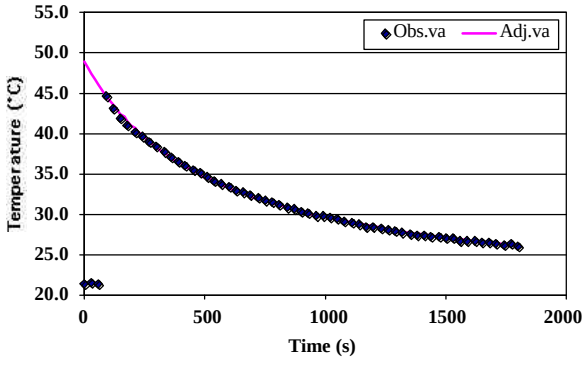

Figure 2. Control thermometric curve.

EXPERIMENTAL DESIGN :

Table I. Definition of factors and levels in the experimental design

Factor	Definition	Low Level	High

			Level
A	Polymer*	HA	HPMC
B	Sulfate	Plaster	Sulf. Ac.
C	Magnesium°	0 %wt	8 %wt
D	Porosity	35%vol	45%vol

* HA : Hyaluronic acid ; HPMC : Hydroxypropylmethyl cellulose. ° In the form of $Mg.HPO_4.2H_2O$ (Newberryite).

Experimental factors summarized in Table I have been selected on the basis of previous *in vivo* and *in vitro* studie, which have shown considerable changes in biodegradability of brushite cements according to the presence of Mg, sulfate ions and on the nature of hydrosoluble polymers incorporated for rheological control. The experiments were organised into a 2^4 multifactorial statistical design. The results were analysed using the ANOVA technique.

RESULTS AND DISCUSSION:

Thermometric observations show a systematic decrease of the maximum temperature for Mg–containing samples. Statistical analysis of the results expressed in terms of maximum β–TCP conversion (Fig. 5) demonstrates clearly a marked inhibitory effect of Mg on the consolidation reactions ; the effect is more contrasted for samples with 35%vol porosity containing hyaluronic acid. The presence of sulfate in any form does not seem to play any significant role.

Thus the presence of Mg, especially in conjunction with hyaluronic acid appears to inhibit strongly the chemical reactions leading to the formation of brushite.

CONCLUSIONS: A new experimental approach based on thermometric measurements allows to calculate the kinetics of enthalpy production, and hence the kinetics of transformation of calcium phosphate cements. These kinetic curves allow to calculate several working characteristics of the cements : working and setting times, maximum fraction of converted β-TCP, reaction rate, maximum temperature increase upon cement consolidation.

Based on thermometric analysis, the inhibiting effect of magnesium on the setting reaction of Brushite cement has been clearly evidenced.

REFERENCES:

[1] A.A Mirtchi, J.Lemaître, N.Terao. Calcium phosphate cements : study of the β-Tricalcium phosphate-monocalcium phosphate system. Biomaterials, 10 [septembre] 475-480 (1989).

[2] C. Pittet "Development and Characterisation of Injectable Calcium Phosphate Cements for Use in Vertebroplasty." Thesis n° 2509, EPFL, 2001.

ACKNOWLEDGEMENTS: The support of the Robert Mathys Foundation and of Stratec Medical is gratefully acknowledged.

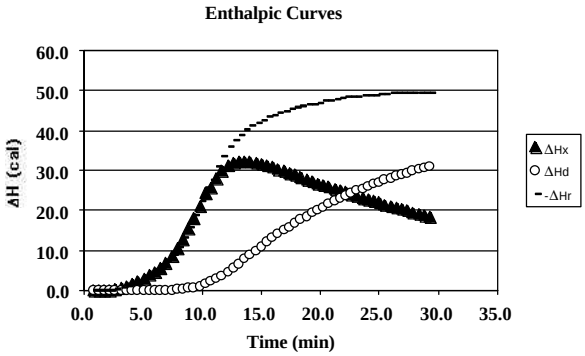

Figure 3. Enthalpic curves : $\bullet H_x$ experimental enthalpy vs time ; $\bullet H_d$ dissipated enthalpy.

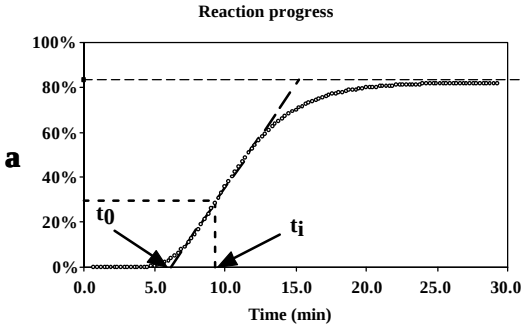

Figure 4. Reaction progress *vs* time. t_o : working time ; t_i setting time.

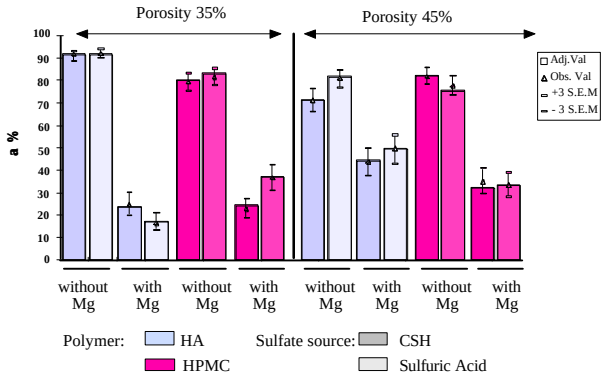

Figure 5. Evolution Effects of experimental factors on the ultimate conversion of the cement.

HEMOCOMPATIBILITY OF SEMI-CONDUCTING BIOMATERIALS

K. Unal[1], Y. Mugnier[1], N. Nurdin[1], J. Krumeich[2], P. François[3], B.-O. Aronsson[1] & P.Descouts[1]

[1]*GAP Biomedical, University of Geneva, CH,* [2] *Sulzer Innotec, Winterthur, CH ,*
[3]*Div. of Infectious Diseases, University Hospital of Geneva, CH*

INTRODUCTION: Hemocompatibility of an implant is determined by its surface properties. According to recent suggestions [1], the involvement of electron exchange can occur in adsorption process from physiological media. This electron transfer may induce conformation changes of adsorbed proteins and cause their degeneration. Therefore materials with large band gaps and high work function could be advantageous and the knowledge of the surface electronic properties of biomaterials at the nanometer scale is crucial.

In addition to the physico-chemical characterization, tests to determine the interactions between the modified surface and the blood proteins and platelets are important to perform. For this the measurements of both fibrinogen adsorption and platelets adhesion are important for determining the relative thrombogenic potential of a material. Today, it is proved that synthetic materials adsorbing less fibrinogen from blood plasma do also adhere fewer platelets and thereby exhibit improved blood compatibility. The aim of this project is to characterize the surface electronic properties of different semi-conducting biomaterials using Electrostatic Force Microscopy (EFM) with AFM instrumentation, and to observe by confocal microscopy the platelet adhesion and aggregation from platelet-rich human blood plasma.

METHODS: In EFM [2], the Contact Potential Differences (CPD) are measured at the nanometer scale in an analogous manner to conventional Kelvin Probe Spectroscopy. An electrostatic force is induced between the conductive tip of an AFM and the sample surface by applying an AC bias voltage of frequency ν to the tip (already vibrating at its resonance frequency ν_0). The convoluted signal of the CPD between the sample and the tip and the gradient of the capacitance is obtained from the amplitude at ν, while at 2ν only the gradient of the capacitance is measured. The local work function of different DLC coatings was obtained by performing spectroscopy. The AFM tip was kept stationary on a desired surface point and a DC voltage was applied on either the tip or the sample. At a certain voltage, the amplitude at ν can be reduced to zero. This DC voltage corresponds to the difference of work function ($\Delta\phi$) between the sample and the tip coated with 10 nm of Pt. A commercial AFM working in controlled atmosphere (Relative humidity = 30% ±5%) was used. DLC coatings with a thickness of ca. 3 μm were deposited on Si wafers using plasma assisted CVD in a mixture of acetylene and argon. Three different types of coatings were studied. The first one is a standard DLC coating co-deposited with the sputtering of Ti. A dense DLC coating was produced using a sample potential of 75 V and a density gradient DLC coating was deposited by varying the sample potential from 25 to 75 V. These two latter coatings were deposited in a metal free procedure.

To observe the platelet adhesion on previously described materials, confocal laser microscopy (CLM) and/or epi-fluorescence measurements will be used. A custom-made set-up was thus implemented on a commercial inverted microscope (Nikon Eclipse TE300) in order to combine CLM, epi-fluorescence and classical optical imaging. The sample is scanned in a confocal arrangement on a servo-controlled x,y,z scanner. Using either a 40* (0.6 NA dry), or a 100* (1.3 NA oil immersion) objective, the lateral resolution (depth discrimination) are, respectively 0.5 μm (5 μm) and 0.3 μm (0.9 μm), as determined from response curves measured on fluorescent micro-spheres. For a high s/n-ratio, the fluorescence signal is detected by an avalanche photo-diode (EG&G) and the image constructed in a PC.

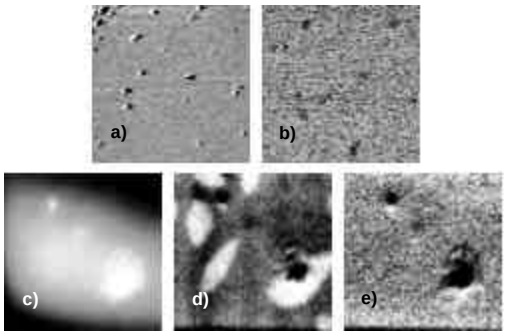

Fig. 1: Convoluted surface potential and capacitance gradient image for a) dense and b) density gradient DLC coating (scan size 2 mm); c) Topography, d) Surface potential and Capacitance gradient, e) Capacitance gradient image of standard DLC coating (scan size 10 mm).

RESULTS: The dense and the density gradient DLC coatings showed smooth topographical AFM images. Homogeneous surface potential (Figure 1a and 1b) and capacitance gradient images were found. The CPD for the different DLC coatings and the reference Si wafer are shown in Table 1. The topography of the standard DLC coating was found to be rougher than the other two. As shown in Figure 1, the surface potential image (1d) exhibited spots of ca. 2-4 μm wide with a different surface potential which was not observed on the capacitance gradient image (1e).

Table 1. CPD of DLC coatings measured by EFM.

Sample	CPD [eV]
Ref. Si wafer	-0.68±0.02 eV
Dense DLC	0.11±0.05 eV
Density Gradient DLC	0.08±0.02 eV
Standard DLC	-0.33±0.02 eV

DISCUSSION & CONCLUSIONS: The metal free coatings show similar topographical and surface electronic properties, although the coating densities are different. The inhomogeneities observed for the standard DLC coating are interpreted as a TiC clustering during the co-deposition of Ti. This is evidenced by traces of Ti detected in the Auger spectra. In conclusion, an EFM was implemented with a resolution less than 40 nm. EFM on standard DLC coating showed surface inhomogeneities (metal clusters), not seen in a metal free deposition process. The CPD of different DLC coatings was determined. By confocal microscopy of platelet-rich blood incubated samples the platelet adsorption on the surfaces will be quantified.

REFERENCES: [1]A. Boltz *et al*. (1996) Coating of Cardiovascular Stents with a Semi-conductor to improve Their Hemocompatibility *Tex. Heart. Inst. J.*, **23** (2),162-166.[2]. M. Nonnenmacher *et al*. Kelvin probe force microscopy (1991) *Appl. Phys. Lett.*, **58** (25), 2921-2923.

ACKNOWLEDGEMENTS: M. Moret (GAP-biomedical) is gratefully acknowledged for technical support. This work is supported from the COST action 527 OFES No C01.0051.

2- AND 3-YEAR RESULTS OF ZIRCONIA POSTERIOR FIXED PARTIAL DENTURES, MADE BY DIRECT CERAMIC MACHINING (DCM)

I Zembic, H Lüthy, M Schumacher, P Schärer, C H F Hämmerle

Clinic for Fixed and Removable Prosthodontics and Dental Materials, School of Dentistry, University of Zurich, CH

INTRODUCTION: Today, Fixed Partial Dentures (FPD), made of a metallic framework covered by tooth colored ceramics exhibit a well documented long-term stability for the molar region. However, the use of some metals in the oral cavity has been disputed because of the risk of biological incompatibility. Furthermore, a grayish mucosal discoloration of the marginal region may leed to esthetic problems despite the ceramic veneering. Hence, there is a need for all-ceramic restorations offering sufficient stability for molar replacement. Zirconia combines excellent mechanical properties, widely documented biocompatibility and desired esthetic advantages due to its white color. The purpose of this study was to evaluate the clinical behaviour of zirconia posterior FPDs fabricated by direct ceramic machining (DCM).

METHODS: In 45 patients 58 zirconia FPDs replacing 1 to 3 posterior teeth were cemented with two composite cements (Variolink®, Panavia®). The zirconia frameworks were fabricated out of a porous pre-sintered TZP (tetragonal zirconia polycrystals) blank by milling a linearly enlarged copy of a framework model. Thereafter the frameworks were sintered to full density (DCM; ETH Zurich, Switzerland), allowing shrinkage to their final dimension. Subsequently they were veneered with porcelain. After 2 or 3 years respectively, the patients were re-examined and the following data were recorded on test- and control-teeth (neighbouring teeth, antagonists): i.)examination of the bridge for framework-fracture and chipping/fracture of the veneering material; ii.)recordings of pocket probing depth (PPD), probing attachment level (PAL), bleeding on probing (BOP), Plaque Index (PlI) and tooth mobility (TM); iii.)radiographical examination using single tooth films.

RESULTS: 2-year follow-up: 23 patients with 29 bridges were examined. No framework-fracture was observed. 2 bridges had to be replaced due to biological complications (root fracture, endodontic problem). Therefore, the survival-rate in this group was 93%. Minor porcelain chipping was reported in 10% (n=3), and 18% (n=16) of the abutments exhibited marginal discrepancies leading to secondary caries in 3% of the cases. No statistically significant differences were found between test- and control-teeth regarding PPD, PAL, BOP, PlI and TM ($p>0.5$; Wilcoxon Signed Rank Test).

3-year follow-up: 13 patients with 18 bridges were examined. Again, no framework-fracture was observed. 3 bridges had to be replaced: 1 due to a biological complication (endodontic problem), 1 because it was not correctly cemented and 1 because of loss of retention. Therefore, the survival-rate in this group was 83%. Minor porcelain chipping was reported in 5% (n=1) and 18% (n=6) of the abutments showed marginal discrepancies leading to secondary caries in 9% of the cases. No statistically significant differences were found between test- and control-teeth regarding PPD, PAL, BOP, PlI and TM.

DISCUSSION&CONCLUSIONS: Based on the results of this study it can be concluded, that zirconia-frameworks made by direct ceramic machining offer sufficient stability to be used for replacement of posterior teeth. Complications resulting from marginal discrepancies of the reconstructions need to be reduced by further refinements of the prototype DCM.

REFERENCES: [1]F Filser, H. Lüthy, P. Schärer, L. Gauckler (1998) *All-Ceramic Dental Bridges by Direct Ceramic Machining (DCM)* in: *Materials in Medicine*, Eds. M.O. Speidel et al.: vdf Hochschulverlag, ETH Zurich: Zurich.p.165-189. [2]B Sturzenegger et al. (2000) *Klinische Studie von Zirkonoxidbrücken im Seitenzahngebiet hergestellt mit dem DCM-Verfahren;* Acta Med Dent Helv 5: 131-139

ACKNOWLEDGEMENTS: This work was supported by the Swiss Priority Program for Materials Research.

European Cells and Materials Vol. 3. Suppl. 1, 2002 (pages 1-2) ISSN 1473-2262

MICROSTRUCTURE DESIGN OF ADVANCED BIOCERAMICS

P. Greil and F. Mueller, University of Erlangen-Nuernberg, Erlangen, FRG

INTRODUCTION: Bioceramics are increasingly being used clinically due to their compatibility with the physiological environment. While load bearing implants are made of high strength and wear resistant oxides such as Al_2O_3 and ZrO_2 a number of bioactive glasses and glass ceramics in the system Na_2O-CaO-SiO_2-P_2O_5-CaF_2 and Ca-Phosphate ceramics showing osteoconductive behavior serve for bone-repair and reconstruction of deseased or damaged skeletal parts [1]. Thus, applications of bioceramics include implants and restaurations in dentistry, joint replacements in orthopedics, bone reconstruction in maxillofacial surgery, and drug release and tissue engineering systems in pharmaceutical technology.

In the field of materials science and engineering zero shrinkage manufacturing, fiber composites processing and biomimetic interface bonding are among the current topics of advanced bioceramics development. In the following, recent work on microstructure design involving volume compensating reaction bonding systems, bioceramic fiber composite architecture, and *in situ* formation of calcium phosphate reaction layer at the implant/ tissue interface will be discussed.

RESULTS AND DISCUSSION:

A) Zero Shrinkage Manufacturing: Volume compensation of a bonding reaction which takes place between a matrix phase and a filler phase has recently become a promising approach for achieving a dimensional invariant shaping and densification of bioceramic components. Ideally, the volume change associated with the formation of the ceramic body from a starting powder mixture, Ψ, is given as

$$\Psi = \sum V_{educts} + P_{educt} - \sum V_{products} - P_{product} \ .$$

Making use of a selective expansion reaction in the educt powder mixture, zero shrinkage with $\Psi = 0$ can be obtained upon densification (e.g. porosity in the product $P_{product} \rightarrow 0$) when the volume of the reaction product, $\sum V_{products}$, equals that of the green body, $\sum V_{educts} + P_{educts}$. Possible reactions involving metal powders (Al, $ZrSi_2$, Ti) and gaseous (O_2) or liquid and solid polymeric ($CH_3SiO_{1.5}$) reactants are for example [2-4]

$2Al+3/2\ O_2 \rightarrow Al_2O_3$

$ZrSi_2+3O_2 \rightarrow ZrSiO_4+SiO_2$

$Ti+2(CH_3SiO_{1.5}) \rightarrow TiC+SiO_2+SiC+(H_2O+2H_2)\uparrow$

Typical reaction bonding temperatures can be rather low (< 1100°C) and the reaction bonded ceramics are distinguished by excellent mechanical properties (strength of RBAO Al_2O_3 > 700 MPa) which may further be improved by ZrO_2-toughening. Zero shrinkage manufacturing of bioceramic components is of particular relevance for complex shaped dental restaurations.

B) Bioceramic Fiber Composite Architecture: Bioactive as well as bioresorbable fibers are of particular interest for reinforcement of osteosynthetic biopolymer matrix composites and for cell carrying scaffold substrates. Hollow fibers of hydroxylapatite (HAP) ($Ca_5(PO_4)_3/OH$) and tricalciumphosphate (ß-TCP) ($Ca_3(PO_4)_2$) can be prepared by coating a template fiber with a powder slurry of controlled rheology, removal of the template and subsequent sintering. Continous as well as short fibers with an outer and inner diameter ranging from 50 to 200 µm and 10 to 100 µm, respectively, were prepared by coating polyamide or cellulose template fibers, Fig. 1, and subsequently used for reinforcement of polylactide composites.

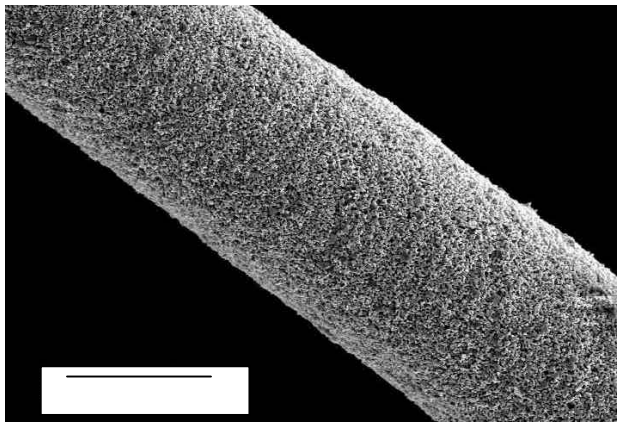

Fig. 1: ß-TCP hollow fiber derived by a continuous slurry coating process.

Electrochemical and electrophoretic deposition of the calcium phosphate phases from aqueous solutions or powder suspensions on fibrillar biocarbon templates derived from plant tissue is a novel approach which makes use of the hierarchical cellular anatomy of naturally grown tissue. Templates of appropriate cellular morphology mimicking the anatomical features of bone can be selected from a huge variety of biostructures as for example the one shown in Fig. 2.

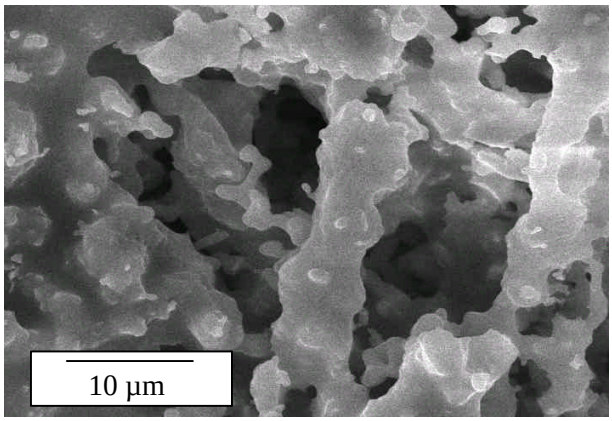

Fig. 2: Cellular HAP-bioceramic derived from a lingocellulosic template.

C) Biomimetic in situ formation of HAP interface layers: Todays implants have a variety of shortcomings related to their fixation behavior, and unlike living tissues, cannot self-repair or adapt to local physiological conditions. Conventionally physical (plasma spraying) and chemical (sol-gel) deposition processes are applied to form ceramic coatings on the implant surface. *In situ* formation of biologically active bone-like calcium phosphate interface bonding layers on metals, polymers and ceramics can be triggered in the physiological environment via a cation exchange process which induces local pH variation [5,6].

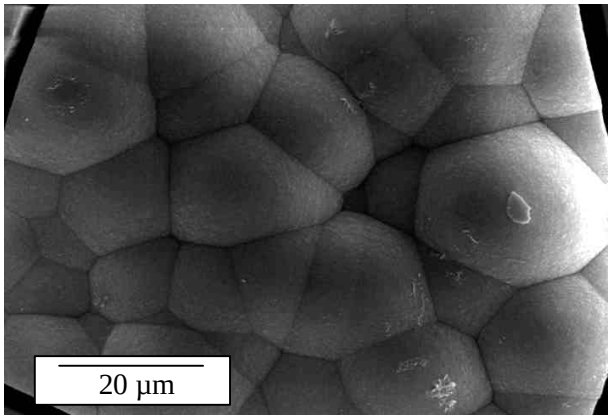

Fig. 3: SEM micrograph of Ti surface soaked for 14 days in SBF showing in situ grown HAP reaction layer.

Fig. 3 shows typical HAP surface structure of alkaline treated Ti after soaking in simulated body fluid (SBF) for 14 days. Formation of interface apatite at low alkaline concentrations is of particular relevance in order to reduce inflammatory response at the early stages of implant fixation [7].

The long-term alternatives to the more traditional use of bioceramics and bioceramic fabrications processes include the use of nanoceramics coupled with biofunctional molecules [8]. Enzymes, anti-bodies or specific receptors linked to nanoceramic particles are supposed to make new applications possible such as diffusible bio-markers and bio-sensors for medical diagnostics or nanoparticle carrier systems to be applied in therapeutics. Hierarchically structured biomaterial surfaces with a porous microstructure extending over several length scales provide the opportunity of improving the biomaterial/ tissue interface with respect to molecular, supramolecular and cellular interaction.

CONCLUSIONS: Tailoring the microstructure on various hierarchical levels is of particular significance for the development of advanced bioceramics with improved biomechanical and biochemical behavior. Novel approaches such as zero shrinkage and biomimetic processing offer the possibility for manufacturing of bioceramics which exhibit a better adaption to the physiological environment, performance and reliability.

REFERENCES: [1]L.L. Hench, Bioceramics, *J.Am.Ceram.Soc. 81* (1998) 1705-28. [2]S. Wu, D. Holz, N. Claussen, Mechanisms and kinetics of reaction-bonded aluminium oxide ceramics, *J.Am. Ceram.Soc. 76* (1993) 970-80. [3]V.D. Hennige, J. Haußelt, H.J. Ritzhaupt-Kleissl, T. Windmann, Shrinkage-free $ZrSiO_4$-ceramics: Characterisation and Applications, *J.Europ.Ceram.Soc. 19* (1999) 2901-08. [4]P. Greil, Pyrolysis of Active and Passive Filler-Loaded Preceramic Polymers, in *Handbook Advanced Ceramic Materials Science*, edt. S. Somiya, Academic Press. (2002), [5]T. Kokubo, Forma-tion of biologically active bone-like apatite on metals and polymers by a biomimetic process, *Thermoch.Acta 280/281* (1996) 479-90. [6]H. Barrere, P. Layrolle, C.A. Van Blitterswijk, K. De Groot, Biomimetic coatings on titanium: a crystal growth study of octacalcium phosphate, *J.Mat.Sci. Med. 12* (2001) 529-34. [7]L. Janasova, F.A. Müller, A. Helebrant, J. Strnad, P. Greil, Hydroxyapatite formation on alkali-treated titanium with different content of Na^+ in the surface layer, to be publ. in *Biomaterials* (2002). [8]C.M. Niemeyer, Nanopartikel, Proteine und Nucleinsäuren: Die Biotechnologie begegnet den Materialswissenschaften, *Angew. Chem. 113* (2001) 4254-87.

European Cells and Materials Vol. 3. Suppl. 1, 2002 (pages 3-4) ISSN 1473-2262

CONTROLLED LOCALIZED DELIVERY OF INSULIN LIKE GROWTH FACTOR I (IGF I) INDUCES NEW BONE FORMATION: THE SIGNIFICANCE OF RELEASE KINETICS

V. Luginbühl[1], B. v. Rechenberg[2], J. Zapf[3], E. Zoidis[3], J. A. Auer[2], H. P. Merkle[1], L. Meinel[1]

[1]Drug formulation and delivery, ETH Zürich, CH, [2]Department of Veterinary Surgery, University of Zürich, CH, [3]Division of Endocrinology, University of Zürich, CH

INTRODUCTION: It is estimated that five to ten percent of the 6.2 million fractures occurring annually in the United States result in delayed or impaired healing. Osteoinductive agents are a possible avenue to augment surgical procedures or treat the plethora of standard fractures. A great challenge presented in the science of biological bone growth factors at this time seems to be developing the best delivery mechanism and kinetic. Direct injection or oral applications do not present appropriate remedy, but the controlled localized delivery of osteoinductive therapeutics from polymeric biodegradable implants is a valid alternative. We have demonstrated a marked capacity of IGF I to bridge non-union defects, when delivered in a controlled localized fashion[1,2]. We report the impact of release kinetics and polymer choice on new bone formation within sheep fracture models and concomitant changes in the expression of various marker genes relevant for bone formation, resorption, and turnover.

METHODS: IGF I was encapsulated in various types of poly (lactide-co-glycolide) (PLGA 502H, 502, 503H, 752) and poly-lactide (PLA 202) microspheres (MS) using solvent evaporation (loading 0,1%). IGF I in vitro release kinetics from the microspheres were monitored for 72 days by radioimmunoassay (RIA) analysis. The in vivo study was performed in 6 sheeps in an 8 mm drill hole defect model (8 defects per animal). Each defect received either (i) 100 mg unloaded microspheres or (ii) 100 mg MS loaded with 100 µg IGF I (IGF I-MS) or (iii) were left unfilled (negative control). Three animals were sacrificed after 3 weeks and another three 6 weeks post operation. The bones were cut, and slices prepared for histology (acrylic resin embedding, grinding and thin sections were stained with toluidine blue/von Kossa) and for RNA extraction[3]. Upon reverse transcription, the gene expression of pro- and inflammatory proteins (interleukins 1α and 6, cyclooxygenase 2), inducible NO synthetase, and morphogeneic factors (platelet derived growth factor A, transforming growth factor β 1, fibroblast growth factor, IGF I) was analysed by real-time polymerase chain reaction.

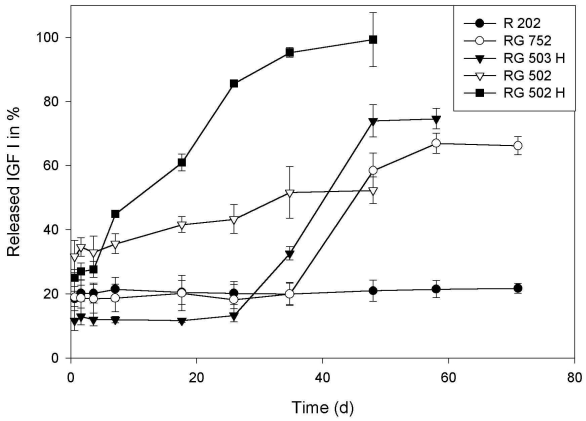

Fig. 1: In vitro release of IGF I from different microsphere formulations.

RESULTS: IGF I in vitro release was monitored over 72 days (Fig. 1).

Three weeks postoperatively, all IGF I treated defects showed consistent new bone formation adjacent to the defect borders. In case of defects treated with IGF I encapsulated in faster degrading PLGA 502H an increased density of granulation tissue and capillaries was observed in the interior defect. Hypertrophic osteoblasts lined the bone surfaces, actively depositing osteoid. In all IGF I treated defects the inflammatory infiltrate characteristic for early reparative changes of fracture healing was highly reduced and foreign body cells were rarely found.

Defects treated with unloaded microspheres showed a fatty in-growth, some granulation tissue formation and an increased inflammatory reaction. This inflammation was more pronounced in defects treated with faster degrading microspheres. On a genome level this finding is corroborated by a reduced expression of inflammatory genes in IGF I treated defects. Little numbers of osteoblasts lining bone surfaces laid down significantly less osteoid compared to IGF I treated defects.

After six weeks, all IGF I-MS treated defects showed a well-organized network of woven bone

within the defects and the pre-existing trabeculae were lined with hypertrophic osteoblasts that laid down thick layers of osteoid (except IGF I loaded PLGA 502 MS). Osteoblast number and matrix deposition rates were especially advanced in defects receiving slow degrading IGF I microspheres prepared with either PLGA 752 or PLA 202 (Fig. 2), respectively.

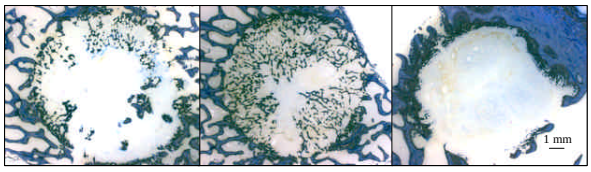

Fig. 2: Grinding sections of IGF I-MS loaded defects 6 weeks post operation (staining toluidine blue).

In defects treated with unloaded microspheres, osteoblasts were inactive depositing few osteoid. In some of these defects the bone ends were covered by fibrous and fibrocartilaginous tissue and showed signs of increased osteoclastic activity.

DISCUSSION & CONCLUSIONS: Controlled localized delivery of IGF I induces efficiently new bone formation. The degree of new bone formation largely depends on release kinetics. This new bone formation is due to an increased osteoblastic and a decreased osteoclastic activity upon IGF I delivery compared to control defects and those treated with unloaded MS. Presence of inflammatory cells is low in IGF I treated defects and this finding is corroborated by a reduced expression of inflammatory marker genes in IGF I-MS treated defects.

REFERENCES: [1] Meinel L, Auer JA , Schneider R, Illi OE, Merkle HP, Rechenberg B (2001) Complete bridging of critical-size bone defects in sheep following controlled localized delivery of insulin-like growth factor I. *submitted*. [2] Meinel L, Zapf J, Zoidis E, Auer JA, Illi OE, Gander B, Merkle HP, Rechenberg B (2001) Enhanced bridging of experimental bone defects in sheep by controlled localized delivery of insulin like growth factor I. *submitted*. [3] Chirgwin JM Przybyla AE MacDonald RJ Rutter WJ (1979) Isolation of biologically active ribonucleic acid from sources enriched in ribonuclease. *Biochemistry*, **18**, 5294-5299.

ACKNOWLEDGEMENTS: We are deeply indepted to Kati Zilinsky, Sabrina Wunderlin and Jessica Müller.

European Cells and Materials Vol. 3. Suppl. 1, 2002 (pages 5-6) ISSN 1473-2262

EARLY DURAL REACTION TO POLYLACTIDE IN CRANIAL DEFECTS OF RABBITS

A. A. Mueller[1], C. S. Leiggener[2], R. Curtis[3], B. Rahn[4]

[1,4]*AO Research Institute, Davos, CH,* [2]*University Hospital Basel, CH,* [3]*AO Development Institute, Davos , CH*

INTRODUCTION: Cranial through-and-through defects, exceeding a certain size do not heal spontaneously[1] and therefore frequently require surgical treatment. One approach uses the principle of guided tissue regeneration[2] by placing a mechanical barrier to preclude soft tissue ingrowth and thus to enhance the regeneration of new bone. The application of biodegradable instead of non-biodegradable material leads to various advantages e.g.: no second surgical procedure for membrane removal, no sequels due to permanent membrane retention, no growth restrictions, spontaneous disintegration in case of passive translocation during growth. These advantages are very useful in cranial surgery, particularly in the growing skull.

Before application in the neurocranium and therefore in vicinity to neural tissue can be considered any hazards must be excluded. In the early stage of polymer degradation biological reaction depends on the material itself and on possible chemical residues from the processing, while in the later stage the biological reaction depends mainly on the degradation products and their molecular weight.

In this study we investigated the dural reaction during the early stage after implantation of polylactide implants into cranial defects in rabbits.

METHODS: We used two implant systems, which consisted of a burr hole cover, four fixation dowels, a perforated strip and an endocranial membrane. One series was manufactured from poly(L/DL-lactide) 70:30 the other was manufactured from poly(L/DL-lactide) 80:20. The membranes were all 0.3 mm thick.

The burr hole covers, endocranial membranes and perforated strips were manufactured by the melt extrusion process, followed by laser cutting. Fixation dowels were injection moulded. The molecular weight of the raw materials was approximately 600’000 Daltons. All implants were sterilised by 30 kGy gamma irradiation.

Implants were applied to the bone in a sandwich manner. The endocranial membrane was placed at the inner surface of the neurocranium in direct contact to the dural tissue without mechanical fixation. The perforated polylactide strip of 3 x 15 mm was then formed in a “z” shape and placed perpendicular to the inner membrane to maintain the bone thickness of approximately 3 mm. The burr hole cover was then fixed onto the outer surface of the skull with four fixation dowels.

Twenty clinically healthy adult female New Zealand rabbits were used in this study. Sixteen underwent surgery and four served as controls. Two 8.3 mm diameter full thickness cranial defects were made, one in each parietal bone, and not touching any cranial sutures. Implants from poly(L/DL-lactide) 70:30 were applied to the first defect and implants from poly(L/DL-lactide) 80:20 were applied to the second defect. The side distribution was randomly assigned in each rabbit.

The animals were sacrificed eight weeks postoperatively. The undecalcified specimens were plastic embedded and sectioned in a coronal direction for contact radiographs, Giemsa/Eosin staining and microradiographs. The light-microscopic evaluation focused on the endocranial polylactide membrane, the interface and the underlying dural tissue. The findings were compared to non-operated specimens and to specimens having only burr hole covers on the outer surface of the skull[3].

RESULTS: All 16 rabbits recovered with no neurological complications. Macroscopically there were no signs of inflammation and no implant was rejected. Microscopically all endocranial membranes prevented the intracranial tissues from herniation into the bony defect. 3 out of 32 membranes had an oblique position protruding into the osseous defect. The formerly transparent polylactide turned to a milky white color. The periphery of the membrane was still continuous with few signs of polymer degradation while the core of the membrane showed variable structural changes.

Along the membrane-dura interface only few giant cells were detected, equal in both types of poly(L/DL-lactide). They were more numerous on the membrane-dura interface than on the bone defect side. The dura had a smooth surface towards

the brain as well as towards the poly(L/DL-lactide) membrane.

In about 80% of all specimens a formation of osseous islets within the dura was detected, equal in both types of poly(L/DL-lactide). The formation of the osseous islets was limited to the dura section along the poly(L/DL-lactide) and raised at any place in the dura. The thickness was variable up to 1 mm while the cranial bone thickness was about 3 mm.

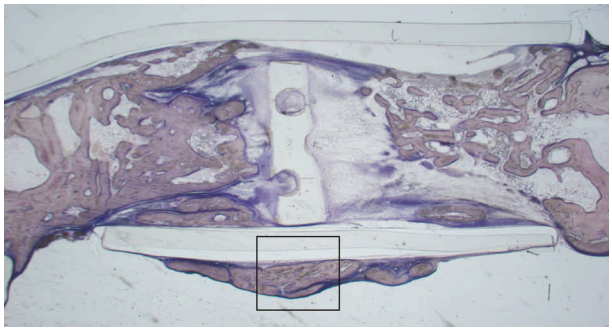

Fig. 1: Osseous islets formation within the dura 8 weeks after insertion of a polylactide disk into a full thickness cranial defect in a rabbit.

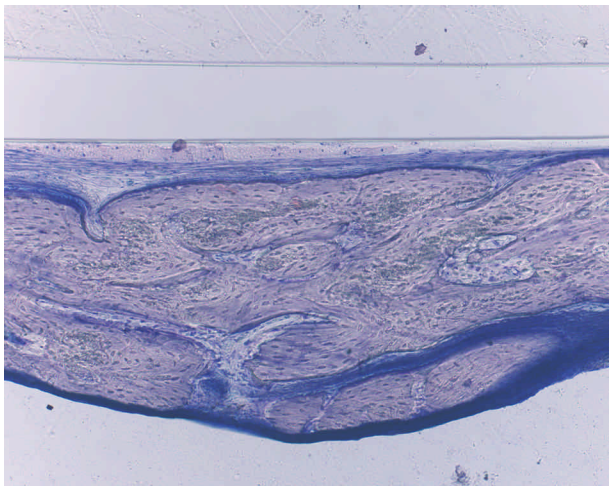

Fig. 2: Details of the osseous islet. The bone is completely lined with connective tissue.

The osseous islets were always limited by a thin dural layer and never stayed in direct contact neither to the poly(L/DL-lactide) membrane nor to the underlying neural tissue. No signs of acute inflammation and no granulation tissue were seen.

The non-operated control specimens showed a normal dura consisting only of dense connective tissue. The specimens having only burr hole covers on the outer surface of the skull showed regular bone formation from the dura towards the defect areas. These bone formations mixed and merged with islets of proper bone regeneration originating from the burr hole edges.

DISCUSSION & CONCLUSIONS: During the observed time the biodegradable poly(L/DL-lactide) membranes were well tolerated by the neurocranium. The dura showed neither acute inflammation nor marked connective tissue reaction. No differences between the two types of poly(L/DL-lactide) were detected. The ectopic osseous formation within the dura shows the osteogenic potential of the dura. This dural bone formation takes place regardless of dura being in direct contact to the regenerating tissue or being separated from the defect by a polylactide membrane. The dural bone formation showed no adverse effect during the observed time, as the amount of bone formation was limited. The biocompatibility of both types of polylactide was good during the observed early stage of biodegradation disclosing no adverse processing residues.

A long-term study would be necessary to investigate first the biocompatibility during the later stage of biodegradation. Second this would demonstrate whether the dural bone islets merge with the cranial bone or not after complete degradation of the endocranial membrane. A persistence of larger zones of dural calcification would be undesired especially in the growing skull of young patients.

REFERENCES: [1] J. P. Schmitz (1986) *The Critical Size Defect as an Experimental Model for Craniomandibulofacial Nonunions*. Clin Orthop (205):299-308. [2] S. Nyman (1982) *The Regenerative Potential of the Periodontal Ligament. An Experimental Study in the Monkey*. J Clin Periodontol 9(3):257-65. [3] C. S. Leiggener (2002) *Effect of Perforations in Burr Hole Covers on Cranial Bone Regeneration in Rabbits.* J Biomed Mater Res (in press).

ACKNOWLEDGEMENTS: Financial support for this work was obtained from the Margarete und Walther Lichtenstein Stiftung, Basel, Switzerland.

European Cells and Materials Vol. 3. Suppl. 1, 2002 (pages 7-8) ISSN 1473-2262

SURFACE MODIFICATION OF POLY(VINYL CHLORIDE) INTUBATION TUBES TO CONTROL BACTERIAL ADHESION : TEFLON-LIKE AND PLURONICS®

D.J. Balazs[1], C. Hollenstein[2] & H.J. Mathieu[1]

[1] *Materials Institute, Swiss Federal Institute of Technology, Lausanne, CH,*
[2] *Plasma Physics Research Center, Swiss Federal Institute of Technology, Lausanne, CH*

INTRODUCTION: *Pseudomonas aeruginosa* is one of the most prevalent bacterial strains in a clinical environment, responsible for 30% of nosocomial pneumonia cases occurring in intubated and mechanically ventilated patients [1]. Colonization of the intubation device leads to mortality for over 40% of these cases, despite aggressive antibiotic therapy. Therefore, a strategy to reduce bacterial adhesion to intubation tubes is desirable. We are developing an approach based on the surface modification of the polymer used for this application, medical grade poly(vinyl chloride) (PVC). This paper investigates a method to prevent protein adsorption and eventual bacterial adhesion, as protein adhesion is believed to be a key event responsible for specific adhesion of bacteria to a surface.

The strategy is to mask the PVC substrate with a chemically inert Teflon-like fluoropolymer layer, which serves as an ideal platform for further surface modification due to its low surface energy properties[2]. By exploiting hydrophobic-hydrophobic interactions, we then bind protein and bacterial resistant[3,4] molecules, such as amphiphilic Pluronics®, to the fluoropolymer film.

METHODS:

This paper investigates fluoropolymer films created on PVC substrates through plasma-enhanced chemical vapor deposition. The films are deposited in a RF-plasma reactor, using C_2F_6 as a precursor and H_2 as a carrier gas. The PVC substrates were 1cm^2 sections cut from Mallinckrodt Medical Hi-Lo endotracheal tubes, which were flattened to allow the eventual microscopic counting of bacteria.

Further surface modification of the Teflon-like surfaces is completed through an incubation in Pluronic® (BASF) F108, a tri-block copolymer containing hydrophilic PEO and hydrophobic PPO chains.

Protein adhesion to the various surfaces is studied by incubating the samples in bovine serum albumin and fibrinogen, for a period of 3 h, at 37°C. The concentrations of albumin and firinogen used were 1 mg/ml, and 0.2 mg/ml, respectively.

XPS analysis of the various surfaces is performed using an imaging Kratos Axis Ultra (UK) X-ray photoelectron spectrometer equipped with a hemispherical analyser. The X-ray source employed is a monochromatized Al *Kα*.

Surface wettability is determined by contact angle measurements of deionized water sessile drops, using a microscope equipped with a goniometer (Krüss GmbH, Hamburg, Germany).

RESULTS: Teflon-like deposition on PVC yields a 21° increase in contact angle to a value of 104° for an 80% flow of C_2F_6 (*Fig. 1*). When C_2F_6 percentage is varied from 20% up to 80%, the contact angle increase is shown to be directly related to the quantity of CF_x groups incorporated in the film (data not shown), where 80% C_2F_6 shows the highest amount of fluorinated groups.

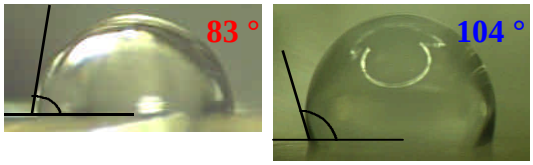

Fig. 1:Effect of Teflon-like deposition on surface wettability: native (left) and Teflon-like (right).

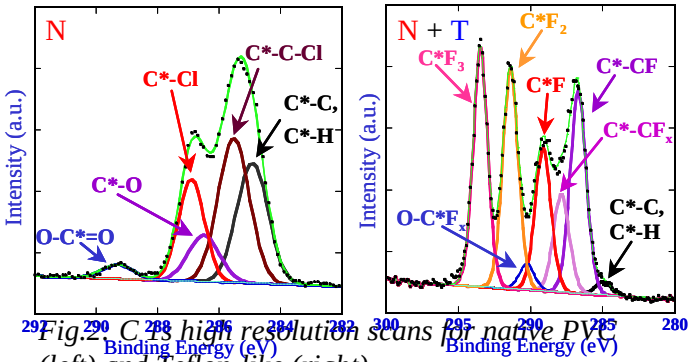

Fig.2: C 1s high resolution scans for native PVC (left) and Teflon-like (right).

The C 1s high resolution scans of the Teflon-like films show that the native PVC is completely masked as there are no signatures, such as C-Cl, remaining (*Fig. 2*). Moreover, there is significant fluorocarbon group incorporation, including C-CF_x, C-F, C-F_2, C-F_3, which are all indicative of a Teflon-like layer. Pluronic® F108 does not adsorb to untreated native PVC. There is no change in contact angle for the native PVC following incubation with the F108 (Fig.3). Pluronic® F108 adsorption is achieved following Teflon-like

deposition on native PVC. Contact angle measurements confirm this as the contact angle of Teflon-like decreases by 14° following the F108 incubation (Fig.3). The O 1s high resolution scan of F108 incubates samples shows the incorporation of O-C groups, which are not present prior to incubation (data not shown).

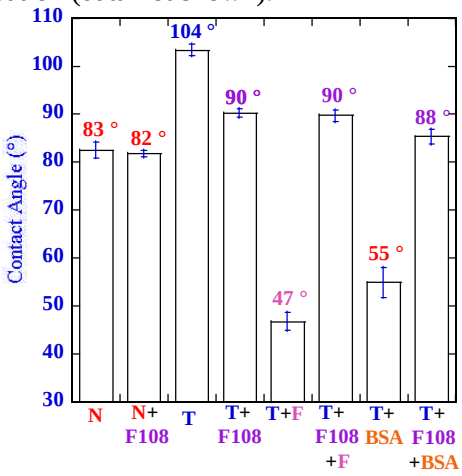

Fig.3: Contact angle evolution for native, Teflon-like and F108 modified samples. The graph also illustrates the evaluation of protein adhesion.

Pluronic® F108 incubation prevents fibrinogen adsorption to Teflon-like coated Native PVC. The T + F108 + Fibrinogen contact angle is identical to T + F108 (Fig.3), and nitrogenated functional groups representative of fibrinogen adsorption are absent on the O 1s high resolution scan following F108 modification. Pluronic® F108 also prevents albumin adsorption, as the contact angle follows the same trend as fibrinogen (Fig.3).

DISCUSSION & CONCLUSIONS: Teflon-like deposition on native PVC yields, a reproducible, hydrophobic surface modification, which serves as an excellent platform for further surface modification with Pluronic® F108. As shown by XPS analysis, the fluoropolymer completely masks the native surface, as no signatures of PVC are detectable following deposition. Contact angle measurements of the Teflon-like surfaces show that the PE-CVD techniques used yield a highly hydrophobic film (104°), where the contact angle achieved directly depends on the feed of C_2F_6 used during the deposition. Higher feeds of C_2F_6 allow for a greater incorporation of hydrophobic fluorocarbon groups in the film.

Pluronic® F108 does not adsorb to untreated native PVC, because the hydrophobic interactions are not strong enough to attract and bind the molecule. Pluronic® adsorption to PVC is only achieved following deposition of a Teflon-like film. XPS analysis shows evidence of F108 adsorption to Teflon-like surfaces through the detection of O-C functional groups, which are not present following incubation of the molecule with native PVC. The reason for the adsorption to the Teflon-like film is the increased hydrophobicity, a 21° increase compared to native PVC surfaces. Contact angle measurements confirm the XPS data. Following Pluronic® F108 incubation with the Teflon-like samples there is a 14° decrease in contact angle, which indicates a surface modification. Following incubation with native PVC substrates, the contact angle remains unchanged.

Pluronic® F108 incubation is capable of preventing albumin and fibrinogen adsorption to Teflon-like coated PVC. Following incubation of fibrinogen and albumin to Teflon-like surfaces the contact angle drops from 104° to 47° and 55°, respectively. This decrease in contact angle indicates adsorption of proteins to the Teflon-like surface. This hypothesis is confirmed by XPS analysis, which detects nitrogenated functional groups characteristic of protein adsorption, such as O=C-N. However, following F108 modification of the Teflon-like surfaces, XPS analysis does not detect the functional groups indicative of protein adsorption. The O 1s high resolution spectra for the F108 modified samples which had been incubated in the protein solutions is identical to that of the F108 modified samples. Moreover, the contact angle of F108 modified surfaces following protein incubation, remains unchanged demonstrating the anti-fouling properties of the Pluronic® F108 molecules.

In conclusion, data from XPS analysis and contact angle measurements confirms that Pluronic® F108 modification of Teflon-like films is capable of producing surfaces resistant to protein adhesion. As protein adhesion is believed to be the triggering event in the inflammatory response and eventual failure of biomaterials, this method could prove to be useful in creating anti-fouling surfaces.

REFERENCES: [1] J. L. Vincent, D. J. Bihari, P. M. Suter et al (1995) *JAMA* **274**: 639-644. [2] I. Noh, K. Chittur, S. Goodman, J. Hubbell (1997) *J Polym Sci Poly Chem* **35**: 1499-1514. [3] M. J. Bridgett, M.C. Davies, S. P. Denyer (1992) *Biomaterials* **13**: 411-416. [4] M. Paulsson, M. Kober, C. Freij-Larsson et al (1993) *Biomaterials* **14**: 845-853.

ACKNOWLEDGEMENTS: We acknowledge financial support of Common Program on Bio-medical Engineering and Research, Univ.of Geneva and EPFL, (1999-2002).

European Cells and Materials Vol. 3. Suppl. 1, 2002 (pages 9-10) ISSN 1473-2262

ELECTRON MICROSCOPY ON TITANIUM IMPLANTS FOR BONE REPLACEMENT AFTER "SLA" SURFACE TREATMENT

E. Conforto[1], D. Caillard[2], B-O. Aronsson[3]& P. Descouts[3]

[1]*Swiss Federal Institute of Technology, Lausanne, CH,* [2]*CEMES/CNRS, Toulouse, FR,*
[3]*GAP Biomedical, University of Geneva, CH*

INTRODUCTION: Because the chemical interaction between the implant and the biological tissue is too weak to account for the fixation, the implant stability depends on good mechanical interlocking. The interest for the influence of surface roughness on biological interactions has recently increased as well as that for bone-anchored implants. Titanium is a very good material for this kind of implant due to its biocompatibility.

The SLA ("Sand-blasting and acid etching") surface treatment on Ti implants has as goal to control the surface roughness, to improve osseointegration and to increase the stability of bone-anchored dental implants. This treatment consists of bombarding the surface with a jet of Al_2O_3 particles followed by an acid etching. From this treatment results a two-level roughness: sub-micron porosity, caused by the acid etching, superimposed to the 30-200 µm roughness, due to the bombardment.

Previous works[1] highlighted the presence of hydrogen in the sub-surface layer after acid etching. Authors have formulated the hypothesis of the formation of another phase, a titanium hydride. The aim of this work is to identify this layer highlighting the crystallographic relationships with the substrate. The layer adherence will be evaluated as well as its mechanical properties.

METHODS: Commercially pure titanium disks were submitted to the SLA surface treatment after polishing. Samples were provided by Institut Straumann AG, Waldenburg, CH. Surface observations after SLA treatment were performed by scanning electron microscopy (Philips XL-30, 10 kV). Crystallographic relationships between the surface layer and the substrate as well as dislocations in the layer were observed in cross-sectional specimens by transmission electron microscopy (Philips EM-430, 300 KV). Specimens were prepared by mechanical polishing followed by ion bombardment. Observation techniques were: Bright and Dark Field images and Electron Diffraction.

RESULTS: SEM observations clearly show the desired porosity (Fig. 1) after SLA treatment on Ti surface. TEM cross-sectional observations confirmed the expected surface profile and also revealed the existence of an interface between the α-Ti substrate, with a hexagonal structure, and tips formed during the acid etching (Fig. 2, top). No other layers, either interfacial or superficial, were detected. In all cases examined these tips are constituted of one or several grains of an FCC phase identified as $TiH_{1.971}$.

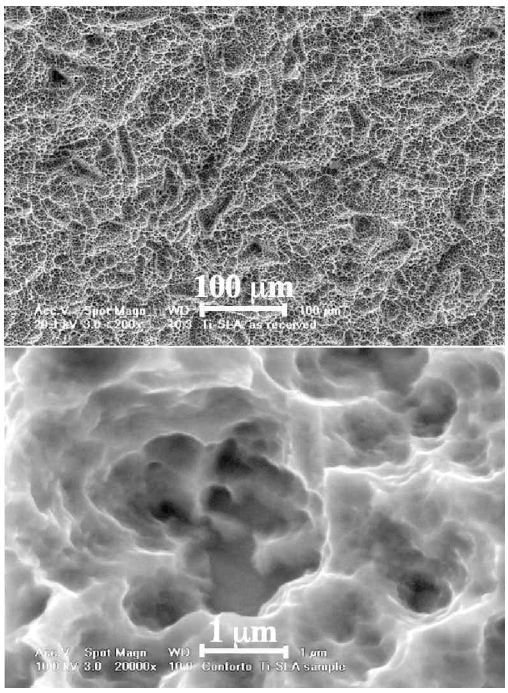

Fig. 1: Ti surface after SLA treatment: general view showing the 30 µm roughness (left); detail, showing micro-porosities (right).

These grains can be of round or column-shape and show, in all samples examined, a crystallographic orientation relationship at the interface with α-Ti grains that have, in average, several tens microns in size. Differences between the two types of hydride grains are not only in shape, but also in the parallelism of their orientation and that of the Ti. Fig. 2 shows the interface between columnar $TiH_{1.971}$ grains and the adjacent Ti, in Bright (Fig. 2, middle) and Dark Field (Fig. 2, bottom) views. The latter was obtained with the diffraction of (311) family of atomic planes of the FCC structure. These grains

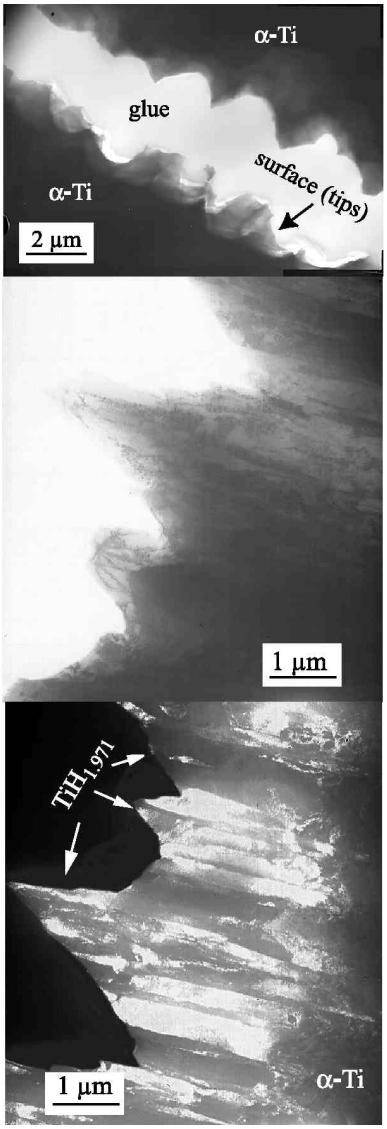

Fig. 2: Cross-sectional TEM observations of the $TiH_{1.971}$/α-Ti interface: low magnification bright field image of the profile (top); Detail, showing $TiH_{1.971}$ FCC columnar grains (middle); Dark Field image of the same region, obtained with the diffraction of (3-11) planes (bottom).

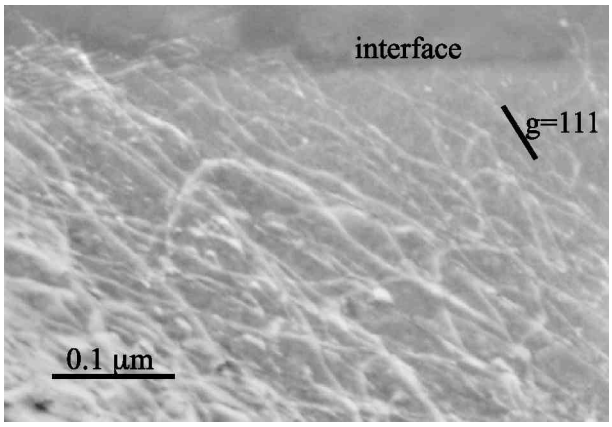

Fig. 3 - Dislocations in a $TiH_{1.971}$ grain close to the interface with the Ti substrate.

extend from the interface up to the surface and belong to one (311) family among three equivalent ones that exhibit an epitaxial relationship with the Ti substrate. These three families can exist simultaneously due to the six-fold symmetry of the adjacent Ti grain in the substrate, in [0001] orientation.

Fig. 3 shows high density of dislocations in the hydride layer forming a three-dimensional network. Using the classical extinction rules, their Burgers vectors are found to be of the 1/2<110> type, as in FCC metals and alloys.

DISCUSSION & CONCLUSIONS: The formation of the hydride layer directly on the Ti substrate, without any interfacial layer, as observed even in very high magnification images, suggests that the acid etching reduced the superficial native titanium oxide layer. Moreover, the crystallographic relationship between the two structures is an evidence that the hydride layer grows epitaxially to the immediate neighbor grain in the substrate. The crystallographic coherence between the two phases at the interface guarantees the best possible adherence of the hydride layer to the Ti substrate.

The dislocation arrangement observed in Fig.3 is typical of a fairly ductile but highly plastically deformed material, which denotes a substantial strain accommodation during the elaboration process. Our observations are in good agreement with previous studies[2] demonstrating the plastic deformation of TiH_x (x = 1.58 – 1.99). According to the Hall-Petch law, good mechanical properties can be expected a priori, since the hydride layer is formed by slightly misoriented subgrains smaller in size than the roughness.

REFERENCES: [1] Aronsson B-O, Hjörvarsson B, Frauchiger L, Taborelli M, Valloton P-H, and Descouts P (2001) Hydrogen desorption from sand-blasted and acid-etched titanium surfaces after glow-discharge treatment. *J. Biomed. Mater. Res.* **54**(1), 20-29. [2] Irving PE, and Beevers CJ (1972) Some observations on the deformation characteristics of titanium hydrides. *J. Mater. Sci.* **7**, 23-30.

ACKNOWLEDGEMENTS: This research was supported by Swiss National Science Foundation that is gratefully acknowledged.

European Cells and Materials Vol. 3. Suppl. 1, 2002 (pages 11-12) ISSN 1473-2262

INVESTIGATION OF FERROFLUIDS FOR BIOMEDICAL APPLICATIONS

M. Chastellain[1], A. Petri[1], M. Hofmann and H. Hofmann[1]

[1]*Powder Technology Laboratory, DMX, EPFL, Lausanne, Switzerland;* [2]*Laboratoire de Photonique et Interfaces (SB/ICMB/LPI) EPFL.*

INTRODUCTION: The recent development of a large variety of ferrofluids has led to a range of new biomedical and diagnostic applications. A major drawback for a lot of applications remains the lack of well-defined and well characterized particles.
Growing attention is paid to iron oxide nanoparticles embedded in a polymer matrix. The matrix fulfills several demands: on the one hand it acts as a stabilizer, or even controls the particle formation, on the other hand it determines the physicochemical properties of the material, or allows surface functionalization.
In this study magnetic nanoparticles were prepared either in the presence of polyvinylic alcohol or were redispersed after precipitation and isolation of iron oxide powder. Aqueous suspensions of magnetic particles were obtained under identical reaction conditions by coprecipitation of Iron(III)- and Iron(II)-salts using aqueous ammonia. The suspensions were finally dialyzed against distilled water to approximately pH 6.5.

METHODS: For a better understanding of the colloidal and magnetic properties, an extensive characterization of the ferrofluids must be carried out. Four major points are discussed in this work: composition, size distribution, magnetic properties, and first tests with human endothelial and synovial cells.

Composition: The iron oxide particles were analyzed with and without coating using XRD as well as FTIR. High resolution TEM measurements were also carried out to obtain qualitative information about the presence of an amorphous phase.

Size distribution: Different techniques were applied in order to obtain information about the iron oxide particle size distribution. Among these are: X-ray diffraction peak broadening, TEM picture analysis, magnetic characterization techniques, photon correlation spectroscopy, or analytical ultracentrifugation. Although the obtained results are not always comparable, valuable information is provided by their interconnection.

Cell survival tests: In collaboration with the Tierspital Zuerich (Musculoskeletal Research Unit) first tests with human endothelial cells and synovial cells have been carried out. The cell survival after different time periods has been

compared for different concentrations as well as different methods of synthesis.

RESULTS: The main characterization results are summarized in the following.

Composition: XRD patterns show a large amorphous zone as well as typical peaks, which can be attributed to nanocrystalline magnetite (Fe_3O_4) or maghemite (γ-Fe_2O_3). After close examination the presence of two distinct phases was excluded and the composition is thought to consist of a defect magnetite structure with a lattice parameter in between the one of bulk magnetite and bulk maghemite. FTIR investigations yield the same results.

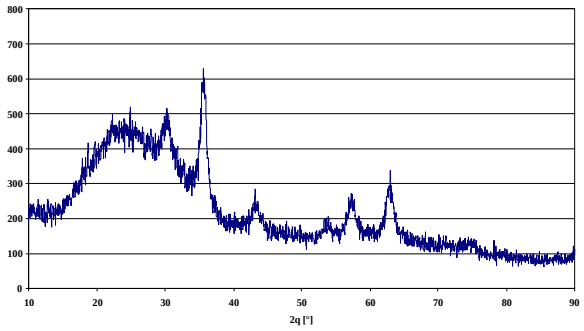

Fig. 1: XRD pattern of uncoated iron oxide nanoparicles showing a wide amorphous zone and typical inverse spinel peaks.

Size distribution: Typical monomodal distributions were found with an average size slightly smaller than 10nm.

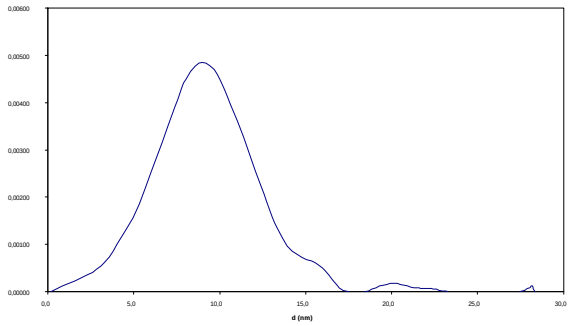

Fig. 2: AUC size distribution of bare iron oxide

The differences in size distribution determined by various methods show the necessity of combined size characterization for particles of that size. The comparison of the results also gives qualitative information about other properties such as the density or the refractive index. In particular the spherical assumption for the particles shape proved to be satisfactory.

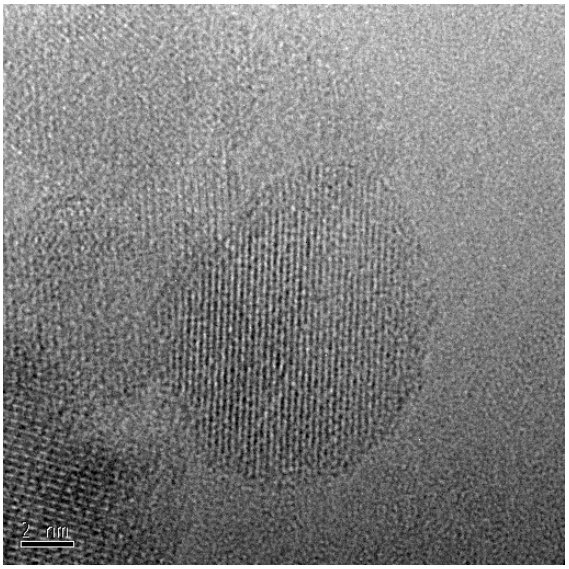

Fig. 3: High resolution TEM picture showing crystalline iron oxide particles.

Cell survival tests: It could be shown that the concentration the polymer as well as the ammonia concentration plays a very important role in the cell survival tests. As a first result it can be concluded that a minimum concentration of ammonia and polymer is essential for cell survival.

CONCLUSION: Ferrofluids were synthesized using PVA to ensure a colloidal stability at neutral pH. The composition, structure and size distribution characterization of iron oxide particles was carried out, showing the influence of the synthesis parameters. After the first tests, the obtained ferrofluids seem to be non-toxic to human endothelial as well as synovial cells.

ACKNOWLEDGMENTS: This project is supported by EU - under the project NANOMAG - Magnetic Nanoparticles for Medical and Biological Diagnostics and Devices.

WORKING CHARACTERISTICS OF RADIO-OPACIFIED BRUSHITE CEMENTS

C. Pittet, J. Lemaître

Laboratoire de Technologie des Poudres, EPFL, MX-Ecublens, 1015-Lausanne

INTRODUCTION: X-Ray opacification of calcium phosphate hydraulic cements (CPHC) is a pre-requisite prior to use them safely in image-guided vertebroplasty. Theoretical calculations (1) have shown that injectable CPHC presently available on the market exhibit linear attenuation coefficients below 1.6 cm^{-1}, whereas the recommended value should be close to 2.5 cm^{-1} in order to achieve enough contrast between the injected cement and the surrounding tissues (2).

According to theoretical calculations, injectable CHPC of the Brushite family – i.e. based on mixtures of $Ca(H_2PO_4)_2•H_2O$ (MCPM) and β-$Ca_3(PO_4)_2$ (β-TCP) transformed into $CaHPO_4•2H_2O$ (Brushite, DCPD) upon consolidation – can be obtained with the requested radio-opacity by incorporating about 100 mg iodine per mL of freshly mixed cement.

This work investigates the effects of different iodine sources on the working characteristics of an injectable Brushite cement formulation containing plaster of Paris (CSH, $CaSO_4•2.H_2O$) as a setting regulator.

METHODS: The Brushite cements were made of 1.201 g β-TCP, 0.781 g MCPM, 0.339 g CSH and mixed with 1.080 mL of distilled water ; 0.09 g of di-sodium di-hydrogen pyrophosphate (NHPP) (Fluka) was added to the mixture in order to adjust the setting time at approximately 20 min.

Four different iodine compounds were tested : NaI, $NaIO_3$ (Merck, pro analysis) Iopentol® (Imagopaque from Nycomed Imaging AS) and Iopamidol® (Iopamiro from Bracco SpA). The two latter compounds are tri-iodinated benzoic molecules commonly used for angiographic diagnosis. In all cases, theamount of iodine-containing substance represented 100 mg of iodine per mL of fresh cement, so as to achieve a theoretical linear attenuation coefficient of 2.47 cm^{-1}. The radio-opacifiers were incorporated by dissolution in the mixing water ; given the low aqueous solubility of $NaIO_3$, only partial dissolution of the additive was achieved. The other ingredients were added in the following order : NHPP, MCPM, CSH, β-TCP ; thorough mixing was effected after each addition. A iodine-free cement was used as control.

The setting times of the cements were measured with the Vicat needle technique (neddle ø = 2 mm, weight 98.4 g). Their mechanial properties were tested on wet cylindrical specimens aged for 24 h at 37 °C and 100 % relative humidity in the uniaxial (ø x h. = 8.7 x 18 mm) and diametral (ø x h = 8.7 x 6 mm) compression modes at a loading rate of 0.3 mm/min ; each composition was tested 4 times.

RESULTS AND DISCUSSION:

Setting times. No significant differences were found between the iodine-containing cements and the control (ST = 24 ± 1 min).

Mechanical properties. The results are summarised in Fig. 1. In diametral compressive strength, cements containing NaI, Iopentol® and Iopamidol® perform better compared to the control and the $NaIO_3$–containing cements In uniaxial compressive strength, Iopentol®–containing cements are significantly better than those containing Iopamidol®, the latter performing the same as the control ; $NaIO_3$ and NaI–loaded cements are worse than the control.

CONCLUSIONS: Brushite cements can be opacified with various iodine–containing additives : NaI, $NaIO_3$ Iopentol® and Iopamidol®. None of these additives affects significantly the setting times of the cements. In general, they do not affect to a large extent the mechanical performances of the consolidated cements, even though NaI appears to improve significantly the diametral compressive strength (3.1 *vs* 2.1 ± 0.8 MPa), immediately followed by Iopentol® ; the latter also improves significantly the uniaxial compressive strength (14.5 *vs* 10.5 ± 2.5 MPa). Thus, from the viewpoint of the working properties, Iopentol® appears to be the first–choice radio-opacifying additive.

REFERENCES:

1 C. Pittet "Development and Characterisation of Injectable Calcium Phosphate Cements for Use in Vertebroplasty." Thesis n° 2509, EPFL, 2001.

2 Deramond H., Wright N.T., Belkoff S.M. Bone 1999, 2 17S-21S.

ACKNOWLEDGEMENTS: This work has been granted by the Foundation of the "Hôpital Orthopédique de la Suisse Romande". Dr A. Uske

(Service de Radiologie, CHUV) is ackowledged for his help in collecting the radio-opacity data.

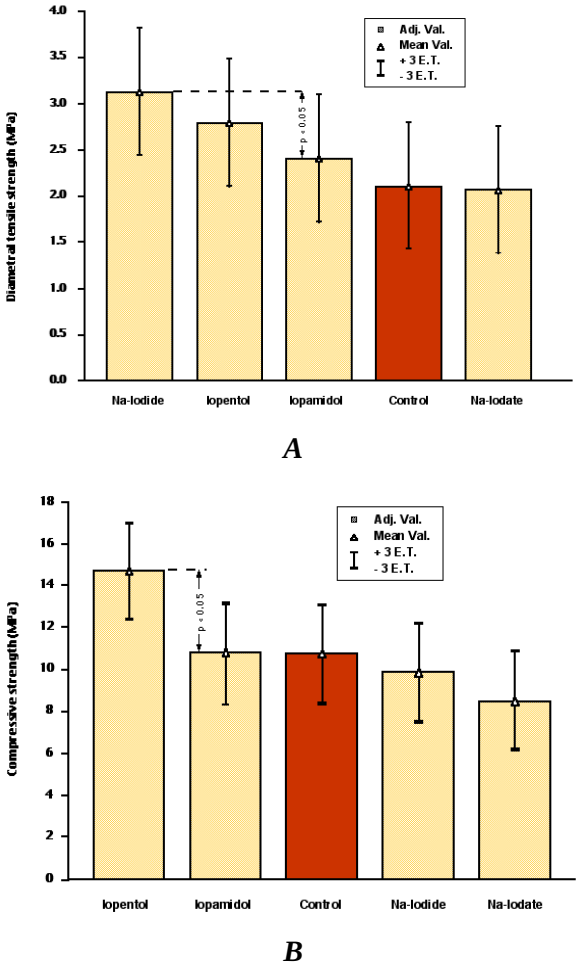

Fig. 1: Mechanical properties of radio-opacified Brushite cements. A) Diametral compressive strength ; B) Uniaxial compressive strength.

THE IMMEDIATE TISSUE REACTION TO A BIORESORBABLE BRUSHITE CEMENT IN EXPERIMENTAL METAPHYSEAL DEFECTS IN SHEEP

F. Theiss[1], D. Apelt[1], M. Bohner[2], Ch. Frei[3], K. Zlinsky[1], J. A. Auer[1], B. von Rechenberg[1]

[1]MSRU, Dept. of Veterinary Surgery, University of Zurich, Winterthurerstr. 260, CH-8057 Zürich, [2]RMS Foundation, Bischmattstrasse 12, CH-2544 Bettlach, [3]STRATEC Medical, Eimattstrasse 3, CH-4436 Oberdorf

INTRODUCTION: Resorbable cements as synthetic bone replacement have been introduced into orthopedic surgery for various applications, such as bone defect filling, augmentation and reinforcement in combination with autogenous grafts. Among those, brushite cements ($CaHPO_4 \cdot 2H_2O$) showed good resorbability and solubility. If applied as a biphasic cement in combination with large granules of β-tricalcium phosphate (β-TCP; β-$Ca_3(PO_4)_2$) <0.5mm in diameter), they proved to be resorbed and replaced with new bone within 4-6 months in a drill hole model in long bone metaphyseal and epiphyseal application in sheep. Although, their biocompatibility was considered optimal at 2, 4 and 6 months, the immediate reaction of the tissue to the biphasic cement was unknown. In this study, the immediate reaction of a brushite biphasic liquid cement (ChronOs Inject) was studied.

METHODS: Eight (8) adult, Swiss Alpine sheep served as experimental animals and were divided in fours groups with 2 animals each. An osteotomy in the proximal tibia was performed, where a rectangular bone wedge of 0.7cm height was removed at the cranial aspect of the tibia plateau. The osteotomy extended ca.60% (2.4 cm) caudally into the tibia shaft and was made according to a standardized template. The defects were stabilized using a 3.5 mm T-plate and 7 x 3.5 mm screws and they were filled with the cements. The hind limbs were operated alternately and additional immobilization of the limbs was provided with splint bandages. A suspension system was used for 4 weeks to protect the animals from refracturing their limbs. The study period until sacrifice of animals was 2,4,6 and 8 weeks. After sacrifice, the bone samples were immediately harvested, macroscopically assessed and processed for histology. Non-decalcified bone specimens were embedded in acrylic resin (HistoDur®). Ground sections (30-40µm) and thin (5µm) were prepared, and stained with either toluidine blue or von Kossa/McNeal.

RESULTS: All cement samples were well integrated at the time of sacrifice, and were easily visible from outside of the bone. Histologic evaluation was performed focusing on cellular reactions and ways of cement degradation. Both cortices of the tibia defects were not remodeled yet at all time points. However, periosteal reactions and new bone formations had started at 6 weeks. A small resorption zone between the old bone matrix and the bulk of the cement was noticed (≈1-2 mm) mainly in the 2 weeks group. It gradually decreased over time. Resorption of the cement matrix (brushite) was quicker compared to the TCP granules. The gap within the resorption zone of the cement was filled with mesenchymal or osteoprogenitor cells and close to the old bone matrix active osteoblasts producing new osteoid were found at the bone surface already at 4 weeks. Small areas of new bone deposition were already noticed on the TCP granules in the 6 weeks group. Only in the 2 weeks group multinuclear foreign body cells were found. Macrophages digesting the cement particles were abundant after 4 weeks as well as actively osteoid synthesizing osteoblasts.

DISCUSSION & CONCLUSIONS: The biphasic resorbable brushite cement (ChronOs Inject) showed good biocompatibility also in short-term experiments. The immediate tissue reaction at short intervals revealed excellent tissue compatibility, such that no significant inflammatory reaction was present at 2,4, 6, and 8 weeks. Foreign body cells were seen only transiently at 2 weeks and were already completely replaced by cement digesting macrophages at 4 weeks. In any case, macrophages are normally involved in cellular debridement and are not considered to be inflammatory cells, at least in bone. The front of cement resorption and bone formation was parallel over time, although the resorption zone of the cement matrix was slightly larger initially at 2 weeks. In conclusion, the brushite cement as investigated in this study appears to be an excellent synthetic bone replacement also in short-term experiments.

ACKNOWLEDGEMENTS: Mathys Medical (Bettlach, Switzerland) and STRATEC Medical (Oberdorf, Switzerland) are thanked for their financial support.

European Cells and Materials Vol. 3. Suppl. 1, 2002 (pages 16-17) ISSN 1473-2262

IMPROVEMENT OF RELIABILITY OF CERAMIC HIP JOINTS

W.Weber[1], M.Zahner[2], W.Rieger[1]

[1] *Metoxit AG, , Thayngen, CH* [2] *EMPA, Dübendorf, CH*

INTRODUCTION:. Ceramic heads have been used for total hip joint replacements successfully for many years due to excellent biocompatibility, low friction and wear and high strength. The failure rate of the ceramic head is very low. However there is still a remaining minimal probability of fracture. This probability is a result of the fracture mechanical behavior of ceramic materials, which is characterized by the Weibull distribution. While metals have a narrow strength distribution, ceramics have a certain probability of low strength elements (figure1).

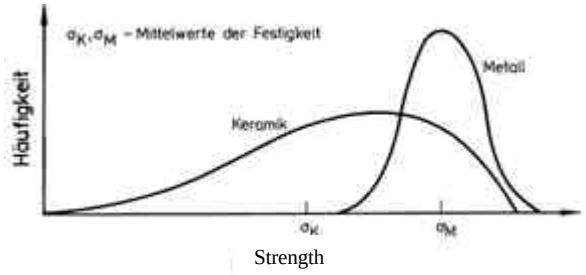

Fig. 1 Strength distribution of metals and ceramic

Therefor proof testing of ceramic hip joints heads has become an accepted method to improve reliability of ceramic hip joints: A static load is applied which is higher than the expected maximum physiological load. Ball heads with a lower strength will be eliminated.

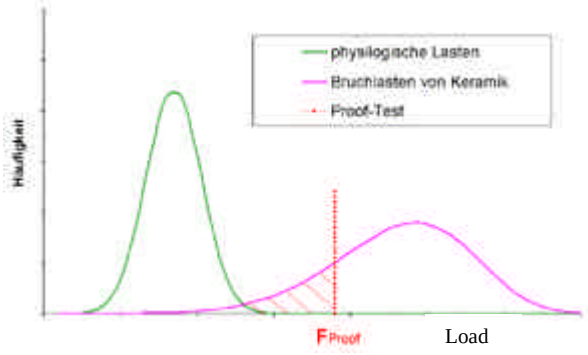

Fig. 2: Effect of proof testing on the strength distribution

While the destructive testing of ceramic heads is described in the standards[1] the way how to perform proof testing is not defined. It is obvious, that proof testing is only of value, if the stress is equivalent to that applied to the component in vivo. Otherwise, failures would not be detected or the test may lead to destruction of good products.

METHODS: The stress distribution in the ceramic head was calculated by finite element methods. The non linear calculation was validated and calibrated by experimental measurements. This was done by measuring the strains and calculating the stresses in dependence of the load by strain gauges. The measurements were carried out for the proof test as well as for the static fracture test according to ISO 7206-5[1] and an "in vivo near" model.

Strain measurement

For the strain measurement each ball head was provided with three strain gauges on the surface. The arrangement of the gauges on the head is shown in fig. 3.

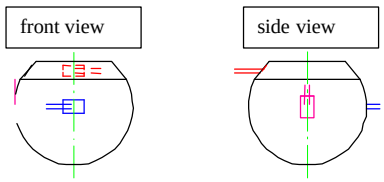

Fig. 3: Arrangement of the strain gauges on the ceramic heads (left side: radial in 38° and 0° position, right side in axial 0° position)

FEM Calculation

In a first step the contact definitions had to be validated by measuring the displacement of the conical shaft and the conical bore of the ceramic head (figure 4) under a definite load.

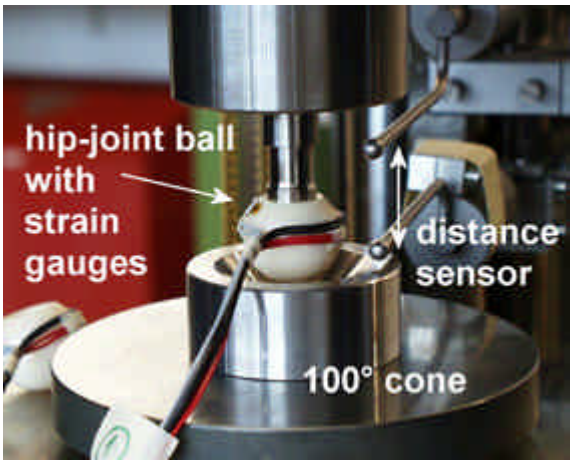

Fig. 4: Test set up for displacement measurement

For two types (cone length L and S) of alumina standard BIO-HIP® ball heads the FEM models for the three load cases were calculated and compared with each other: The static fracture test according to ISO 7206-5, a proof test with hydrostatic pressure inside the cone, and an in vivo near 3D-model.

RESULTS:

Static fracture test

After the calibration of the FEM model, a good agreement between the measured and calculated strains was found. A comparison chart is shown in fig. 5. The best fit was reached with a Youngs-Modulus of 380 MPa for alumina.

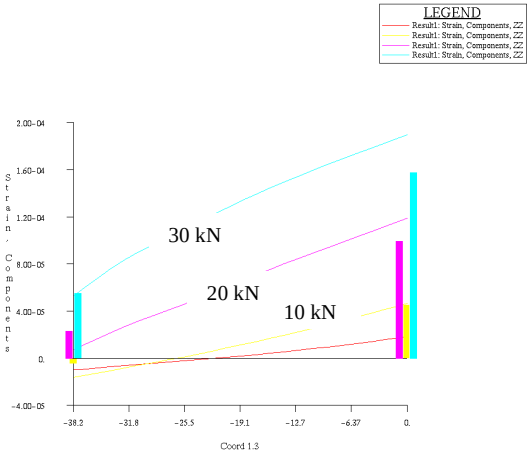

Fig. 5: Calculated (lines) and measured (bars) strains along the outer diameter from the 38° position to the equator for ball head S.

Proof test

The proof test was now designed in order to give a similar strain as in the load case against a 100 ° cone. Figure 6 shows the calculated result of an optimized proof test configuration.

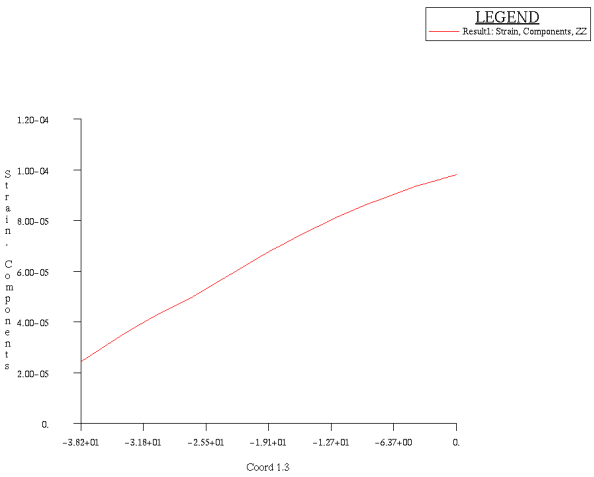

Fig. 6: Calculated strains along the outer diameter from the 38° position to the equator for ball head S.

DISCUSSION: As a result of the calibration of the FEM calculation and a comparison between the three load cases a reliable proof test could be developed. The FEM plots in figure 7 demonstrate good agreement in the stress distribution between the optimized proof test and the static fracture test.

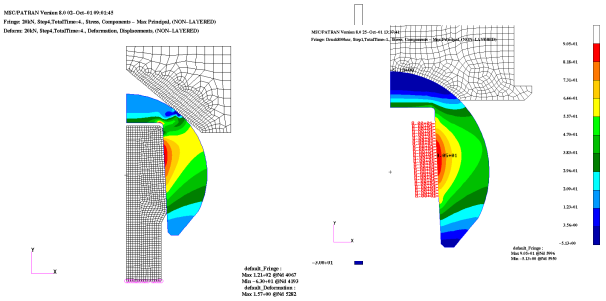

Fig. 7: Stress distribution in the ceramic head type S. Left: static fracture test, right: Optimized proof test.

In addition, for the head type L an “in vivo near” 3D-model with non axial load was also calculated.

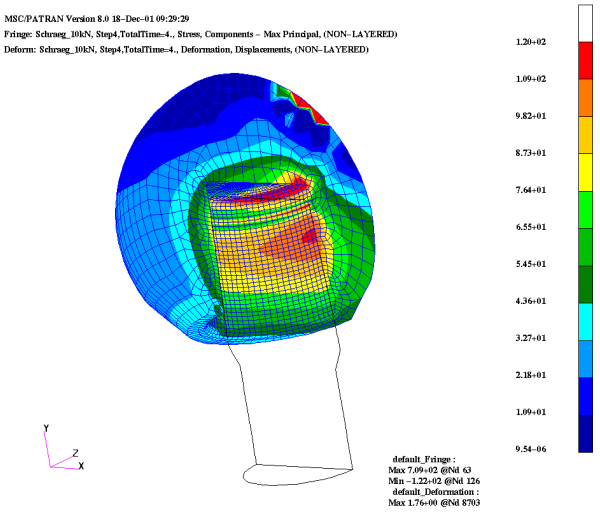

Fig. 8: 3D –model of stress distribution in the ceramic head type L with non axial load.

The influence of the asymmetric load can clearly be seen. However, no principal differences of the stress distribution compared to the axial load cases are found.

CONCLUSIONS: Proof testing of ceramic ball heads was adjusted by strain measurements under load and consecutive FEM calculation to obtain an optimized proof test geometry for increased product reliability.

REFERENCES: [1]ISO 7206-5 “Implants for surgery”

ACKNOWLEDGEMENTS: This study was financially supported by the swiss KTI (Commission for technology and innovation).

European Cells and Materials Vol. 3. Suppl. 1, 2002 (pages 18-19) ISSN 1473-2262

IN VITRO DEGRADATION OF PSEUDOWOLLASTONITE AND IN VITRO CYTOTOXICITY EVALUATION

D. Dufrane [1], M. Anseau [2], I. Mc Kay [3], P. de Asa [4], YJ. Schneider [5], C. Delloye [1].
[1]: Orthopaedic research laboratory: Université catholique de Louvain, Belgium; [2]: Université de Mons-Hainaut; [3]:St Bartholomew's and the Royal London School of Medicine and Dentistry, University of London, UK; [4]: Departamento de Ciencia y Tecnologia de Materiales; Universidad Miguel Hernandez, Spain; [5]: Cell Biochemical Laboratory: Université catholique de Louvain; Louvain-La-Neuve, Belgium.
Mail: denis.dufrane@clin.ucl.ac.be

INTRODUCTION: Bioactive materials including a chain silicate minerals as pseudowollastonite ($CaSiO_3$) (psW) have demonstrated the formation of hydroxyapatite-like layer on their surface both *in vivo* and *in vitro*[1,2,3]. This ceramic material appears to offer therapeutic potential in situation requiring bone augmentation or replacement[4,5]. In previous study, we have demonstrated that psW can released substances able to induce an impact on cellular viability with a kinetic reaction. Indeed, a decrease of cellular viability was observed in the early phase of psW degradation and a better cells viability in function of psW degradation time[6] (Fig.1). Our hypothesis is that the interaction between Silicate and Calcium, released by psW, can play an important role on cell metabolism. The aim of this work consists in the study of calcium and silicate effects on cellular viability.

METHODS: **Cytotoxic assays on silicate and calcium:** Human osteosarcoma cell lines (SaOS-2; ATCC: HTB-85) were incubated with medium [DMEM/HAM-F12 (50% v/v), 10% (v/v) fetal bovine serum, 100 u/ml penicillin, 100µg/ml streptomycin) supplemented with different concentrations of calcium (+ 50%, +100%, +150%) and silicate (sodium silicate solution; 1.6 and 6.25 mM). At 24 and 48 hours after incubation, cells were incubated for 30 min in DMEM/HAM-F12 (no serum) containing 8 µmole/L 2',7'-bis-carboxyethyl)-5- carboxyfluorescein acetoxymethylester (BCECF-AM, Molecular Probes), an esterified dye that, when internalized by living cells, is hydrolyzed by cellular esterases to a membrane-impermeable fluorescent species. The cells were then lyzed by incubation with 1% Triton X-100, and the released dye collected in the supernatant for quantification by spectrofluorimetry (485 nm excitation and 535 nm emission). **Silicon and calcium released of psW pellets:** PsW pellets were incubated in conditioning medium at different concentrations (10, 15, 50 and 100 mg/ml) during 1,2,3,7 and 9 days. Silicon and calcium released were performed by inductively coupled plasma atomic emission spectroscopy (ICP-AES).

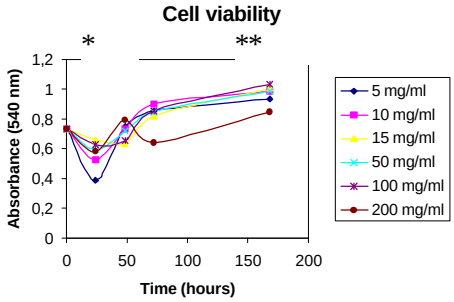

Fig. 1. Cell viability: Relative MTT formazan formation by SaOS-2 cells incubated, during 24 hours, with psW extracts (24, 48, 72, 168 hours of extraction) (n=8) (*: $p<0.005$; **: $p<0.05$).

RESULTS: No significant modification of cellular viability was observed for SaOS-2 cells incubated with medium supplemented with different concentrations of calcium (at 24 and 48 hours) (Fig.2). However, a significant decrease of cell viability was observed for cells exposed to silicate solutions (Fig.2,3). ICP-AES has confirmed that psW samples, incubated in medium, released at day 1 and day 2, a major quantity of silicon compared with sample incubated during 3,7 and 9 days.

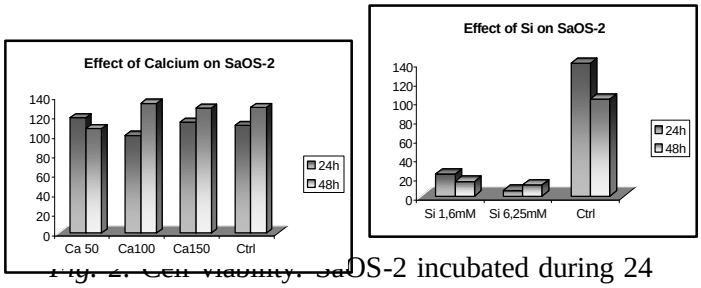

Fig. 2. Cell viability: SaOS-2 incubated during 24 and 48 hours with medium supplemented with calcium (left) and silicon (right).

DISCUSSION & CONCLUSIONS: No cytotoxic effect was demonstrated for psW. However, we

have observed few changes in cell viability or stress for cell exposed to psW extract in the early phase of extraction (24 hours). This phenomenon could be correlated with an increase of silicon released by psW which can initiate a cellular toxicity. Further studies will be necessary to obtain a better understanding of psW degradation which will be primordial to obtain a better interaction between cell and bioactive ceramic.

REFERENCES: [1] Siriphannon P et al (2000) *J Biomed Mater Res* **52**: 30-9.[2] De Aza PN et al (1999) *J Dent* **27**: 107-13.[3] Nishio K et al (2001) *J Biomed Mater Res* **55**: 164-76.[4] Mousa WF et al (2000) *Biomaterials* **21**: 2137-46.[5] Fujita H et al (2000) *J Bone Joint Surg Br* **82**: 614-18.[6] Dufrane D et al (2001) *European Cells and Materials* **1 (supplement 2)**: 64.

European Cells and Materials Vol. 3. Suppl. 1, 2002 (pages 20-21) ISSN 1473-2262

RF-PLASM DEPOSITION AND SURFACE CHARACTERIZATION OF A BIODEGRADABELE THIN FILM COATING

D. Favez [1], D. G. Castner [2], B.D. Ratner [2], H.J. Mathieu [1]

[1] *EPFL, Materials Institute, Lausanne, CH,* [2] *University of Washington, NESAC/BIO, Seattle, USA*

INTRODUCTION: Synthetic biodegradable polymers have become very important materials for applications in biomaterials, tissue engineering and controlled drug delivery. Among these materials, poly(L-lactic acid) (PLLA) has been widely utilized either as temporary scaffolds for cell transplantation in tissue regeneration or as carriers for delivery of bioactive molecules. PLLA breaks down in the body to lactic acid, a component of the normal metabolism [1]. RF-plasma deposition has also been found to be a useful technology for biomaterials applications because of its ability to coat complex shapes with a tightly adherent thin film [2].

The surface analytical techniques X-ray photoelectron spectroscopy (XPS) and Time-of-Flight Secondary Ion Mass Spectrometry (ToF-SIMS) have been used to study the surface chemical nature of many polymeric materials, including plasma deposited polymers [3-4] and degradation of polymers [2]. These techniques probe the chemistry of the polymer surface to a depth of between 20 and 100 Å for XPS and approximately 10 Å for ToF-SIMS. Atomic Force Microscopy (AFM) is also commonly used to probe the topography of plasma deposited polymers [5] or the evolution of polymer degradation, an example being the hydrolysis of polyester [6-7].

The aim of this study is to use plasma deposition techniques to form a thin PLLA coating using the cyclic lactide as a monomer and to study its degradation in a phosphate buffer solution (PBS, pH 7.4) at 37°C (reproducing the saline conditions of human blood) using state-of-the-art surface analysis techniques.

MATERIALS/ METHODS: The substrates used for this experiment were either glass disks (for coating optimization) or silicon wafers (for the degradation studies). The borosilicate glass disks were obtained from Carolina Biological Supply Company (NC, USA) Cat. # D8-63-3029. Their diameter was 12 mm and thickness was 0.13-0.17 mm. The Si wafers were obtained from Silicon Valley Microelectronics, Inc., (CA, USA). The precursor used to form the plasma was L-lactide or (3 S)-cis –3,6-Dimethyl-1,4-dioxane-2,5-dione, purchased from Aldrich Chemical Company, Inc. (Milwaukee, WI, USA), reference 36,704-4.

The plasma chamber consists of a Pyrex tubular glass cylinder, 25.5 in. in length and 4 in. in diameter, wrapped with heating tapes to control the temperature. Two copper capacitor plates are coupled to the 13.56 MHz RF generator via a matching network to increase the power dissipation in the discharge and protect the reactor. A capacitance manometer gauge measures the pressure, using a feedback controller which moves the throttle valve to maintain the pressure as directed.

XPS (ESCA) analyses was performed at the University of Washington (NESAC/BIO) on a Surface Science S-probe or X-probe Instruments. This instrument permits analysis of the outermost 20-100 Angstroms of a sample using a square spot size that can be adjusted from 100 µm x 100 µm to 800 µm x 800 µm. For the present set of measurements the largest spot size (800 microns) was used.

ToF SIMS analysis was conducted using a Physical Electronics Model 7200 time-of-flight secondary ion mass spectrometer at NESAC/BIO. The instrument is equipped with a Cs+ ion source operated at 8keV, a reflectron mass analyzer, and chevron-type multichannel plate detectors. A bunched primary Cs+ beam (50 micron diameter, approximately 1 ns pulse width) is used and the bin width of the time-to-digital converter (TDC) is set at 1.25ns, resulting in mass resolutions (m/Δm) of >7000 at m/z=27 for electrically conducting samples. The beam is rastered over a square area that is 100 microns on a side. Charge neutralization is achieved with a pulsed electron flood gun.

RESULTS / DISCUSSION:

Plasma deposition of cyclic L-lactide has been successfully optimized to yield a poly(lactic acid)-like thin film. The XPS, ToF-SIMS and AFM characterization of such films deposited using a pulsed RF plasma showed that the chemical structure, deposition rate and degradation in phosphate buffer solution (pH 7.4, 37°C) of such

films are strongly dependent on the duty cycle of the pulses. A typical XPS spectrum is shown in Fig. 1.

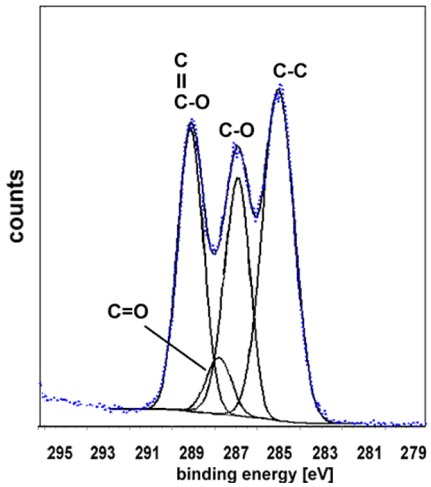

Fig. 1: Four peaks fit of C1s high resolution peak duty cycle = 2%

During the optimization process, it has been shown that the input power is the major parameter which affects the chemical structure of the deposited film. Lowering the input power increases the monomer structure retention. Since the degree of monomer retention was continuing to increase as the lower limit of continuous wave (CW) plasma stability was reached, it was necessary to use a pulsed RF plasma to reach even lower effective powers by decreasing the duty cycles. Other parameters such as sample position or deposition time were shown not to be as significant as the input power for monomer structure retention.

The characterization of the pulsed plasma deposited film showed an increase of oxygen functionalities, present as ester or alcohol groups, with decreasing duty cycle as shown in Fig. 2. The proportion of ketone groups seemed to be independent of the duty cycle. In addition, the deposition rate with a duty cycle of 33% is nearly three times the one corresponding to a duty cycle of 2%. Compared to PLLA, plasma deposited films contain more hydrocarbon species. However, the plasma-deposited PLLA films have several of the same ToF-SIMS fragments observed from a conventionally polymerized PLLA film.

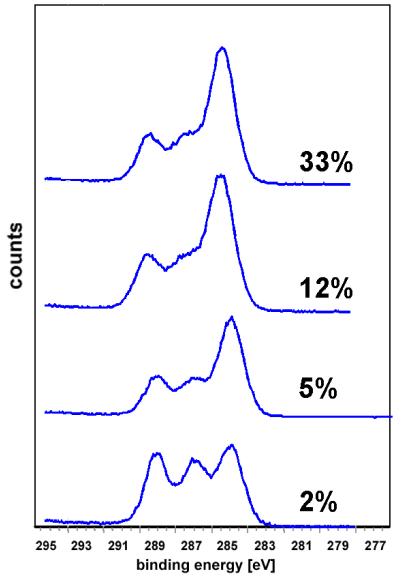

Fig. 2 C1s high-resolution peaks of pulsed plasma polymerized films for various duty cycles..

REFERENCES: [1] Amass, W., A. Amass, et al., *A review of biodegradable polymers: Uses, current developments in the synthesis and characterization of biodegradable polyesters, blends of biodegradable polymers and recent advances in biodegradation studies*, Polymer International, **1998** *47*(2): 89-144; [2] Ratner, B. D. and E. E. Johnston, *Surface characterization of plasma deposited organic thin films*, Journal of Electron Spectroscopy and Related Phenomena, **1996** *81*(3): 303-317; [3] Mackie, N. M., D. G. Castner, et al., *Characterization of pulsed-plasma-polymerized aromatic films*, Langmuir, **1998** *14*(5): 1227-1235; [4] Chen, J. X. and J. A. Gardella, *Time-of-flight secondary ion mass spectrometry studies of in vitro hydrolytic degradation of biodegradable polymers*, Macromolecules, **1999** *32*(22): 7380-7388; [5] Wang, J. H., J. J. Chen, et al., *Plasma Synthesis of a Novel CF3 Dominated Fluorocarbon Film*, Chemistry of Materials, **1996** *8*: 2212-2214; [6] Leadley, S. R., K. M. Shakesheff, et al., *The use of SIMS, XPS and in situ AFM to probe the acid catalyzed hydrolysis of poly(orthoesters)*, Biomaterials, **1998** *19*(15): 1353-1360;[7] Davies, M. C., K. M. Shakesheff, et al., *Surface analysis of biodegradable polymer blends of poly(sebacic anhydride) and poly(DL-lactic acid)*, Macromolecules, **1996** *29*(6): 2205-2212.

ACKNOWLEDGEMENTS: The XPS and ToF-SIMS experiments at NESAC/BIO were funded by NIH grant RR-01296.

European Cells and Materials Vol. 3. Suppl. 1, 2002 (pages 22-23) ISSN 1473-2262

IMMOBILISATION OF STREPTAVIDIN ON POLYSTYRENE

C. Houphouet-Boigny [1], Xin Gao [1] , M. Schawaller [2], H.J. Mathieu [1]

(1) EPFL, Materials Institute, 1015 Lausanne, CH

(2) DiaMed / ADS Applied Diagnostic Systems AG, 1785 Cressier sur Morat, CH

INTRODUCTION: The measurement of certain analytes in blood is an important aspect of clinical diagnosis. There is a need for tests (immuno assays) with high sensitivity to identify and detect enzymes, therapeutic drugs or other specific proteins. In order to achieve this we use a biosensor based on fluorescence measurement [1] To improve analytical performance, allyldextran monolayers were coated on gamma-irradiated polystyrene wells (γ-PS). This study reports the coating of polystyrene wells with allyldextran and chemical properties of the surface analyzed by X-ray Photoelectron Spectroscopy (XPS), contact angle and Total Internal Reflectance Fluorescence Spectroscopy (TIRF) measurements based on a diploma work of one of the authors [2].

METHODS: Surface modification procedures are based on allyldextran layer absorbed on the bottom surface of the polystyrene wells. Allyldextran grade (MW 150'000, Pharmacia 253758-01) provided by Pharmacia is used for all experiments. It is a form of dextran substituted with allyl groups.

Allyldextran solutions with different concentrations 0 –10'000 µg/ml of allyldextran are prepared in water (18.2 MΩcm at 25°C) which has been degassed with nitrogen for about 1h. The wells are filled with the allyldextran solution and stored in a closed box for 16 ± 3 hours. After washing again with water the γ-PS chips are used for further treated with 30mM sodium (meta)periodate $NaIO_4$ (Fluka 71859). After washing with PBS and coupling in a bicarbonate solution (100mM $NaHCO_3$, pH 9.3) with 40µg/ml of Streptavidin (Pierce cat. No. 21122) or Neutravidin (Pierce cat. No. 31000)

The avidin-biotin system has many applications in both research and technology. Due to the very high affinity ($Ka=10^{-15}M^{-1}$) of the complex.

XPS scans were performed to determinethe surface composition in order to analyze changes due to the transformations induced by surface treatment and to detect otherwise contamination. XPS of the samples was performed on a Kratos AXIS Ultra System, utilizing an aluminum Ká monochromatized X-ray source (E=1486.6 eV) and a hemispherical energy analyzer. For this study, XPS spectra were recorded at take-off angles of 0°, 45°, 70° and 80° with respect to the surface. Spectral binding energies were referenced to the C-H peak assigned to 285.0 eV. Evaluation of the XPS data was done by CasaXPS (v. 2.11) and Tougaard-Quasas software packages.

The surface modification and its effects on wettability were analyzed using contact angle measurements. They were performed with a contact angle measuring system G10 by Krüss GmbH (Hamburg, Germany) at the DGR of EPFL (Prof. H. Harms). The contact angle measurements were performed on air-dried sample by placing a water drop on the polystyrene surface. The measured contact angle was the advancing angle between the surface and the water drop.

Total Internal Reflectance Fluorescence measurements were performed at DiaMed by an immunosensor device [3].

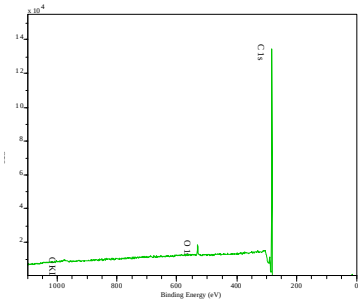

Fig. 1 XPS survey of g-PS radiated Polysytrene

RESULTS:

A typical XPS survey for a polystyrene surface is shown in Figure 1. Carbon C1s peak and the oxygen O 1s are observed. This survey is the standard survey for the gamma irradiated

polystyrene wells prior to any surface treatment. The oxygen amount of the pure gamma irradiated samples (ã-PS) is less than approx. 2 atom%).

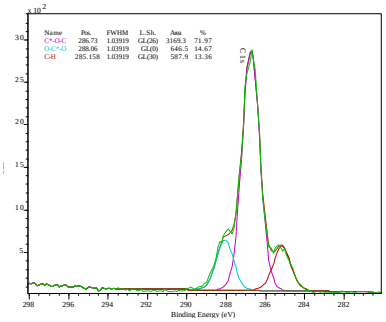

Fig. 2 C1s high resolution XPS of pure allyldextran powder

Fig.2 shows AC1s high resolution scan of pure allyldextran powder is shown in Figure 2, which is compared to allyldextran coating as shown in figure 3.

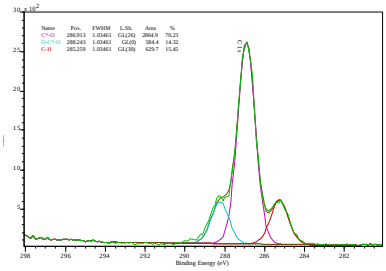

Fig. 3 C1s high resolution XPS of g-radiated Polystyrene coated with an allyldextran layer; è = 0°

SUMMARY: The allyldextran coating provides a stable, hydrophilic surface on γ-radiated Polystyrene wells with repetitive XPS results. Surface treatments were optimised using XPS and contact angle measurements. Functional biotin binding assay using fluorescence measurements of surfaces treated with allyldextran acitvated with iodate and coupled to Neutravidin seem to indicate that the Neutravidin is immobilised. Surfaces treated with allyldextran followed by iodate activation and and Neutravidin are highly hydrophilic and express very good non-specific adsorption characteristics.

REFERENCES: ; [1] Pierce catalogue 2001-2002 ; [2] C. Houhouet-Boigny, EPFL diploma thesis submitted Feb. 2002 to the Mat. Institute;[3] Patent Application WO 01/14859 A1

ACKNOWLEDGEMENTS : The project was partially funded by CTI/KTI, Bern, contract no. 5170.1 MTS. We like to thank N. Xanthopoulos, C. Aeby and M.C. Morandi for their experimental advice and assistance.

European Cells and Materials Vol. 3. Suppl. 1, 2002 (pages 24-25) ISSN 1473-2262

REINFORCEMENT OF COMPOSITE RESINS WITH UNIDIRECTIONAL GLASS FIBERS

J. Kosoric, M. Cattani, S. Bouillaguet, Ch. Godin, & J.-M. Meyer

School of Dentistry, University of Geneva, CH,

INTRODUCTION: Glass fibers have been introduced as reinforcement for composite resins in dentistry more than 20 years ago. They are available in different forms : unidirectional, braid, woven, mesh. They can also be found as pre-impregnated or as material to be impregnated with resin before use when needed. Among different clinical applications we can cite : dentures, overdentures, reinforced temporary/long-term (interim) bridges etc. Even after more than ten years of first clinical experiments the conclusion is that they can be used as long temporary solution (few months up to two years), in case of fixed partial denture (Vallittu[1], Vallittu and Sevelius[2]).

In current research on dental implants there are some intentions for immediate loading : « The results suggest that immediate loading of Branemark System implants at the time of placement in edentulous patients can be a valuable adjunct to therapy and as predictable as delayed loading, in both mandibular and maxillary arches. » Horiuchi K[3], Gatti et al[4] and Copper et al[5] have come to the same results in their own works. We therefore decided to point our research in that direction.

By selecting materials which have a lower rigidity than a cast metal alloy we might be providing better conditions for healing process in the bone surrounding the implant.

First we have decided to evaluate improvement in mechanical behavior, both with laboratory composite resins and with a provisional resin. Thanks to those preliminary results it seemed reasonable to continue our research in making samples shaped like real bridges and to evaluate them under loading.

The aim of this work was to evaluate reinforcement with glass fibers of two dental materials : laboratory composite resins and provisional resins, in order to obtain preliminary results for further studies of provisional bridges as a suprastructure for immediate loading of implants.

METHODS: We have used two different laboratory composite resins (Sinfony, *ESPE* and Cristobal+, *IDR*) and one provisional resin (Protemp Garant 3, *ESPE*) reinforced with unidirectional glass fibers (Stick, *Stick Tech Ltd.*). For all the materials we have used Sinfony Transparent, a flowable composite resin, for a 10 minutes impregnation of glass fibers, in a closed plastic bag. The samples with composite resins were prepared in a 25x2x2 mm mould and cured for 15 sec with a halogen curing lamp Elipar TriLight (*ESPE*), followed by additional curing in the Mpa 2000 light-curing unit for 90 sec, and at the end treated with temperature of 80 degrees C for 8 minutes in the Mpa 2000 Post Cure unit. The samples with provisional resins have been light-cured differently : 15 sec with the Elipar TriLight curing lamp, followed by a post-cure treatment in *ESPE* Beta-Unit, auxiliary program 1. Flexural strength and elastic modulus have been examined with 3 and 4 points bending tests, using an Instron Universal testing machine 1114, at a crosshead speed of 0.5 mm/min. Statistical analysis was performed by multifactorial ANOVA.

RESULTS:

Table 1. Modulus of elasticity of fiber-reinforced composite resins in GPa

4 points test	Without fibers	
	24 h	7 d
Cristobal	13.8 (1.8)	22.7 (6)
Synfony	7.2 (0.5)	7.1 (1.2)
	With fibers	
	24 h	7 d
Cristobal	17.2 (5.3)	15.4 (8.5)
Synfony	16.8 (1.3)	10.5 (1.1)

Table 2. Flexural strength of fiber-reinforced composite resins in MPa

4 points test	Without fibers	
	24 h	7 d
Cristobal	140 (28)	159 (22)
Synfony	163.4 (13)	162 (14)
	With fibers	
	24 h	7 d
Cristobal	460 (130)	340.3 (51)
Synfony	525.6 (36)	462.3 (91)

Multifactorial analysis has shown that glass fibers reinforce the laboratory composite resins but they do not have any influence on their elastic modulus. On the other hand samples become less resistant with time, but their modulus does not change.

Table 3. Flexural strength of fiber-reinforced provisional resins in MPa

4 points test	Without fibers	
Flex strength	24 h	7 d
Protemp Garant 3	134(60)	180(19)
	With fibers	
	24 h	7 d
Protemp Garant 3	110(24)	207(61)

Table 4. Modulus of elasticity of fiber-reinforced provisional resins in GPa

4 points test	Without fibers	
Flex modulus	24 h	7 d
Protemp Garant 3	2.2(0.6)	2.6(0.7)
	With fibers	
	24 h	7 d
Protemp Garant 3	2.9(0.8)	6(2)

Multifactorial analysis has shown that only aging in water has significant influence on flexural strength of provisional resins, but the reinforcement has not. For flexural modulus both, aging in water and reinforcement, give significant difference for tested material.

DISCUSSION & CONCLUSIONS: Post-curing provides better mechanical properties in a short period of time. Glass fibers reinforce significantly the flexural strength of the laboratory composite resins, but strength is more material dependent than condition specific (aging in water, reinforcement) – this is more obvious for Sinfony, a less charged material. On the contrary, flexural strength of provisional resins is condition dependent (aging in water). Also their flexural modulus has become more elevated in simultaneous action of aging and reinforcement.

The work is continuing by the evaluation of provisional reinforced resin characteristics and the development of bridges which simulate more closely the clinical situation.

REFERENCES: [1] Vallittu(1999) *Case report: a glass fibre reinforced composite resin bonded fixed partial denture* (Eur J Prosthodont Restor Dent 2001 Mar;9(1):35-8).[2] Vallittu, Sevelius(2000) *Resin-bonded, glass fiber-reinforced composite fixed partial dentures: Clinical study* (J of Prost Dent 2000 Oct, 413-18,[3] Horiuchi K(2000) *Immediate loading of Branemark system implants following placement in edentulous patients: a clinical report* (Int J Oral Maxillofac Implants 2000 Nov-Dec;15(6):824-30), 4,5 Sadowsky SJ. (2001) *Mandibular implant-retained overdentures: a literature review* J Prosthet Dent 2001 Nov;86(5):468-73

ACKNOWLEDGEMENTS : We would like to thank ESPE, Germany and IDR, France for their generous support in providing theirs material and curing units.

European Cells and Materials Vol. 3. Suppl. 1, 2002 (pages 26-27) ISSN 1473-2262

CORROSION CHARACTERISATION OF PASSIVE FILMS ON CoCrMo WITH ELECTROCHEMICAL TECHNIQUES IN SALINE AND SIMULATED BIOLOGICAL SOLUTIONS

S. Kurz[1], A.W.E Hodgson[1], S. Virtanen[1], V. Fervel[2] & S. Mischler[2]

[1] Institute for Materials Chemistry and Corrosion & Department of Materials, Swiss Federal Institute of Technology Zurich,8093 Zurich, CH, [2] Laboratory of Metallurgical Chemistry, Department of Materials, Swiss Federal Institute of Technology Lausanne, University of Geneva, 1015 Lausanne, CH

INTRODUCTION: CoCrMo alloy is regarded as a highly biocompatible material and has been employed in the fabrication of hip prostheses since the 1940's. Its biocompatibility is linked to the spontaneous formation of a stable oxide film. Nonetheless, the release of metal into the body takes place, which can be the result of uniform passive dissolution, of local breakdown of passivity as a consequence of localized forms of corrosion, or of mechanical events such as fretting corrosion. However, the exact chemical, electrochemical and triboelectrochemical mechanisms that lead to the release of metal from CoCrMo prostheses are not known. In this work an electrochemical characterisation of CoCrMo alloy under simulated biological conditions was sought. In particular, the effects of specific ions present in the electrolyte solution and of time on the properties of the passive film were investigated.

METHODS: CoCrMo disc-shaped samples (Protasul-20, Sulzer Winterthur) of 1 cm^2 area and 5 mm thickness were employed throughout the study. Experiments were performed in simulated body fluid (SBF) and in 0.14 M NaCl solution buffered to pH 7.4 via the use of tris(hydroxyaminomethane) buffer, or to pH 2 and pH 10 by the addition of concentrated HCl and 1 M NaOH. (Table1) The solutions were thermostatted via the use of a water bath to 37 ºC, unless otherwise stated. Potentiodynamic measurements and electrochemical impedance spectroscopy (EIS) were carried out to characterise the alloy and to monitor changes in the passive film as a result of exposure to different environments with time.

***Table 1**: Electrolyte solutions employed in the study. All solutions were adjusted to the desired pH by the addition of HCl (37%) or NaOH (1 M).*

Background Electrolyte	Added ions
0.14 M NaCl	—
0.14 M NaCl	1 mM KH_2PO_4, 2.5 mM $CaCl_2$, 3 mM KCl, 1.5 mM $MgCl_2$, 4.2 mM $NaHCO_3$, 0.5 mM Na_2SO_4 - **Simulated body fluid -**

RESULTS: In Figure 1, potentiodynamic curves acquired after exposure times of 6 min, 90 min, 18 h, 24 h and 7 d to simulated body fluid adjusted to pH 7.4 at 37 ºC are shown. It is evident from the curves that the time of exposure to the solution plays an important role, both on the cathodic and the anodic currents recorded. During the first 18 h the cathodic currents are very similar and the open circuit potentials fall close to one another. In the anodic potential range, the currents are passive, but once again, after 18 h the passive current appears to be much smaller indicating that the passive film has become more protective (e.g. by thickening, by becoming more compact or by changing in composition). At potentials positive to + 0.5 V vs. SCE the peak superimposed upon H_2O oxidation, is due to the transpassive dissolution of Cr. It is important to note that the increase with immediate decrease in current observed at potentials positive to the open circuit potential is not necessarily to be attributed to an active-passive transition but possibly to the discharge of hydrogen ions adsorbed onto the surface under cathodic potentials.

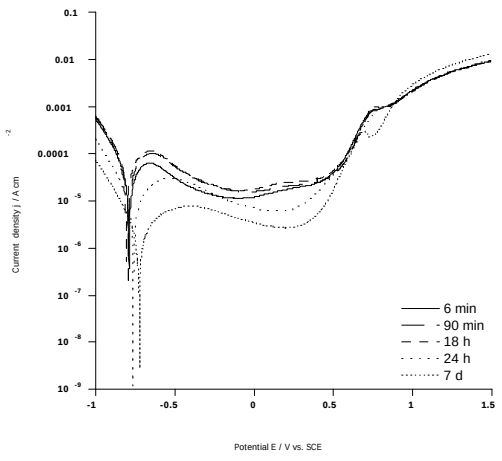

Fig. 1: Current-potential curve recorded at CoCrMo sample at different times of exposure to simulated body fluid adjusted to pH 7.4 at 37 ºC. Sweep rate 5 mVs^{-1}.

Electrochemical impedance spectra acquired under the same solution conditions at different times of exposure ranging from 10 minutes to 7 days, clearly showed an increase in the protectiveness of the passive film with time, which could be observed in the increase in impedance values at low frequency with time and in broadening of the capacitive behaviour of the phase angle to lower frequencies with time.

The effects of ions on the passive film properties were also studied. More specifically, the effects of ions present in simulated body fluid, such as Ca^{2+}, PO_4^{3-}, K^+, Mg^{2+}, were investigated by comparing electrochemical impedance spectra and potentiodynamic measurements with those obtained in 0.14 M NaCl solution also adjusted to pH 7.4 via the use of the same buffer and at 37 ºC. The results clearly showed that, unlike Ti and its alloys[1] which selectively adsorbed Ca^{2+} and PO_4^{3-} ions, CoCrMo does not interact with the ions in the electrolyte and the evolution of the spectra with time obtained in the two solutions are very similar.

Experiments were also performed to investigate the effects of exposure of the CoCrMo sample to air prior to immersion into the electrolyte solution. It was found that the passive films formed in air were different to those formed in solution, but that once the sample had been placed in solution a reconstruction of the passive film takes place.

DISCUSSION & CONCLUSIONS: The electrochemical study showed that the passive film formation on CoCrMo is very sensitive to the conditions under which it takes place, therefore affecting the properties of the films, such as protectiveness and degree of metal ion release. Although the passive film is mainly composed of Cr_2O_3, oxides of Co and Mo can also be present depending on the environment conditions. However the ions present in simulated body fluid do not appear to adsorb or interact with the oxide film. Further studies to investigate the composition of the passive film are currently underway[2].

REFERENCES: [1] A.W.E Hodgson, Y. Mueller, D. Forster, S. Virtanen, (2001) Electrochemical characterisation of passive films on Ti alloys under simulated biological conditions. *Electrochim. Acta* in print. [2] A.W.E. Hodgson, S. Kurz, V. Fervel, S. Virtanen, S. Mischler, (2002) Electrochemical and surface characterization of passive films on CoCrMo in saline and simulated biological solutions, in preparation.

ACKNOWLEDGEMENTS: The authors thank the Foundation "Entwiclungsfonds Seltene Metalle", Switzerland for financial support of the project.

European Cells and Materials Vol. 3. Suppl. 1, 2002 (pages 28-29) ISSN 1473-2262

TRIBOLOGICAL BEHAVIOR OF TITANIUM SLIDING AGAINST BONE

S. Mischler & G. Pax

Laboratoire de Métallurgie Chimique, Ecole Polytechnique Fédérale de Lausanne, CH

INTRODUCTION: In orthopedic implants micro motions are likely to occur at the bone – implant interface. The bone and implant surfaces are thus subject to friction which can cause wear and fretting-corrosion with consequent inflammatory tissue reaction. For this reason, tribological phenomena at bone-implant interface are thought to play a relevant role in aseptic loosening of hip joint implants. Wear and friction are system properties and not materials properties, i.e. the tribological behavior of a material depends, among others, on the nature of the sliding partner. While the tribological behavior of biomedical alloys such as titanium alloys was already investigated when sliding against metals, polymers and ceramics, no results are known for friction against bone.

The goal of this study is to explore possible degradation phenomena (wear, corrosion, changes in surface composition) arising from friction between bone and a Ti6Al4V alloy, a widely used biomedical metal.

METHODS: Tribocorrosion tests were performed using a reciprocating motion plate-on-plate tribometer already described elsewhere. Tests were carried out in a PVC cell that contains 60 ml of solution. The corrosion potential of Ti6Al4V was continuously measured using a silver/silver chloride (+196 mV vs. SHE) reference electrode. Figure 1 shows the details of the contact.

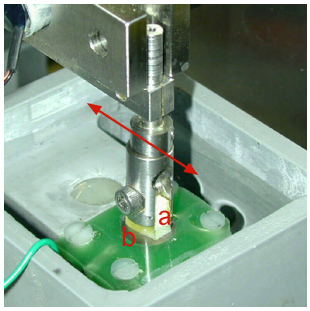

Fig. 1: Detail of the bone (a) – Ti6Al4V (b) contact immersed in 0.14M NaCl at 37°C.

Ti6Al4V discs (10 mm in diameter) were machined from annealed bars supplied by Sieber&Hegner (323HV). The disc were embedded in Technovit, polished using emery paper 240 and subsequently sand blasted. Cow bone specimens were cut in approximately rectangular shape (6 x 4 x 8 mm) from a piece of shin purchased in a butchery. Bone hardness ranged from 35 up to 45 HB62.5 Prior to tests, the samples were cleaned in an ultrasonic ethanol bath. The contact was immersed in a 0.14 M NaCl solution prepared using pa reagent and osmoses de-ionized water. The test procedures involved following steps: first stabilization of the corrosion potential, rubbing at 5 Hz oscillation frequency to establish steady state friction and wear rate (1 hour duration), short rubbing periods (few minutes) at variable motion amplitude by constant oscillation frequency of 1 Hz to monitor changes in corrosion properties. All tests were carried out at 37°C ± 2°C with a normal force of 3 N corresponding to an average load of 0.1 MPa. After tests, the metallic samples were analyzed using optical microscopy, Auger Scanning Electron microscopy (AES), Scanning Electron Microscopy and laser profilometry (UBM apparatus).

RESULTS: The running in period was characterized by severe wear of the bone as evidenced by the large amount of bone debris particles ejected from the contact and the continuous decrease in vertical position of the contact (linear wear). Average of 5 measurements yielded an average bone wear rate of 1.6 ± 0.3 nm/stroke. To check for wear the Ti6Al4V samples were cleaned (after surface analysis) in acetic acid for 12 hours to removed residual bone material. No significant material damage could be observed after rubbing using laser profilometry, SEM and optical microscopy.

The coefficient of friction during rubbing attained, after a few minutes run in, a steady state average value characterized however by large noise (±50% of the average value) due to the large amount of particles trapped within the contact area. Typical average coefficient of friction ranged from 0.34 up to 0.39 for five independent experiments.

Table 1. Shift of the corrosion potential of Ti6Al4V due to rubbing at selected amplitudes.

Motion amplitude	Cathodic shift
1.8 mm	12.7 ± 3.1 mV
0.9 mm	4.5 ± 0.5 mV
0.3 mm	0.3 mV

Rubbing of bone against Ti6Al4V induced a small cathodic shift of the corrosion potential. The shift amplitude was found to depend on the motion amplitude as indicated in Table 1.

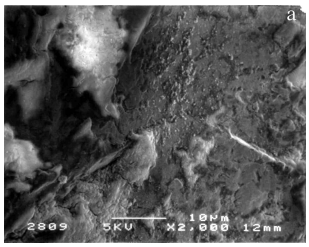

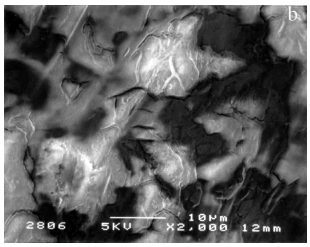

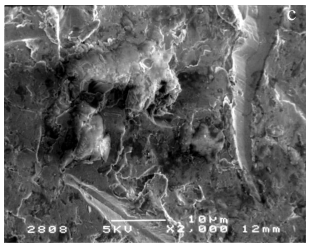

Figure 2: SEM images taken on Ti6Al4V after rubbing against bone in the center (a, top left), at the edge (b, top right) and outside (c) the sliding track.

The rubbed area of all Ti6Al4V samples was found covered by transferred bone material as evidenced by SEM analysis (Figure 2). The transfer morphology was found to depend on whenever the contact was continuous (surface always in contact with the bone) or intermittent (rubbed area exposed to the solution between two strokes). In the intermittent contact area the transfer layer is homogeneous (Figure 2b) while several µm thick patches of bone material characterized the central area (Figure 2a). Interestingly, the transferred bone could not be detached by repeated ultrasonic cleaning but only by dissolution in acetic acid. This indicates a good mechanical adhesion.

AES sputter depth analysis was carried out on three different locations corresponding respectively to thick patches of transfer, areas of the track between patches and areas outside the track. The atomic concentration ratio of the thick patches corresponds to 46% Ca, 32% O, 14% C with P concentrations well below 5%. Areas 2 and 3 are characterized by a passive film of titanium oxide with some contamination by Ca and P, the contamination being more pronounced in the track. The thickness of the passive film is approximately 10 nm. For comparison AES analysis was also carried out on a Ti6Al4V disc loaded against bone (3 N load) during immersion for 2 hours at open circuit potential without sliding. Only carbon (air contamination) oxygen and titanium could be observed. This indicates that friction is necessary to obtain bone transfer onto the metal under the present conditions.

DISCUSSION & CONCLUSIONS: The present work is of preliminary nature and implied several major simplifications of the analyzed tribosystem compared to the complex situation prevailing in vivo. In particular the selected cow bone does not correspond necessarily with clinical situations. The same holds for the applied load and amplitudes. Further the test duration of 1 hour used here is relatively short because it corresponds to an in-vivo activity of only few days assuming a frequency of 10^6 steps per year. Thus, the possibility to extrapolate the present observations to clinical cases is somehow limited.

However, the obtained results clearly illustrate that complex phenomena may occur during rubbing of titanium against bone, phenomena leading to significant bone wear, adhesive transfer of bone onto the metal and modification of the titanium surface composition by contamination of the passive film by Ca and P.

REFERENCES: [1] A, Meunier, L. Sedel (2000), Influence de l'endommagement tribologique des implants orthopédiques sur le milieu biologique: réactions tissulaires et descellement prothétique, *Tribologie et corrosion*. SIRPE pp 193-200. [2] S. Mischler, S. Debaud, D. Landolt (1998) Wear accelerated corrosion of passive metals in tribocorrosion systems. J. Electrochem. Soc **145(3)** pp 750-758.

ACKNOWLEDGEMENTS: Thanks to the Entwicklungsfonds Seltene Metalle, Zürich for financial support.

European Cells and Materials Vol. 3. Suppl. 1, 2002 (pages 30-31) ISSN 1473-2262

EFFICIENCY OF CURING DEVICES FOR DENTAL COMPOSITES

P. Payot*, M. Cattani-Lorente, Ch. Godin, S. Bouillaguet, J. Forchelet* and J.M. Meyer

*Dental School, University of Geneva, * EI-VD, University of applied science, Yverdon-les-bains*

INTRODUCTION: The setting reaction of dental composites is a light-activated radical addition. A high monomer-polymer conversion (DC) is sought, as it is associated with high mechanical properties. The DC depends on the efficiency of the initiator system and on the efficacy of the curing devices. For most dental composites, camphorquinone (CQ) is used as photo initiator. Currently, three different technologies are used in the commercial curing units. The light sources are either halogen lamps, ARC plasma lamps or light emitting diodes (LED).

The aim of the present study is to compare the efficiency of five different curing devices. For that purpose, the curing devices were characterized by their spectra and their irradiance. To test their efficiency, the depth of cure of a dental composite was measured after illumination with different exposure times.

The hypothesis tested is that the efficiency of the curing devices depend on the quantity of energy effectively absorbed by the photo initiator, instead of the total energy supplied by the curing device.

METHODS: The hybrid dental composite Herculite VXR, A2 was used. Two LEDs (Freelight /ESPE; E-light/GC), a halogen (Trilight/ESPE) and two ARC sources (Aurys/DegréK; Flipo/Lokki) were evaluated in the standard mode.

The irradiance was measured using an Avantes fiber optic spectrometer AVS-USB2000 working in the 190 to 850 wavelength range. The irradiance was measured at different distances from the source, as the spectrometer was saturated beyond 4 mW/cm^2.

The depth of cure was determined by measuring the height of cured samples with a micrometer. A PVC opaque mould with a cylindrical cavity of 4mm in diameter and 4 mm in depth was used. The top of the specimens was illuminated using different exposure times (Table 2). The samples were taken out the mold and the uncured material was eventually gently removed. Three samples were made for each illumination condition.Statistical differences in the data were evaluated with a one way analysis of variance, followed by a LSD multiple range test ($p<0.05$).

RESULTS: The obtained spectra are shown in Figure 1.

Fig. 1: Luminous spectra of the five curing units. Their irradiance (mW/cm^2) is given for each

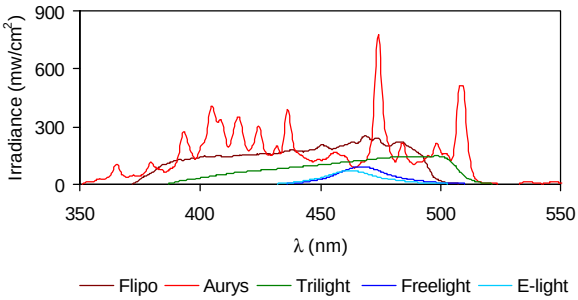

emitted wavelength. The total irradiance is a value integrated over the whole spectrum.

The irradience is given in the Figure 2 for different distances between the source tip and the detector.

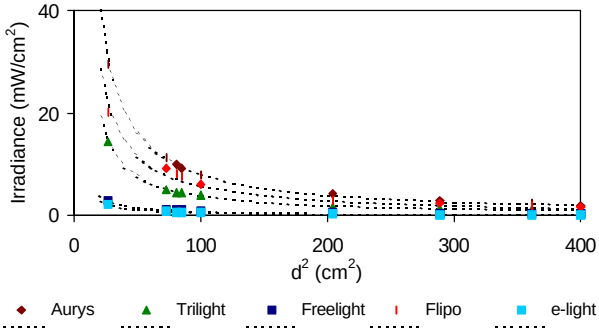

Fig. 2: Irradiance measured at different distances of the source for the five curing devices.

The irradiance in contact with the source was extrapolated from these values, (Table 1). The depths of cure are reported in Table 2.

Table 1. Irradiance Irr (mW/cm2) integrated over two wavelength ranges. Irr are the values given by the manufacturers of the curing devices.*

Curing unit	$Irr_{350-600}$	Irr *	$Irr_{450-490}$
Aurys	1856	1650	523
Flipo	1330	1600	544
Trilight	818	800	297
Freelight	177	400	151
E-light	234	750	203

The energies calculated for the whole spectra range ($E_{350-600}$) and the 450-490 wavelength range (E_{450-}

$_{490}$) are reported in the same table. Values marked with the same letter are not significantly different.

Table 2. Depth of cure for the different conditions and their corresponding energy E (J) emitted over two wavelength ranges .

Curing unit	t (s)	$E_{350-600}$	$E_{450-490}$	Depth (mm)
Flipo	1	0.54	0.23	2.19 ± 0.01 b,c
	2	1.07	0.47	2.34 ± 0.02 c
	3	1.61	0.7	2.79 ± 0.11 d,e
	5	2.68	1.17	3.04 ± 0.16 f
	10	5.37	2.34	4.17 ± 0.01 i
Aurys	1	0.74	0.22	1.42 ± 0.03 a
	2	1.48	0.45	2.09 ± 0.04 b
	3	2.21	0.67	2.84 ± 0.03 e
	5	3.69	1.12	3.05 ± 0.08 f
	10	7.38	2.25	4.06 ± 0.06 i
Freelight	10	0.75	0.65	3.36 ± 0.08 g
	20	1.49	1.3	4.05 ± 0.02 i
	40	2.99	2.6	4.17 ± 0.01 i
E-light	10	0.58	0.49	2.65 ± 0.16 d
	20	1.17	0.98	2.81 ± 0.03 e
	40	2.34	1.95	4.19 ± 0.02 i
Elipar	10	3.1	1.39	3.58 ± 0.14 h
	20	6.2	2.79	4.15 ± 0.02 i
	40	12.4	5.58	4.17 ± 0.01 i

DISCUSSION & CONCLUSIONS: In this work, a single composite was used to exclude the effects of chemical composition on the depth of cure. The maximum depth was obtained by illuminating 10s with the ARC devices, 20s with Elipar and Freelight and 40s with E-light.

The irradiance values given by the manufacturers Irr* are given for the whole emitted. These values correspond to the radiation flux per unit of surface in direct contact with the source. In the present study, the irradiance couldn't be measured in these conditions, because the detector used was saturated at close distances to the sources. However, these values were extrapolated and can be compared to the Irr* (Tab 1). An advantage of measuring the light intensity at different distances is that the source can be considered as being punctual.

To test our hypothesis, the energy emitted by the different sources was calculated by the equation 1,

$$E = IrrSt \quad (1)$$

where S is the surface of the source tip. A relationship between the depth of cure and the emitted energy was established (Figure 3). The data were best fitted by the equation 2,

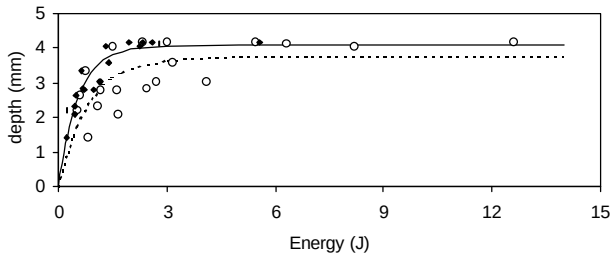

$$Depth = a(1-e^{-bE}) \quad (2)$$

where a and b are constants.

Fig. 3: Relationship between the depth of cure and the energy emitted by the sources at the different exposure conditions.

A poor correlation was obtained between the depth of cure and the total amount of energy $E_{350-600}$ (a:3.77; b:1.21; r:0.81; se:0.66). However, it is well known that only the light emitted in the wavelength interval which corresponds to the absorption of the photo initiator is useful to initiate the composite polymerization. The CQ absorption peak in methacryliate resins ranges from 380 to 510 nm with a maximum at 468 nm [1]. Moreover, Nomoto [2] showed that radiation in the 450-490 nm range activated more efficiently the CQ. Consequently, the energy emitted in this range ($E_{450-490}$) was also calculated. $E_{450-490}$ corresponded to 43% of $E_{350-600}$ for the halogen and the Flipo ARC sources, to 30% for the Aurys ARC and to more than 80% for the LEDs. As expected, a better correlation was obtained between the depth of cure and the $E_{450-490}$ variable (a:4.08; b:1.82; r:0.95; se:0.35), corroborating our working hypothesis.

In conclusion, the five curing devices showed marked differences in the shape and intensity of their emitted light spectra. Despite that the irradiance of the LEDs sources is the lowest, more than 80% of their emitted energy is in the 450-490 wavelength range. 20s were necessary to obtain the maximum depth with the Freelight LED and the halogen source. The exposure time could be reduced by a half by using the two ARC sources. However, for these devices, only 30 % and 43% of the emitted energy is in the wavelength range efficiently absorbed by the CQ.

REFERENCES: [1] F Stahl et al. (2001) *Biomaterials* **21**:1370-1385. [2] R. Nomoto et al. (1997) *Dent Mater J* **16**:60-73.

ACKNOWLEDGEMENTS: We gratefully acknowledge the manufacturers for supplying the unit curing devices.

EXTRACTION OF PLASMA SPRAYED TITANIUM THROUGH A BONE CEMENT USING ELECTROCHEMICAL TECHNIQUES.

L. Reclaru*, A. Blatter*, R. Lerf**, P. Y. Echler*, J. M. Meyer***

** PX Tech SA R&D La Chaux-de-Fonds, ** PI Precision Implant AG , Aarau, ***School of Dentistry, University of Geneva*

Introduction: Titanium and titanium alloys are widely used as orthopedic implants because of their favorable mechanical properties and good biocompatibility. However, some specific cases are known, where highly loaded cemented implants made from Ti alloys produced unsatisfactory results in clinical practise (e.g. 1). Prior *in-vitro* experiments showed that micromotion alone could not explain debonding and osteolysis reported for such cemented implants (2). Electrochemical test on samples of cement + titanium revealed the ability of the polymer to transport electrical charges in the polymer – metal interface (3).

The cement is an ionic conductor and therefore participates in the corrosion process. The corrosion phenomenon is in this case accompanied by titanium cation diffusion into the electrolyte and chloride anions towards the titanium through the cement. In the present study, we have evaluated the corrosion behavior of titanium vacuum plasma spray coating (Ti VPS) with and without bone cement. Electrochemical extraction tests were carried out, with ICP-MS analysis of the electrolyte, in order to verify the ionic permeability of the polymer.

Materials and methods : A layer of CEMEX® bone cement, approximately 0.9 mm thick, was manually pressed onto Ti VPS sample discs of diameter 11 mm.

The quantities of titanium in the electolyte, extracted from the samples by cyclic and potentiostatic voltametry, were determined by the technique of ICP-MS.

After the tests, we eliminated part of the cement on the disc to check for the presence of chloride ions using EDX analysis.

Results and discussion : Figure 1 shows the sweeping curves corresponding to the first and last (#48) cycle recorded during cyclic. The measured current is of the order of a few hundred nano-amperes.

For the second technique used are displayed in Figure 2 the potentiostatic curves of the ten cycles at 650 mV SCE.

The concentrations of titanium cations found in the electrolyte by ICP-MS were smaller than 0.5 ìg/L in both tests.

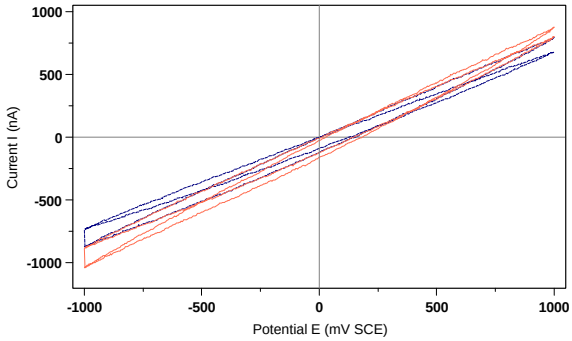

Fig.1 Potentiodynamic curves obtained by the cyclic voltametry technique. First cycle and the last , # 48 .

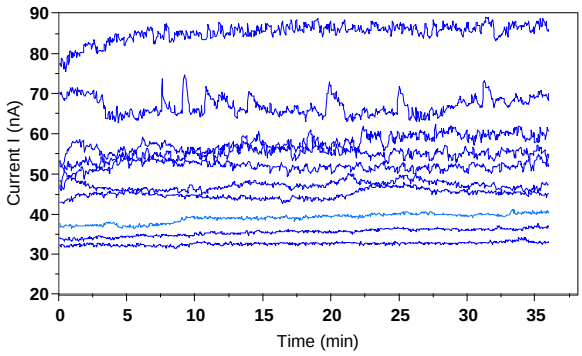

Fig. 2 Potentiostatic curves recorded during 36 minutes, number of cycles, 10 / level

The total quantity of charge recorded during the extraction test was 6106, 6 °C. Based on Faraday's law, which assumes that all the measured electrical charge is used to extricate the Ti^{2+} cations from the disc sample through the membrane of bone cement into the electrolyte, we expect a theoretical quantity of 1.515 ìg of titanium in the solution, corresponding to a titanium concentration of 75ìg/liter. This theoretical concentration by far exceeds the measured quantities of less than 0.5 ìg/liter. This indicates that most of the electrical charges are consumed in the cement by other ions (sodium and chloride), and probably also by the growth of the titanium oxide layer. After the extraction test, we find indeed chloride ions on the surface of the sample disc using EDX analysis.

The presence of titanium in the solution and of chloride on the sample surface confirms the suggested transfer mechanism (Fig.3).

Conclusion: From our results we conclude that the bone cement is permeable for titanium cations, leading to a corrosion process of the titanium underneath the cement. The corrosion process comprises the formation of titanium cations as well as the growth of the titanium oxide layer.

References:

1Willert HG. et al., 1996, Clin Orthop, 333: 51-75.
2 Schmotzer H. et al., 2000, ORS Orlando, 0572.
3 Deportes C., Duclo M., Fabry P., Fouletier J., Hammou A., Kleitz M., Siebert E., Souquet J-L., Electrochimie des Solides, Ed. Presses Universitaires de Grenoble, 1994, 1782-186, 300-320.

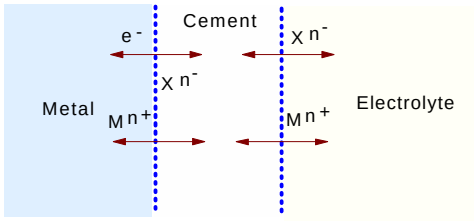

Fig. 3 Schematic representation of the exchange process between the metal - cement – electrolyte**.**

European Cells and Materials Vol. 3. Suppl. 1, 2002 (pages 34-35) ISSN 1473-2262

THERMOMETRIC STUDY OF BRUSHITE CEMENTS

S. Rousseau, M. Bühler, J. Lemaître

Laboratoire de Technologie des Poudres, EPFL, MX-Ecublens, 1015-Lausanne

INTRODUCTION: This study is part of a broader work on Brushite cements [1]. The effects of various experimental factors on the working characteristics of Brushite cements are being investigated, with the aim of understanding the physico-chemical aspects of the setting and consolidation processes, and the mechanisms of the chemical reactions leading to consolidation.

In the present study, thermometric measurements are being used in order to monitor the early stages of the setting and hardenig processes of Brushite cements. The thermometric approach gives acces to useful working characteristics such as working and setting times, in very good agreement with standard experimental techniques such as the Vicat needle method.

METHODS:

Principle of the method : Advantage is taken of the fact that the setting reactions leading to brushite formation are slightly exothermic.

A freshly prepared cement paste (about 2 mL) is inserted into a polyurethane foam block placed within a Dewar flask, and covered with an insulating lid ; thus, the sample is thermally insulated in a way similar as it would be upon implantation into cancellous bone. A thermocouple is stuck in the middle of the cement sample. Temperature is sampled every few seconds and recorded by a computer (Fig. 1). The thermometric curve results from two competing processes : heat is generated by the chemical reactions responsible for the consolidation of the cement and slowly dissipated by thermal conduction through the walls of the container and through the thermocouple. Compensation for thermal dissipation can be calculated from a control thermometric curve (Fig. 2), obtained by placing in the measuring cell a sample of hardened cement preheated to about 45°C, and recording its cooling curve.

The kinetics of enthalpy production due to the consolidation reactions is obtained by summing the apparent enthalpic curve and the thermal dissipation curve deduced from the experimental and control thermometric curves (Fig. 3).

The progress of the cementation reaction is calculated by taking the ratio of the measured enthalpy over the theoretical reaction enthalpy (which can be calculated on the basis of known thermochemical data). The kinetic curve (Fig. 4) shows a sigmoidal shape, from which several characteristics of the consolidation process can be deduced : induction (or working) time, setting time, maximum β-TCP conversion.

Full details on the experimental setup and on the treatment of the experimental data are presented in reference [2].

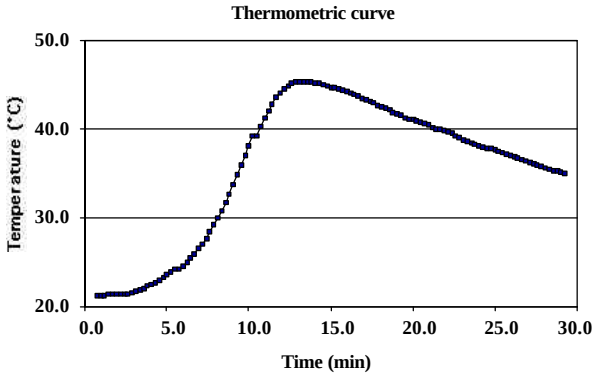

Figure 1. Experimental thermometric curve.

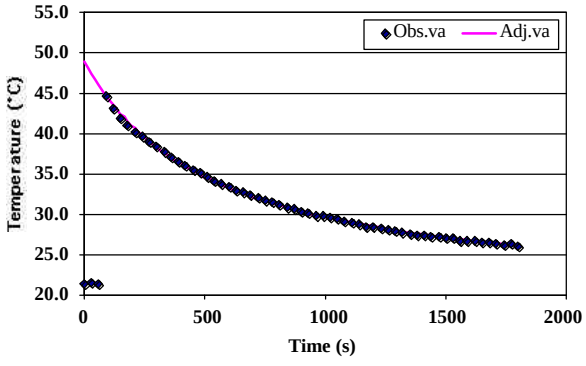

Figure 2. Control thermometric curve.

EXPERIMENTAL DESIGN :

Table I. Definition of factors and levels in the experimental design

Factor	Definition	Low Level	High

			Level
A	Polymer*	HA	HPMC
B	Sulfate	Plaster	Sulf. Ac.
C	Magnesium°	0 %wt	8 %wt
D	Porosity	35%vol	45%vol

* HA : Hyaluronic acid ; HPMC : Hydroxypropylmethyl cellulose. ° In the form of $Mg.HPO_4.2H_2O$ (Newberryite).

Experimental factors summarized in Table I have been selected on the basis of previous *in vivo* and *in vitro* studie, which have shown considerable changes in biodegradability of brushite cements according to the presence of Mg, sulfate ions and on the nature of hydrosoluble polymers incorporated for rheological control. The experiments were organised into a 2^4 multifactorial statistical design. The results were analysed using the ANOVA technique.

RESULTS AND DISCUSSION:

Thermometric observations show a systematic decrease of the maximum temperature for Mg–containing samples. Statistical analysis of the results expressed in terms of maximum β–TCP conversion (Fig. 5) demonstrates clearly a marked inhibitory effect of Mg on the consolidation reactions ; the effect is more contrasted for samples with 35%vol porosity containing hyaluronic acid. The presence of sulfate in any form does not seem to play any significant role.

Thus the presence of Mg, especially in conjunction with hyaluronic acid appears to inhibit strongly the chemical reactions leading to the formation of brushite.

CONCLUSIONS: A new experimental approach based on thermometric measurements allows to calculate the kinetics of enthalpy production, and hence the kinetics of transformation of calcium phosphate cements. These kinetic curves allow to calculate several working characteristics of the cements : working and setting times, maximum fraction of converted β-TCP, reaction rate, maximum temperature increase upon cement consolidation.

Based on thermometric analysis, the inhibiting effect of magnesium on the setting reaction of Brushite cement has been clearly evidenced.

REFERENCES:

[1] A.A Mirtchi, J.Lemaître, N.Terao. Calcium phosphate cements : study of the β-Tricalcium phosphate-monocalcium phosphate system. Biomaterials, 10 [septembre] 475-480 (1989).

[2] C. Pittet "Development and Characterisation of Injectable Calcium Phosphate Cements for Use in Vertebroplasty." Thesis n° 2509, EPFL, 2001.

ACKNOWLEDGEMENTS: The support of the Robert Mathys Foundation and of Stratec Medical is gratefully acknowledged.

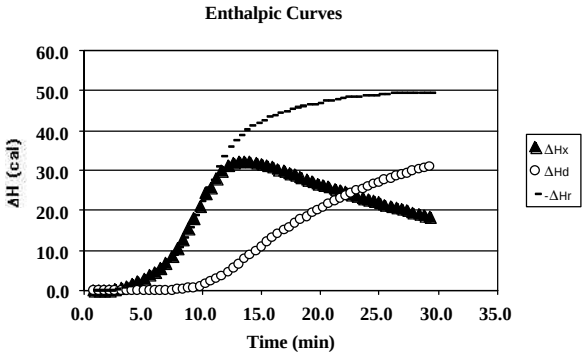

Figure 3. Enthalpic curves : $\bullet H_x$ experimental enthalpy vs time ; $\bullet H_d$ dissipated enthalpy.

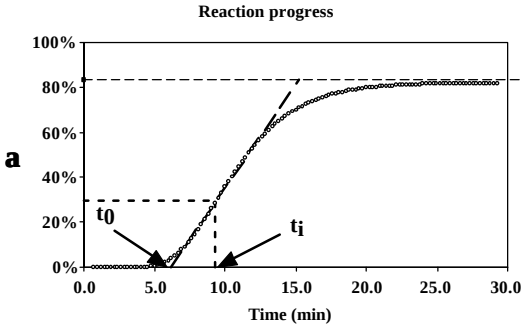

Figure 4. Reaction progress *vs* time. t_o : working time ; t_i setting time.

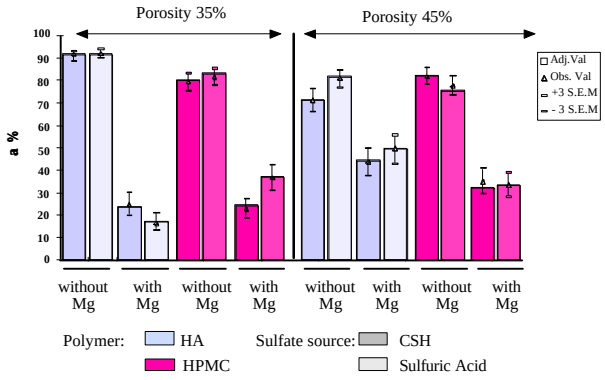

Figure 5. Evolution Effects of experimental factors on the ultimate conversion of the cement.

HEMOCOMPATIBILITY OF SEMI-CONDUCTING BIOMATERIALS

K. Unal[1], Y. Mugnier[1], N. Nurdin[1], J. Krumeich[2], P. François[3], B.-O. Aronsson[1] & P.Descouts[1]

[1]*GAP Biomedical, University of Geneva, CH,* [2] *Sulzer Innotec, Winterthur, CH ,*
[3]*Div. of Infectious Diseases, University Hospital of Geneva, CH*

INTRODUCTION: Hemocompatibility of an implant is determined by its surface properties. According to recent suggestions [1], the involvement of electron exchange can occur in adsorption process from physiological media. This electron transfer may induce conformation changes of adsorbed proteins and cause their degeneration. Therefore materials with large band gaps and high work function could be advantageous and the knowledge of the surface electronic properties of biomaterials at the nanometer scale is crucial.

In addition to the physico-chemical characterization, tests to determine the interactions between the modified surface and the blood proteins and platelets are important to perform. For this the measurements of both fibrinogen adsorption and platelets adhesion are important for determining the relative thrombogenic potential of a material. Today, it is proved that synthetic materials adsorbing less fibrinogen from blood plasma do also adhere fewer platelets and thereby exhibit improved blood compatibility. The aim of this project is to characterize the surface electronic properties of different semi-conducting biomaterials using Electrostatic Force Microscopy (EFM) with AFM instrumentation, and to observe by confocal microscopy the platelet adhesion and aggregation from platelet-rich human blood plasma.

METHODS: In EFM [2], the Contact Potential Differences (CPD) are measured at the nanometer scale in an analogous manner to conventional Kelvin Probe Spectroscopy. An electrostatic force is induced between the conductive tip of an AFM and the sample surface by applying an AC bias voltage of frequency ν to the tip (already vibrating at its resonance frequency ν_0). The convoluted signal of the CPD between the sample and the tip and the gradient of the capacitance is obtained from the amplitude at ν, while at 2ν only the gradient of the capacitance is measured. The local work function of different DLC coatings was obtained by performing spectroscopy. The AFM tip was kept stationary on a desired surface point and a DC voltage was applied on either the tip or the sample. At a certain voltage, the amplitude at ν can be reduced to zero. This DC voltage corresponds to the difference of work function ($\Delta\phi$) between the sample and the tip coated with 10 nm of Pt. A commercial AFM working in controlled atmosphere (Relative humidity = 30% ±5%) was used. DLC coatings with a thickness of ca. 3 μm were deposited on Si wafers using plasma assisted CVD in a mixture of acetylene and argon. Three different types of coatings were studied. The first one is a standard DLC coating co-deposited with the sputtering of Ti. A dense DLC coating was produced using a sample potential of 75 V and a density gradient DLC coating was deposited by varying the sample potential from 25 to 75 V. These two latter coatings were deposited in a metal free procedure.

To observe the platelet adhesion on previously described materials, confocal laser microscopy (CLM) and/or epi-fluorescence measurements will be used. A custom-made set-up was thus implemented on a commercial inverted microscope (Nikon Eclipse TE300) in order to combine CLM, epi-fluorescence and classical optical imaging. The sample is scanned in a confocal arrangement on a servo-controlled x,y,z scanner. Using either a 40* (0.6 NA dry), or a 100* (1.3 NA oil immersion) objective, the lateral resolution (depth discrimination) are, respectively 0.5 μm (5 μm) and 0.3 μm (0.9 μm), as determined from response curves measured on fluorescent micro-spheres. For a high s/n-ratio, the fluorescence signal is detected by an avalanche photo-diode (EG&G) and the image constructed in a PC.

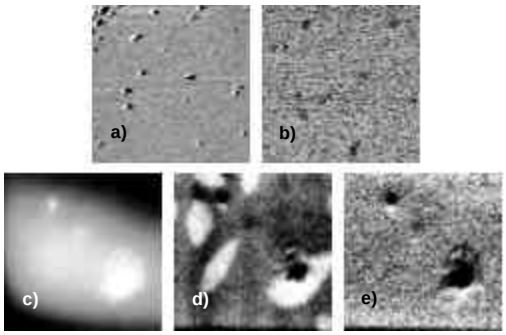

Fig. 1: Convoluted surface potential and capacitance gradient image for a) dense and b) density gradient DLC coating (scan size 2 mm); c) Topography, d) Surface potential and Capacitance gradient, e) Capacitance gradient image of standard DLC coating (scan size 10 mm).

RESULTS: The dense and the density gradient DLC coatings showed smooth topographical AFM images. Homogeneous surface potential (Figure 1a and 1b) and capacitance gradient images were found. The CPD for the different DLC coatings and the reference Si wafer are shown in Table 1. The topography of the standard DLC coating was found to be rougher than the other two. As shown in Figure 1, the surface potential image (1d) exhibited spots of ca. 2-4 μm wide with a different surface potential which was not observed on the capacitance gradient image (1e).

Table 1. CPD of DLC coatings measured by EFM.

Sample	CPD [eV]
Ref. Si wafer	-0.68±0.02 eV
Dense DLC	0.11±0.05 eV
Density Gradient DLC	0.08±0.02 eV
Standard DLC	-0.33±0.02 eV

DISCUSSION & CONCLUSIONS: The metal free coatings show similar topographical and surface electronic properties, although the coating densities are different. The inhomogeneities observed for the standard DLC coating are interpreted as a TiC clustering during the co-deposition of Ti. This is evidenced by traces of Ti detected in the Auger spectra. In conclusion, an EFM was implemented with a resolution less than 40 nm. EFM on standard DLC coating showed surface inhomogeneities (metal clusters), not seen in a metal free deposition process. The CPD of different DLC coatings was determined. By confocal microscopy of platelet-rich blood incubated samples the platelet adsorption on the surfaces will be quantified.

REFERENCES: [1]A. Boltz *et al*. (1996) Coating of Cardiovascular Stents with a Semi-conductor to improve Their Hemocompatibility *Tex. Heart. Inst. J.*, **23** (2),162-166.[2]. M. Nonnenmacher *et al*. Kelvin probe force microscopy (1991) *Appl. Phys. Lett.*, **58** (25), 2921-2923.

ACKNOWLEDGEMENTS: M. Moret (GAP-biomedical) is gratefully acknowledged for technical support. This work is supported from the COST action 527 OFES No C01.0051.

2- AND 3-YEAR RESULTS OF ZIRCONIA POSTERIOR FIXED PARTIAL DENTURES, MADE BY DIRECT CERAMIC MACHINING (DCM)

I Zembic, H Lüthy, M Schumacher, P Schärer, C H F Hämmerle

Clinic for Fixed and Removable Prosthodontics and Dental Materials, School of Dentistry, University of Zurich, CH

INTRODUCTION: Today, Fixed Partial Dentures (FPD), made of a metallic framework covered by tooth colored ceramics exhibit a well documented long-term stability for the molar region. However, the use of some metals in the oral cavity has been disputed because of the risk of biological incompatibility. Furthermore, a grayish mucosal discoloration of the marginal region may leed to esthetic problems despite the ceramic veneering. Hence, there is a need for all-ceramic restorations offering sufficient stability for molar replacement. Zirconia combines excellent mechanical properties, widely documented biocompatibility and desired esthetic advantages due to its white color. The purpose of this study was to evaluate the clinical behaviour of zirconia posterior FPDs fabricated by direct ceramic machining (DCM).

METHODS: In 45 patients 58 zirconia FPDs replacing 1 to 3 posterior teeth were cemented with two composite cements (Variolink®, Panavia®). The zirconia frameworks were fabricated out of a porous pre-sintered TZP (tetragonal zirconia polycrystals) blank by milling a linearly enlarged copy of a framework model. Thereafter the frameworks were sintered to full density (DCM; ETH Zurich, Switzerland), allowing shrinkage to their final dimension. Subsequently they were veneered with porcelain. After 2 or 3 years respectively, the patients were re-examined and the following data were recorded on test- and control-teeth (neighbouring teeth, antagonists): i.)examination of the bridge for framework-fracture and chipping/fracture of the veneering material; ii.)recordings of pocket probing depth (PPD), probing attachment level (PAL), bleeding on probing (BOP), Plaque Index (PlI) and tooth mobility (TM); iii.)radiographical examination using single tooth films.

RESULTS: 2-year follow-up: 23 patients with 29 bridges were examined. No framework-fracture was observed. 2 bridges had to be replaced due to biological complications (root fracture, endodontic problem). Therefore, the survival-rate in this group was 93%. Minor porcelain chipping was reported in 10% (n=3), and 18% (n=16) of the abutments exhibited marginal discrepancies leading to secondary caries in 3% of the cases. No statistically significant differences were found between test- and control-teeth regarding PPD, PAL, BOP, PlI and TM ($p>0.5$; Wilcoxon Signed Rank Test).

3-year follow-up: 13 patients with 18 bridges were examined. Again, no framework-fracture was observed. 3 bridges had to be replaced: 1 due to a biological complication (endodontic problem), 1 because it was not correctly cemented and 1 because of loss of retention. Therefore, the survival-rate in this group was 83%. Minor porcelain chipping was reported in 5% (n=1) and 18% (n=6) of the abutments showed marginal discrepancies leading to secondary caries in 9% of the cases. No statistically significant differences were found between test- and control-teeth regarding PPD, PAL, BOP, PlI and TM.

DISCUSSION&CONCLUSIONS: Based on the results of this study it can be concluded, that zirconia-frameworks made by direct ceramic machining offer sufficient stability to be used for replacement of posterior teeth. Complications resulting from marginal discrepancies of the reconstructions need to be reduced by further refinements of the prototype DCM.

REFERENCES: [1]F Filser, H. Lüthy, P. Schärer, L. Gauckler (1998) *All-Ceramic Dental Bridges by Direct Ceramic Machining (DCM)* in: *Materials in Medicine*, Eds. M.O. Speidel et al.: vdf Hochschulverlag, ETH Zurich: Zurich.p.165-189. [2]B Sturzenegger et al. (2000) *Klinische Studie von Zirkonoxidbrücken im Seitenzahngebiet hergestellt mit dem DCM-Verfahren;* Acta Med Dent Helv 5: 131-139

ACKNOWLEDGEMENTS: This work was supported by the Swiss Priority Program for Materials Research.